

STRUCTURAL LOADS HANDBOOK

Pedro Filipe Fernandes de Albuquerque

Dissertação para a obtenção de Grau de Mestre em
Engenharia Aeroespacial

Júri:

Presidente: Professor Fernando José Parracho Lau (IST)
Orientador: Professor Filipe Szolnoky Ramos Pinto Cunha (IST)
Coorientador: Professor Luís Filipe Galvão dos Reis (IST)
Vogais: Professor Pedro Tavares da Graça Alves Serrão (IST)
Professor Ricardo António Lamberto Duarte Cláudio (IPS)

Outubro 2011

Dedicatória

Aos meus Pais, como tributo pela educação que me deram.

À minha Mãe, a quem nunca poderei retribuir a sua inefável dedicação.

Ao meu Pai que me deu a vida duas vezes, o meu primeiro professor.

À minha Irmã, a quem adivinho e desejo um grande futuro.

Aos meus Avós, pela sua proximidade e constante apoio.

E ainda:

- A todos os professores que contribuíram para a minha educação e formação. Em particular para a Professora de Geografia e Diretora de Turma (2000-2003) na Escola EB 2,3 D. Pedro IV – Queluz, a Professora Teresa Zêzere e para a Professora de Português e Diretora de Turma (2003-2006) na Escola Secundária Stuart Carvalhais, a Professora Ana Paula Assunção. Pelo seu profissionalismo, seriedade, honestidade e competência, sempre foram duas importantes referências para a minha pessoa;
- Ao Professor Fernando Lau da Área Científica de Mecânica Aplicada e Aeroespacial do Instituto Superior Técnico por ter contribuído decisivamente para que no 1º ano, eu e 7 colegas (todos caloiros) fôssemos ao curso *Human Spaceflight and Exploration*, em *Umeå/Kiruna*, na Suécia. Aos amigos Alexandre Antunes, Duarte Boto, Guilherme Trigo, Hugo Lopes, Hugo Marques, Pedro Paulo e Tiago Ferreira com quem partilhei esta experiência;
- Ao meu amigo e Informático António Augusto pela sua inextinguível ajuda na cadeira de Programação e na solução de vários problemas informáticos ao longo de todo o curso;
- Aos camaradas da equipa AERACES 2009 que participaram comigo no Air Cargo Challenge 2009, na Covilhã: Jorge Silva, Hugo Lopes, Nuno Santos, Pedro Ochôa, Pedro Paulo, Pedro Simplício;
- Aos meus amigos e colaboradores da Secção Autónoma de Aeronáutica Aplicada (S3A da AEIST). Ser membro, cofundador e primeiro Presidente deste grupo (2009-2011) foi para mim um enorme orgulho e prazer. A humildade, dedicação, trabalho e espírito de equipa do conjunto são ímpares e fazem-me acreditar no futuro;
- Aos amigos e companheiros da equipa PASSAROLA com quem partilhei a participação no Air Cargo Challenge 2011, em *Stuttgart*, na Alemanha, e um saboroso 6º lugar depois de muitos contratemplos, muito trabalho e muitas noites passadas no laboratório de Engª Aeroespacial: David Melo, Diogo Vicente, João Santos, Hugo Marques, Pedro Precioso e Tiago Ferreira;
- Aos meus amigos e principais companheiros de estudo e de trabalho Kevin Spencer, Duarte Boto, Bruno Tojo e Jorge Baginha.

A todos deixo a minha mais profunda gratidão.

Acknowledgements

The completion of this thesis was only possible with the support and guidance of many people to whom I wish to leave a written testimony of my gratitude.

First of all I would like to thank my advisors. I thank Engineer Carlos Rodrigues for his tireless collaboration during my stay at OGMA, *Indústria Aeronáutica de Portugal, SA*. I am also very grateful to Professor Filipe Szolnoky Cunha and Professor Luís Reis for their crucial help and guidance throughout the whole work.

I would like to express my gratitude to Professor Luís Eça for his precious help with the aerodynamics' analysis. I am extremely indebted for his availability and collaboration on finding simple yet reliable methods for estimating the aerodynamic coefficients of the lifting surfaces.

I thank Professor Relógio Ribeiro for his collaboration on finding the best means to study the landing gear damping system. I acknowledge both his technical help and accessibility.

I thank Professor Viriato Semião for his advice concerning the fuselage's aerodynamics.

I thank Doctor André Marta for having clarified several doubts concerning gust analysis.

I am grateful to my friends and colleagues Bruno Tojo, Diogo Vicente and Stefano Carli for having revised a part of this text.

I thank my colleague Joana Palavras for the data provided on failure criteria.

Last but not least, I would like to thank my family, particularly my parents and sister who have strongly supported me from my first school day onwards. They have also actively contributed for the review of this report.

Resumo

Do ponto de vista de projeto, a determinação das cargas estruturais atuantes numa aeronave reveste-se da maior relevância, pois as suas combinações críticas constituem as limitações de projeto aeronáutico.

O presente trabalho visa consubstanciar o trabalho desenvolvido pelo Departamento de Engenharia Projeto e Modificações na empresa *OGMA, Indústria Aeronáutica de Portugal, SA* através do desenvolvimento de um manual que permita calcular as cargas estruturais máximas atuantes numa aeronave através da utilização de análises simplificadas que sirvam de alternativa e de validação dos métodos mais comumente utilizados, nomeadamente aos programas comerciais de Elementos Finitos e Mecânica dos Fluidos Computacional.

Para concretizar os métodos apresentados, desenvolveu-se um conjunto de documentos em *Microsoft Excel®* que avaliam os carregamentos de uma aeronave genérica – sujeita à introdução por parte do utilizador da geometria e condições de operação da mesma – com o intuito de determinar o carregamento máximo a que cada ponto dos principais componentes de aeronave está sujeito. São analisados os principais carregamentos atuantes nos trens de aterragem, nas asas, no estabilizador horizontal, no estabilizador vertical e na fuselagem.

No sentido de demonstrar os resultados alcançados com os métodos desenvolvidos durante esta investigação, ilustram-se os gráficos do esforço transversal, momento fletor e torção em cada um dos principais componentes da aeronave *Lockheed Hercules C-130*.

Palavras-Chave: Aeronave, Avião, Manual Cargas Estruturais, Manobras.

Abstract

From the design viewpoint, the determination of the acting loads on an aircraft is of outmost relevance, because their critical combinations are the aeronautical designer constraints.

The present work aims to enhance the work developed by the *OGMA, Indústria Aeronáutica de Portugal, SA* Engineering, Design and Modifications Office by developing a Structural Loads Handbook to enable the estimation the maximum structural loads acting on an aircraft using a thorough analysis that can work as an alternative and a validation of the most commonly used methods, namely Computational Fluid Dynamics and Finite Element Methods commercial softwares.

So as to materialize these methods, a number of *Microsoft Excel®* workbooks that evaluate the structural loads acting on a generic aircraft have been developed. The user is required to introduce the geometry and operational conditions. The most relevant loads acting on the landing gears, wing, horizontal stabilizer, vertical stabilizer and fuselage are then analysed.

In order to demonstrate the results obtained with the methods developed throughout this work in a tangible case, the shear force, bending moment and torsion are plotted along each of the main components of the *Lockheed Hercules C-130H*.

Keywords: Aeroplane, Aircraft, Manoeuvre, Structural Loads Handbook.

Contents

1.	Introduction	1
1.1.	Legislation	2
2.	Weight, Balance and Performance	3
2.1.	Aircraft Performance	3
2.1.1.	Atmospheric Conditions	3
2.1.2.	Airspeed Measurement	3
2.2.	Load Requirements	4
2.2.1.	Manoeuvre Envelope	5
2.2.2.	Gust Envelope	7
2.2.3.	Combined Flight Envelope	8
3.	Landing Gear Loads	9
3.1.	Landing Loads Analysis	9
3.1.1.	Landing Loads Conditions and Assumptions	9
3.1.2.	Landing Speed Calculations	12
3.1.3.	One-point Landing	12
3.1.4.	Two-points landing	13
3.1.5.	Three-points landing	14
3.2.	Take-off Landing Gear Analysis	15
3.3.	Ground Load Analysis	16
3.3.1.	Static Load Conditions	16
3.3.2.	Taxi, take-off and Landing Roll Conditions	17
3.3.3.	Braked Roll Condition	18
3.3.4.	Two-Point Braked-Roll	19
3.3.5.	Nose Gear Loads Due to Sudden Application of Brakes	19
3.3.6.	Turning condition	20
3.3.7.	Towing condition	24
3.3.8.	Jacking and Tie-down Provisions	25
4.	Wing loads	27
4.1.	Lift Distribution	27
4.1.1.	Approach 1 – SCHRENK Method	27
4.1.2.	Approach 2 – Joukowski Based Method	28
4.1.3.	Approach 3 – Joukowski Based Modified Method	30
4.2.	Drag Distribution	31
4.3.	Pitching Moment Coefficient	32
4.4.	Compressibility effects	32
4.4.1.	Subsonic Compressibility Correction Methods	33
4.5.	Symmetrical Manoeuvres	35

4.5.1.	Basic Lift and Additional Lift.....	36
4.5.2.	Lift distribution due to pitching velocity	36
4.5.3.	Lift distribution due to pitching acceleration	38
4.5.4.	Lift distribution due to aeroelastic effect of inertia	38
4.5.5.	Lift distribution due to Spoilers.....	38
4.5.6.	Lift distribution due to Aeroelastic Effect.....	40
4.6.	Rolling Manoeuvres	41
4.6.1.	Symmetrical Load Increments	41
4.6.2.	Spanwise Load Distributions during Rolling Manoeuvres	41
4.6.3.	Rolling Manoeuvre Load Factors	42
4.7.	Yawing Conditions	43
5.	Horizontal Tail Loads	47
5.1.	Horizontal Tail Arrangement	47
5.2.	Equilibrium Equations	48
5.3.	Balanced Manoeuvre Analysis	49
5.4.	Abrupt Pitching Manoeuvres.....	50
5.4.1.	Abrupt Unchecked Elevator Conditions	51
5.4.2.	Checked Manoeuvre Conditions.....	51
6.	Vertical Tail Loads	53
6.1.	Rudder Manoeuvre Requirements.....	53
6.2.	Vertical Tail Loads for Yawing Manoeuvre	54
6.3.	Vertical Tail Loads on Engine-Out Condition.....	54
6.3.1.	Engine-Out with Zero Rudder	55
6.3.2.	Engine-Out with Zero Sideslip	55
6.4.	Concluding Remarks.....	56
7.	Fuselage Loads	57
7.1.	Wing, Empennage and Landing Gear Loads	57
7.2.	Pressurization Loads	57
7.3.	Fuselage Airloads	59
7.3.1.	Approach.....	59
7.3.2.	Fuselage Cross Flow	60
7.3.3.	Pressure Distribution on a Body of Revolution in an Uniform Stream	62
7.4.	Combined Loads on the Fuselage.....	63
8.	Miscellaneous loads analysis	65
9.	Results – Case Study	67
9.1.	Presentation of the Lockheed C-130	67
9.2.	Lockheed C-130 Specifications	68
9.3.	Results	69

9.3.1.	Landing Gear Loads	70
9.3.2.	Wing Loads	71
9.3.3.	Horizontal Tail Loads	73
9.3.4.	Vertical Tail Loads	75
9.3.5.	Fuselage Loads	77
9.4.	Validation	78
10.	Conclusions and Future Work	79
10.1.	Conclusions	79
10.2.	Future Work	79
10.2.1.	Improve the Fuselage's Aerodynamics.....	79
10.2.2.	Miscellaneous Loads Analysis.....	80
10.2.3.	Dynamic Analysis.....	80
10.2.4.	Stress Analysis	80
10.2.5.	Final Statement.....	81
References.....		82
A.	Overdamped System ($\xi > 1$).....	85
B.	Underdamped System ($\xi < 1$).....	85
C.	Critically Damped System ($\xi = 1$).....	86
A.	Shear Force and Bending Moment.....	91
B.	Torsion Plot.....	92
A.	Abstract.....	93
B.	Disclaimer	93
C.	Architecture.....	93
C.1.	Colour codes.....	93
D.	System of Units.....	94
E.	Atmospheric Variables	94
F.	Flight Envelope	95
G.	Mass Discretization.....	95
H.	Specific Load Analysis	97
H.1.	Landing Gear Loads	97
H.1.1.	Landing Loads	97
H.1.2.	Ground Loads	98
H.2.	Wing Loads	100
H.3.	Horizontal-Tail Loads	100
H.4.	Vertical Tail Loads	101
H.5.	Fuselage Loads	101
I.	Plots	102
J.	Endnote.....	102

List of Figures

Figure 1 – Typical flight manoeuvring envelope.	5
Figure 2 - Limit wing loading conditions as defined by the aeroplane flight envelope [7].	6
Figure 3 - Stress response acting in the wing box as a function of the angle of attack [7].	7
Figure 4 - Gust envelope according to CS-25 [1].	8
Figure 5 - Combined Flight Envelope.	8
Figure 6 - Simplified landing gear analysis, 1 degree of freedom (left) and 2 degrees of freedom (right).	9
Figure 7 – Displacement versus time for the three possible damping conditions.	10
Figure 8 - One-point landing [1].	12
Figure 9 - Side load landing [1].	14
Figure 10 - Airbus A320 landing gear retraction after take-off.	15
Figure 11 - Reference axis in the wheel.	16
Figure 12 - Ground turning condition [1].	21
Figure 13 - Lockheed Hercules C-130 supported on jacks.	26
Figure 14 - Tied-down aeroplane.	26
Figure 15 - Chordwise fractions (downwards deflected aileron)	30
Figure 16 – Comparison between the similarity laws and experimental data [19].	34
Figure 17 - Wing lift sources scheme.	36
Figure 18 - Pitching velocity induced lift.	37
Figure 19 - Pitching velocity lift scheme.	37
Figure 20 - Positive load factor symmetric manoeuvre.	38
Figure 21 - Negative load factor symmetric manoeuvre.	38
Figure 22 - Spoiler scheme.	40
Figure 23 - Force equilibrium diagram in a coordinated turn.	43
Figure 24 - Swept back wing airflow [23].	44
Figure 25 - Swept forward wing airflow [23].	45
Figure 26 - Swept back wing influence on effective values of the normal airflow and spanwise chord.	45
Figure 27 - Sign convention [5].	49
Figure 28 – Horizontal tail geometric parameters [5].	49
Figure 29 - <i>Lockheed C-130H</i> Pressurization Chart [28].	58
Figure 30 - Hoop and longitudinal tension stresses [29].	59
Figure 31 - Different fuselage sections considered – side view.	59
Figure 32 - Different fuselage sections considered – top view.	59
Figure 33 - Schematic of the cross flow around a cylinder [31].	60
Figure 34 - Possible cross flow configurations around the cylinder [31].	60
Figure 35 - Experimental relation between the Drag coefficient and the Reynolds number in a cylinder under cross flow [31].	61
Figure 36 - Lockheed C-130H (Portuguese Air Force).	67
Figure 37 - Wing maximum shear force on the vertical plane – ($n_z = n_{zmax}$).	71
Figure 38 - Wing maximum bending moment on the vertical plane – ($n_z = n_{zmax}$).	71
Figure 39 - Wing maximum shear force on the vertical plane – static ground condition.	72
Figure 40 - Wing maximum bending moment on the vertical plane – static ground condition.	72
Figure 41 - Wing maximum shear force on the horizontal plane - ($n_z = n_{zmax}$).	72
Figure 42 - Wing maximum bending moment on the horizontal plane ($n_z = n_{zmax}$).	72
Figure 43 - Wing maximum pitching moment (torsion) – ($n_z = n_{zmax}$).	73
Figure 44 - Horizontal tail maximum shear force on the vertical plane.	73
Figure 45 - Horizontal tail maximum bending moment on the vertical plane.	73
Figure 46 - Horizontal tail maximum shear force on the horizontal plane.	74

Figure 47 - Horizontal tail maximum bending moment on the horizontal plane.	74
Figure 48 - Horizontal tail maximum torsion.	74
Figure 49 - Horizontal tail minimum shear force in the vertical plane.	74
Figure 50 - Horizontal tail minimum bending moment in the vertical plane.	75
Figure 51 - Horizontal tail minimum torsion.	75
Figure 52 - Vertical tail maximum shear force in the normal plane (spanwise distribution).	75
Figure 53 - Vertical tail maximum bending moment in the normal plane (spanwise distribution).	76
Figure 54 - Vertical tail maximum shear force in the vertical plane (spanwise distribution).	76
Figure 55 - Vertical tail maximum bending moment in the vertical plane (spanwise distribution).	76
Figure 56 - Vertical tail maximum torsion (spanwise distribution).	76
Figure 57 - Fuselage shear force in level flight (lengthwise distribution).	77
Figure 58 - Fuselage bending moment in level flight (lengthwise distribution).	78

List of Tables

Table 1 - Type of Loads.....	2
Table 2 - Vertical load factor as a function of the landing gear configuration [13].	17
Table 3 - CS-25 specifications for towing condition [1].....	25
Table 4 - CS-25 specification for jacking condition.....	25
Table 5 - Pressure distribution over a spoiler.	39
Table 6 - Sweep and sideslip angles influence on life generation.....	44
Table 7 - Manoeuvres do be investigated [1].	53
Table 8 - Summary scheme with all the conditions to be investigated.....	56
Table 9 - Different loads acting on each fuselage section.....	64
Table 10 - C-130H external dimensions [33].	68
Table 11 - C-130H Aerodynamic and Engines data [28].....	68
Table 12 - C-130H performance data [28].	68
Table 13 - C-130H main materials density [34].	69
Table 14 - Weight Estimates [28].....	69
Table 15 - Maximum Loads due to landing impact on each landing gear.....	70
Table 16 - Maximum ground loads acting on the landing gears.....	70

Acronyms

Acronym	Meaning	Acronym	Meaning
AOA	Angle of attack	MLW	Maximum Landing Weight
AC	Aerodynamic Centre	MTOW	Maximum Take-off Weight
CAS	Calibrated Airspeed	MTW	Maximum Taxi Weight
CG	Centre of Gravity	MZFW	Maximum Zero Fuel Weight
EAS	Equivalent Airspeed	NHAA	Negative high angle of attack
EO	Engine Out	NLAA	Negative low angle of attack
F1	Fuselage Section 1	PHAA	Positive high angle of attack
F2	Fuselage Section 2	PLAA	Positive low angle of attack
F3	Fuselage Section 3	SSL	Static Sea Level
F4	Fuselage Section 4	TAS	True Airspeed
F5	Fuselage Section 5	WWII	World War Two/Second World War
IAS	Indicated Airspeed		

Nomenclature

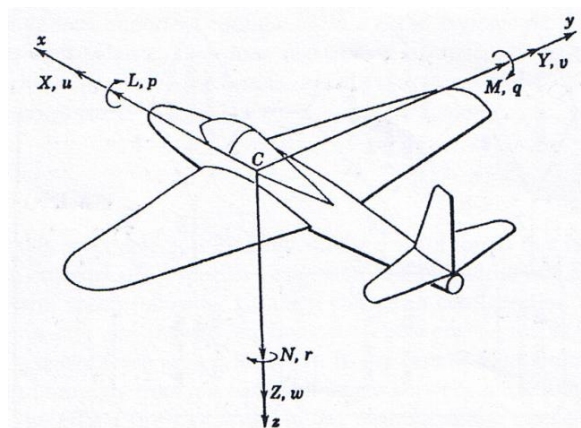
Variable	Meaning	Variable	Meaning
GREEK ALPHABET			
α	Angle of attack	μ_{MG_l}	Left main gear friction coefficient
α_t	Tail Angle of attack	μ_{MG_r}	Right main gear friction coefficient
α_w	Wing Angle of attack	μ_{NG}	Nose gear friction coefficient
β	Symmetrical of the aerofoil zero lift angle	ξ	Damping ratio
β_{comp}	Compressibility factor	ρ	Air density
β_{slip}	Sideslip angle	ρ_0	Reference air density
γ	Specific heats quotient	σ	Sidewash angle
Γ	Circulation	ϕ	Bank angle
δ_e	Elevator deflection	ϕ'	Perturbation velocity potential
δ_r	Rudder deflection	$\dot{\phi}$	Bank velocity
ε	Downwash	$\ddot{\phi}$	Bank acceleration
θ	Pitch angle	ψ	Yaw angle
$\dot{\theta}$	Pitch velocity	ψ_{str}	Stream function
$\ddot{\theta}$	Pitch acceleration	$\dot{\psi}$	Yaw velocity
Λ	Aspect ratio	$\ddot{\psi}$	Yaw acceleration
λ	Taper ratio	ω_n	Undamped natural frequency
μ	Dynamic viscosity		

Variable	Meaning	Variable	Meaning
LATIN ALPHABET			
a	Slope of the aeroplane normal force coefficient curve	p_{∞}	Free stream pressure
A	Horizontal distance from the CG of the aeroplane to the nose wheel	p_{in}	Inner fuselage pressure
b	Wingspan	p_{out}	Outer fuselage pressure
B	Horizontal distance from the CG of the aeroplane to the main wheel	q	Dynamic Pressure
BTL	Balancing tail load	r	Wheels rolling axis
c	Lifting surface local chord	R	Fuselage radius
\bar{c}	Lifting surface average chord	R^*	Constant of gases
C	Damping coefficient	Re	Reynolds number
C_d	2D drag coefficient	s	Laplace transform
C_D	2D lift coefficient	s_i	Specific entropy in state i
C_l	2D lift coefficient	S_{MG_l}	Left main gear side friction force
C_{l_i}	Lift distribution due to i variable	S_{MG_r}	Right gear side friction force
C_L	3D lift coefficient	S_{NG}	Nose gear side friction force
C_m	2D Pitching moment coefficient	S_{HT}	Horizontal tail reference area
C_M	3D Pitching moment coefficient	S_{VT}	Vertical tail reference area
c_p	Constant pressure specific pressure	S_W	Wing reference area
C_p	Pressure coefficient	t	time
c_v	Constant pressure specific volume	th	Fuselage skin thickness
D	Drag Force	t/c	Relative thickness
D_{MG_l}	Left main gear longitudinal friction force	T	Temperature
D_{MG_r}	Right main gear longitudinal friction force	T_0	Reference temperature
D_{NG}	Nose gear longitudinal friction force	T_{eng}	Total Engine Thrust
E	Vertical height of the CG of the aeroplane above the ground	v_i	Specific volume in state i
E_T	Vertical distance from aeroplane CG to engine thrust line	U_{∞}	Free stream velocity
f	Dynamic Response Factor [1]	V_A	Design manoeuvring speed
f_{HT}	Hoop tension	V_B	Design speed for maximum gust intensity
f_{LT}	Longitudinal tension	V_C	Design cruise speed

F_x	Forces along the x-axis	V_D	Design dive speed
F_z	Forces along the z-axis	V_e	Equivalent Airspeed
g	Acceleration of gravity	V_S	Stall speed with flaps retracted
G	Modulus of Elasticity	$V_{S.1g}$	Stall speed at 1g
		V_{S-1g}	Stall speed at -1g
H	Altitude	V_T	True airspeed
H_{max}	Maximum Altitude	V_{MG_l}	Left main gear vertical reaction
I_y	Aeroplane moment of inertia with respect to the y-axis	V_{MG_r}	Right main gear vertical reaction
J	Polar moment of inertia	V_{NG}	Nose gear vertical reaction
k	Spring constant	V_∞	Free stream velocity
K_g	Gust alleviation factor [1]	w	Wing average loading
L_t	Tail lift	W	Weight
m	Mass	W_T	Design Take-off Weight
M	Mach Number	x	Landing gear damper displacement
$M_{sp_hinge_ext}$	Extended spoiler hinge moment	x_{cg}	Lengthwise CG position
$M_{sp_hinge_hold}$	Retracted spoiler hinge moment	x_V	Horizontal distance from wing root leading edge to AC
M_t	Tail pitching moment	\dot{x}	Landing gear damper displacement derivative
n_x	Forward load factor	\ddot{x}	Landing gear damper displacement second derivative
n_y	Side load factor	x_t	Distance from CG to h-tail AC
n_z	Vertical load factor	z_d	Vertical distance from CG to tail drag vector
p	Air pressure	z_e	Vertical distance from CG to thrust line
P_i	Pressure	\emptyset	Fuselage diameter
p_0	Reference air pressure		

	x direction	y direction	z direction
SUBSCRIPTS			
Displacement	x	y	z
Angular velocity	p	q	r
Velocity	u	v	w
Force	X	Y	Z
Moment	l	m	n

Body Axis



1. Introduction

Although the load analysis is the responsibility of the Loads' Engineers group, a global knowledge of the loads is of outmost relevance for the Stresses' Engineers group as well. A comprehensive analysis of the loads acting on an aeroplane is thus of crucial relevance in the context of aeronautical design. The addition or removal of equipment involving changes in weight can affect the structural integrity, weight, balance, flight characteristics, reliability and aircraft performance.

The loading conditions are those found in flight, on the ground and on landing and take-off. Since it is impossible to investigate all the loading conditions that each aeroplane will have to withstand during its life cycle, it is common to select those that will be critical for each member of the structure. These conditions are usually found from investigation and experience and then included in updated versions of the applicable legislation. In Europe, the ruling legislation for large aeroplanes ($W > 5,700kg$) is the European Aviation Safety Agency Certification Specifications for Large Aeroplanes (CS-25) [1]. This document encompasses several differences relative to the North-American Federal Aviation Regulations for Large Aeroplanes (FAR 25) [2]. Despite this study focus is CS-25 requirements, whenever there are differences between these and FAR-25 the reader is reminded. Although these documents can also provide some guidance in the design and certification of military aeroplanes, the military authority is the Air Forces with jurisdiction on the aeroplane, meaning that it is their responsibility to establish the aeroplane's certification criteria rather than the civilian authorities.

There are four main load sources acting on an aeroplane – aerodynamic forces, inertia, ground reactions and thrust. The goal of the current work is it to determine its critical combinations. Not until all these load sources are determined shall the criticality of a particular aeroplane modification be known. Once all the loads have been determined, the challenge is to assess which critical load combinations are likely to happen to conclude about the maximum loads that may be taking place at each point.

The main purpose of this Master Thesis is to enable a much faster analysis of the maximum loads acting on each point of the aeroplane, so that modifications can be made at any point of the aeroplane without putting at risk its overall integrity, thus working in compliance with both the aeroplane's flight manual and the ruling legislation. Furthermore, the simplified approach developed throughout can be rather useful when performing finite element method analysis with commercial programs, enabling the validation of the computational output.

Table 1 [3] summarizes the different type of loads that act on an aeroplane, namely aerodynamics, inertia, take-off, landing, engine, ground and other loads.

Table 1 - Type of Loads.

Type of Loads		
Aerodynamic	Landing	Take-off
	Vertical load factor	Catapult
Manoeuvre	Wheel acceleration	Aborted
Gusts	Strut acceleration	
Controls	Wheel slide	Ground Loads
Buffet	One wheel	Ground Turning
	Brakes	Pivoting
		Towing
		Braking
		Yaw
		Steering
Inertial (Appendix A)	Engine	
	Thrust	
Acceleration	Torque	
Rotation	Gyroscopic effects	
Dynamics	Exhaust Pressure	Others
Vibration	Shock waves in exhaust	Pressurization
Flutter	Propeller stall	Bird Strike
	Break	Crash Landing

1.1. Legislation

In order for the user to make a proper use of the regulations and to clarify the meaning of several words used throughout CS-25 [1] and FAR-25 [2]; it is useful to provide the following definitions:

CAN – Can-requirements are conditional and indicate a possibility open to the user's choice.

MAY – May indicates a course of action that is permissible within the limit of the standards (a permission).

NEED (NOT) – Need (not) indicates that the restriction must (not) be applied.

SHALL – Shall is an absolute requirement which must be followed strictly so as to conform to the standards.

SHOULD – Should is nothing more than a recommendation. Alternative solutions having the same purposes and quality are acceptable.

Verification – Examination to check that an activity, product or service is in accordance with the specified requirements.

2. Weight, Balance and Performance

2.1. Aircraft Performance

2.1.1. Atmospheric Conditions

The maximum operating altitude is defined in each aeroplane's flight manual. The atmospheric properties are computed from the International Standard Atmosphere (ISA) [4] from the International Organization for Standardization.

The equations to compute the static temperature, static pressure and air density are presented below on equations (2.1)-(2.3). The subscript 0 denotes reference values, which, in accordance with ISA's atmosphere are $T_0 = 288.15K$ and $P_0 = 101,325 Pa$.

$$T = T_0 - 0.0065H \quad (2.1)$$

$$p = p_0 \left(1 - \frac{0.0065H}{T_0}\right)^{5.2561} \quad (2.2)$$

Using the state equation for perfect gases,

$$\rho = \frac{p}{RT} \quad (2.3)$$

2.1.2. Airspeed Measurement

This section is devoted to address the problem of understanding the differences between equivalent airspeed, indicated airspeed, calibrated airspeed and true airspeed by engineers without an aeronautical background [5].

The aeroplane lift is defined in terms of a nondimensional lift coefficient (C_L), dynamic pressure (q), which is a function of the true airspeed (V_T) and wing reference area (S_w), as follows:

$$L = C_L q S_w \quad (2.4)$$

Where,

$$q = \frac{1}{2} \rho V_T^2 \quad (2.5)$$

The **Equivalent Airspeed (EAS)** (V_e) is an airspeed at sea level ($\rho_0 = 1.225kg/m^3$) that would result in the same dynamic pressure experienced by the aeroplane flying at altitude at its true airspeed.

$$q = \frac{1}{2} \rho_0 V_e^2 \quad (2.6)$$

A constant equivalent airspeed will give the same lift at all altitudes for the same gross weight and load factor.

The **Indicated Airspeed (IAS)** is the reading of the airspeed indicator. This airspeed is uncorrected for instrument and installation errors, but includes the sea level standard adiabatic compressible flow correction. It differs from calibrated airspeed only in terms of instrument static source error, which may be a function of the aeroplane's flight altitude, Mach number and flap position. Aeroplane manufacturers usually plot the airspeed correction as a function of the indicated airspeed and flap position.

The **Calibrated Airspeed (CAS)** is the indicated airspeed corrected for installation and instrument errors.

The **True Airspeed (TAS)** is the speed at which the aeroplane moves relative to the air mass surrounding it. It can be obtained from knowledge of the equivalent airspeed, as follows:

$$V_T = \frac{V_e}{\sqrt{\frac{\rho}{\rho_0}}} \quad (2.7)$$

As will be shown in the upcoming sections the flight manoeuvring and gust envelopes are drawn as a function of the equivalent airspeed. From now onwards wherever the airspeed is not specified it refers to the equivalent airspeed.

2.2. Load Requirements

When performing a structural load analysis, one of the most important causes of concern is the so-called flight envelope. The aeroplane's flight envelope is the sum of the flight manoeuvring envelope and the gust envelope. In order to clearly understand the combined effect of these two contributions the flight envelope is plotted. This plot enables the structural loads engineer – as well as specialists in other fields of expertise, such as the stresses engineer – to have a much better understanding about the effects that the loads have on the aeroplane's structure.

The 'symmetric' manoeuvre and gust envelopes form the basis of the in-flight stressing cases for a given aircraft design. The manoeuvre envelope gives the range of speeds and pilot induced 'g' loadings which the aircraft will have to withstand [5]. The aircraft is considered in 'symmetric' flight, which means, no side-slipping, rolling or yawing. Just pitching and balanced turning manoeuvres are considered. The gust envelope gives the range of 'g' loadings generated by gusts at various speeds which the aircraft must also withstand. These symmetric flight load cases dictate most of the design of the aircraft structure. Combining these two envelopes yields the aircraft flight envelope. Notice that both the manoeuvring and gust envelopes are calculated with the aircraft at its projected maximum all-up-weight. The exception would be an aerobatic aircraft where both the maximum acrobatic weight and maximum take-off weight would have to be accounted for. Notice that this last consideration will not be addressed since the study of aerobatics aeroplanes is out of the scope of the present work.

In this analysis, the critical design points, which consist of a number of extreme effects, will be determined looking at the aeroplane's flight envelope. A comprehensive way of designing the flight envelope according to the operational limits defined in the aeroplane's flight manual in accordance with the legislation in use will thus be calculated.

2.2.1. Manoeuvre Envelope

According to both CS-25 [1] and FAR-25 [2], the strength requirements must be met at each combination of airspeed and load factor on and within the boundaries of the representative manoeuvring envelope. This envelope, also known as V-n diagram may also be used to determine the aeroplane's structural operating limits. The stall speed in level flight is given by equation (2.8).

$$V_{S1g} = \sqrt{\frac{W}{\frac{1}{2}\rho S_w C_{L_{max}}}} \quad (2.8)$$

At other load factor values, the stall speed is given by $V_S = V_{S1g}\sqrt{n}$. This will give the positive stall curve of the flight envelope. The negative design manoeuvring speed is:

$$V_{S-1g} = \sqrt{\frac{-W}{\frac{1}{2}\rho S_w C_{L_{min}}}} \quad (2.9)$$

At other load factor values, the stall speed is given by $V_S = V_{S-1g}\sqrt{-n}$, where n vary between zero and the minimum admissible load factor. This will give the negative stall curve.

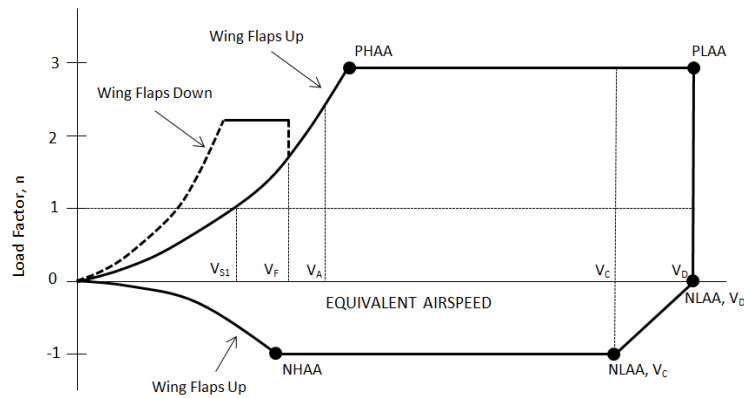


Figure 1 – Typical flight manoeuvring envelope.

The maximum and minimum load factors are determined in accordance with CS-25.337, as follows:

$$n_{max} = 2.1 + \left(\frac{24000}{MTOW+10000} \right) \cap 2.5 \leq n_{max} \leq 3.8 \quad (2.10)$$

$$\begin{cases} n_{min} = -1.0; & V < V_C \\ n_{min} \text{ varies linearly}; & V_C < V < V_D \end{cases} \quad (2.11)$$

Notice that equation (2.10) requires the input of the MTOW in lb. Referring to Figure 1, five basic conditions can be considered relevant for the analysis of the limit load conditions. Accordingly [6]:

- **Positive High Angle of Attack (PHAA)** – It corresponds to the positive stall angle and is the minimum velocity at which the maximum load factor can be achieved. To account for flow irregularities and a possible stall at higher angle – which encompasses would encompass higher loads – it is commonly used $1.25 C_{Lmax}$ instead of C_{Lmax} ;
- **Positive Low Angle of Attack (PLAA)** – It corresponds to the positive angle of attack to generate the maximum lift at dive speed;
- **Negative High Angle of Attack (NHAA)** – It corresponds to the negative stall angle and is the minimum velocity at which the minimum load factor can be achieved;
- **Negative Low Angle of Attack (NLAA, V_C)** – It corresponds to the minimum load factor at design cruise speed;
- **Negative Low Angle of Attack (NLAA, V_D)** – It corresponds to zero load factor at design dive speed.

The reader should note that the negative low angle of attack (NLAA) is usually considered only one and equal to the minimum load factor at dive speed, which would consist of a more conservative estimate without having to perform the load estimations for the negative low angles of attack at cruise and dive speed, to determine which is the most critical.

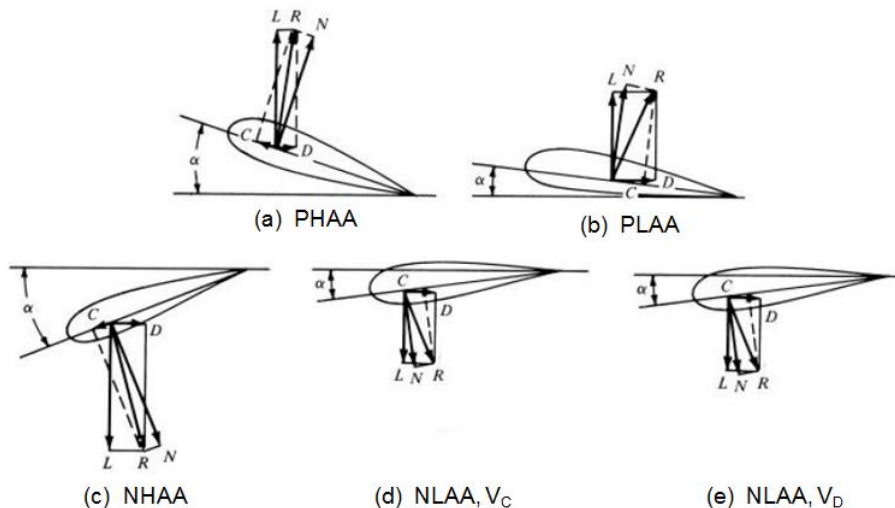


Figure 2 - Limit wing loading conditions as defined by the aeroplane flight envelope [7].

In terms of the stresses acting on the wing on each of these conditions, it is noticeable that the PHAA will reflect the maximum compression in the upper flange of the forward longeron, which means the maximum tension will be acting on the lower flange of the rear longeron. For the same reasons, it can be stated that the NHAA will impose the highest compression in the forward longeron lower flange and the highest tension in the rear longeron upper flange. In the PLAA condition, the centre of pressure will be at its rear most position, which means that it will be critical for compression of the rear longeron upper flange and for tension in the forward longeron lower flange. With an analogous reasoning it can be stated that the NLAA will cause maximum compression in the lower flange rear longeron and in the upper flange forward longeron.

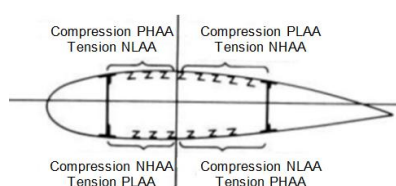


Figure 3 - Stress response acting in the wing box as a function of the angle of attack [7].

2.2.2. Gust Envelope

The gust envelope, commonly known as V-g diagram is determined in a similar pattern to the manoeuvring envelope, except that the boundaries are determined by the gust load factor at cruise airspeed (V_C) and dive airspeed (V_D). The equivalent gust velocity is defined in CS-25 [1] and FAR-25 [2] to be a function of the aeroplane's equivalent airspeed and operating altitude. The gust load factor may be computed as follows:

$$n = 1 \pm \frac{\frac{1}{2}\rho_0 V a K_g U_{de}}{Mg/S} \quad (2.12)$$

Where K_g is the gust alleviation factor and is defined as:

$$K_g = \frac{0.88 \frac{2w}{\rho c a g}}{5.3 + \frac{2w}{\rho c a g}} \quad (2.13)$$

When performing a discrete gust analysis – as the one developed herein – it is assumed that the aeroplane is subjected to symmetrical vertical and lateral gusts in level flight.

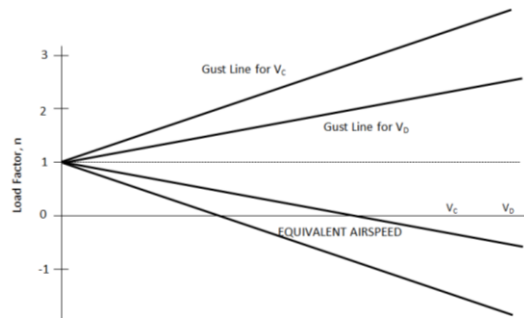


Figure 4 - Gust envelope according to CS-25 [1].

2.2.3. Combined Flight Envelope

Once the manoeuvring and gust envelopes have been determined, the combined flight envelope [8] should be drawn, which is shown in Figure 5. This is the most relevant plot, since it does establish the true limit loads that the aeroplane's structure may experience in the advent of being subject to gust loads coming from any direction and on any flight condition.

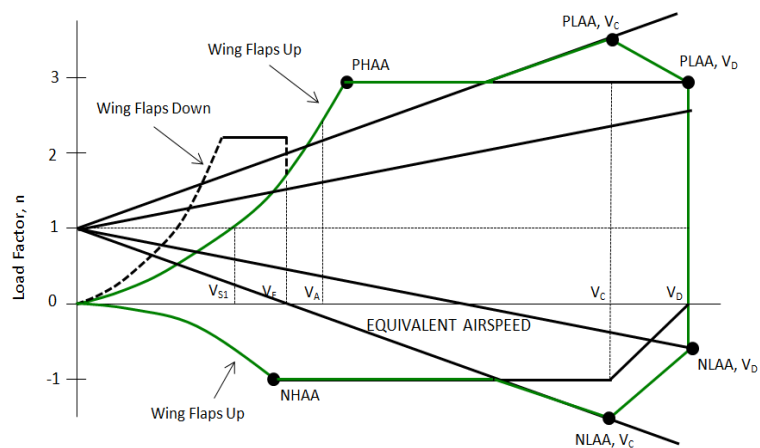


Figure 5 - Combined Flight Envelope.

Each of these limit loading conditions is critical for almost all the aircraft's structure. In the stress analysis of a conventional wing, it is necessary to investigate each of the four main conditions (PHAA, PLAA, NHAA and NLAA). Each stringer and longeron is thus designed for the maximum tension or compression of each of these conditions. It is usually common place to neglect other loading conditions since the structure is likely to withstand all intermediate loadings provided that it bears the limit load conditions shown on Figure 5.

3. Landing Gear Loads

All the below considerations apply for conventional landing gears' arrangements of main and nose gears, or main and tail gears.

3.1. Landing Loads Analysis

3.1.1. Landing Loads Conditions and Assumptions

CS 25.473 [1] defines the conditions under which the aeroplane is assumed to contact the ground:

- 1) "In the attitudes defined in CS 25.479 and 25.481
- 2) With a limit descent velocity of 3.05m/s (10 ft/s) at the design landing weight (maximum weight for landing conditions at maximum descent velocity); and
- 3) With a limit descent velocity of 1.83 m/s (6 ft/s) at the design take-off weight (the maximum weight for landing conditions at a reduced descent velocity)
- 4) The prescribed descent velocities may be modified if it is shown that the aeroplane has design features that make it possible to develop these velocities."

According to CS-25, in order to compute the landing loads acting on the landing gears, the aeroplane lift can be assumed null. In order to know the force acting on the landing gear on the various landing conditions to be studied – one-point landing, two-points landing, side load landing and three-points landing.

At each landing gear a system with one or two degrees of freedom can approximate the physics of the problem. Although the system is better approximated by the system with two springs and two dampers at each landing gear, a system with a single degree of freedom per landing gear will be studied next [9][10][11]. Nevertheless, the results derived are extendable to the two-degrees of freedom analysis.

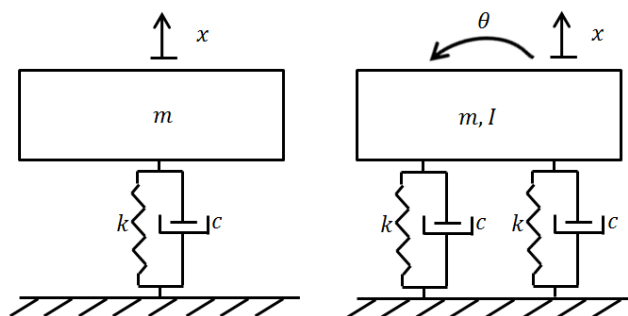


Figure 6 - Simplified landing gear analysis, 1 degree of freedom (left) and 2 degrees of freedom (right).

The viscous damping force can be considered proportional to the first power of the velocity across the damper – always opposes motion – so that the damping force is a linear

continuous function of the velocity. The spring force is proportional to the displacement from the equilibrium position. The equation of motion during the landing is as follows:

$$m\ddot{x} + c\dot{x} + kx = 0 \quad (3.1)$$

The goal is to determine the maximum load to which each landing gear is subject when it is in contact with the ground. Equation (3.1) is a second order differential equation, which can be solved using Laplace transform¹ by assuming a solution of the form:

$$x = X_1 e^{s_1 t} + X_2 e^{s_2 t} \quad (3.2)$$

$$(ms^2 + cs + k)Xe^{st} = 0 \quad (3.3)$$

Excluding the trivial solution – which would correspond to no motion – the roots and respective solution of the equation (3.3) will be:

$$s_{1,2} = -\frac{c}{2m} \pm \frac{\sqrt{c^2 - 4mk}}{2m} \quad (3.4)$$

Three different situations may occur:

- The damping force is dominant and both roots are real numbers ($c^2 > 4mk$) – the system is said to be overdamped;
- Inertial and elastic forces are dominant and the roots are complex conjugate ($c^2 < 4mk$) – the system is said to be underdamped;
- The square root is null and the roots are equal and real – the system is said to be critically damped.

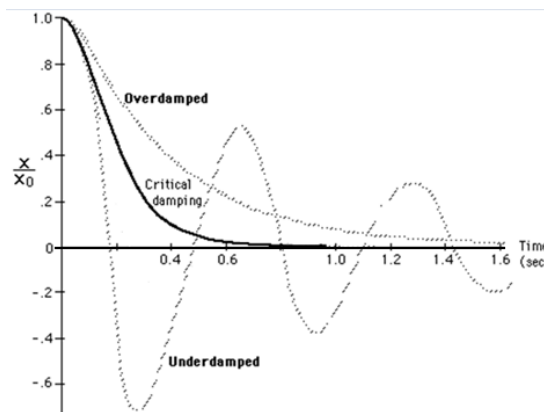


Figure 7 – Displacement versus time for the three possible damping conditions.

From the observations of the last paragraph, it becomes apparent the relevance of the critical damping coefficient, which is defined by:

$$c_c^2 = 4mk \quad (3.5)$$

The damping coefficient (ξ) and the system's undamped natural frequency (ω_n), are defined as follows:

¹ The Laplace transform (1785) (named after Pierre-Simon Laplace), is an integral transform. It is a linear operator of a function $f(t)$ with a real argument that transforms it to a function $F(s)$ with a complex argument s .

$$\xi = \frac{c}{2\sqrt{mk}} \quad (3.6)$$

$$\omega_n = \sqrt{\frac{k}{m}} \quad (3.7)$$

Introducing the initial conditions, which are the same regardless the system's damping coefficient:

$$t = 0; \begin{cases} x(t) = x(0) \\ \dot{x}(t) = \dot{x}(0) \end{cases} \quad (3.8)$$

The initial condition to the displacement refers to the initial spring-damper position, which does not to coincide with its deflection in static ground condition – it will obviously be more extended in the air than in the static ground condition. The velocity is prescribed on the legislation (CS-25) and has already been presented.

3.1.1.1. Overdamped System ($\xi > 1$)

In the case when the damping force is dominant, the roots of the equilibrium equation will be:

$$s_{1,2} = -\omega_n \xi \pm \sqrt{\xi^2 - 1} \quad (3.9)$$

It is shown² that the solution is given by:

$$x(t) = e^{-\xi \omega_n t} \left[x(0) \cosh(\omega_n \sqrt{\xi^2 - 1} t) + \frac{\dot{x}(0) + \xi \omega_n x(0)}{\omega_n \sqrt{\xi^2 - 1}} \sinh(\omega_n \sqrt{\xi^2 - 1} t) \right] \quad (3.10)$$

3.1.1.2. Underdamped System ($\xi < 1$)

If the inertial and spring forces proof dominant over the damping force, the roots of the equilibrium equations will be.

$$s_{1,2} = -\omega_n \xi \pm i \omega_n \sqrt{1 - \xi^2} \quad (3.11)$$

It is shown² that:

$$x(t) = e^{-\xi \omega_n t} \left[x(0) \cos(\omega_n \sqrt{1 - \xi^2} t) + \frac{\dot{x}(0) + \xi \omega_n x(0)}{\omega_n \sqrt{1 - \xi^2}} \sin(\omega_n \sqrt{1 - \xi^2} t) \right] \quad (3.12)$$

3.1.1.3. Critically Damped System ($\xi = 1$)

In this case, the roots of the equilibrium equation will be:

$$s_{1,2} = -\frac{c}{2m} \quad (3.13)$$

In this case, it can be proved² that:

$$x(t) = e^{-\omega_n t} [x(0)(1 + \omega_n t) + \dot{x}(0)t] \quad (3.14)$$

² See appendix B

3.1.2. Landing Speed Calculations

According to CS 25.473 [1], landing loads must be calculated for a limit descent velocity of 3.05 m/s at the design landing weight (MLW) as well as for a limit descent velocity of 1.83 m/s at the design take-off weight (MTOW).

3.1.2.1. Effect of Hot Day on Landing Speeds

To assess the influence that a hot day may have on the landing speeds [5] departing from a standard day 'sd' and from the equation that relates lift to air density and airspeed is:

$$W = 0.5C_{L_s}(\rho V_S^2)_{sd}S_w \quad (3.15)$$

Where the subscript 's' denotes stall conditions. For a hot day 'hd', one may arrive at a similar equation relating the same variables:

$$W = 0.5C_{L_s}(\rho V_S^2)_{hd}S_w \quad (3.16)$$

Thus:

$$(\rho V_S^2)_{sd} = (\rho V_S^2)_{hd} \Rightarrow V_{S_{hd}} = \sqrt{(\rho_{sd}/\rho_{hd})}V_{S_{sd}} \quad (3.17)$$

At a constant altitude, and from the state equation, the relationship between air density and temperature may be stated as:

$$(\rho T)_{hd} = (\rho T)_{sd} \quad (3.18)$$

According to CS-25 [1], the landing conditions to be evaluated are the one-point landing, two-points landing, side load landing and three-points landing.

3.1.3. One-point Landing

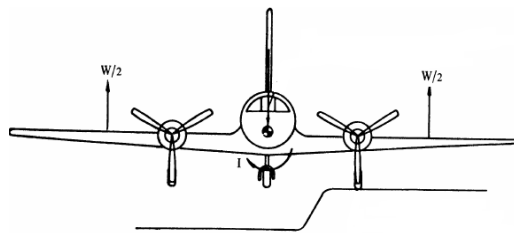


Figure 8 - One-point landing [1].

On a one-point landing condition, the aeroplane is assumed to be levelled and to contact the ground on one main landing gear, in accordance with CS 25.483 [1]. In this attitude, the ground reactions must be the same as those obtained on that side per CS 25.479(d)(1) [1], which states that the landing gear and its directly affected structure must be designed for the maximum vertical ground reaction combined with an aft acting drag component of not less than 25% of this maximum vertical ground reaction.

3.1.4. Two-points landing

A two-point landing is, by definition a type of landing where the aeroplane's nose is held from contact with the ground, until a complete absorption of the energy of descent is accomplished.

3.1.4.1. Two-point Level Landing Condition

The forces and moments acting on the aeroplane during a two-point level landing may be computed as follows [5] (assuming that Lift equals Weight). In the expressions presented below (F_z) is the vertical force, (W) is the weight, (n_z) is the vertical load factor and (V_{MG_r}) and (V_{MG_l}) are the vertical force acting on the main right and left landing gears, respectively.

$$\sum F_z = 0 \Rightarrow V_{MG_r} + V_{MG_l} = n_z W - L \quad (3.19)$$

$$\Leftrightarrow n_z W - L = V_{MG_r} + V_{MG_l} \Leftrightarrow (n_z - 1)W = V_{MG_r} + V_{MG_l} \quad (3.20)$$

$$\Leftrightarrow \Delta n_z = (V_{MG_r} + V_{MG_l})/W \quad (3.21)$$

Adopting a similar approach for the force equilibrium in the horizontal direction (F_x) and assuming that the thrust (T_{eng}) equals the total drag (D):

$$\sum F_x = 0 \Rightarrow D_{MG_r} + D_{MG_l} = n_x W - D + T_{eng} \quad (3.22)$$

$$\Leftrightarrow n_x = (D_{MG_r} + D_{MG_l} + D - T_{eng})/W \quad (3.23)$$

$$\Leftrightarrow n_x = (D_{MG_r} + D_{MG_l})/W \quad (3.24)$$

Finally, for the pitching moment equilibrium, and introducing the vertical distance from the aeroplane CG to the ground plane (E), the vertical distance from aeroplane CG to engine thrust line (E_T), the wheels rolling axis (r) and the pitching acceleration ($\ddot{\theta}$), the following equilibrium equations:

$$\sum M_{cg} = 0 \Rightarrow I_y \ddot{\theta} = B(V_{MG_r} + V_{MG_l}) + E_{ax}(D_{MG_r} + D_{MG_l}) - E_T T_{eng} \quad (3.25)$$

$$\Leftrightarrow \ddot{\theta} = \frac{[B(V_{MG_r} + V_{MG_l}) + E_{ax}(D_{MG_r} + D_{MG_l}) - E_T T_{eng}]}{I_y} \quad (3.26)$$

$$E_{ax} = E - r \quad (3.27)$$

Note that if the engine thrust term is neglected, the resulting pitching acceleration is conservative.

3.1.4.2. Side Load Landing

For the side load condition (CS 25.485), the aeroplane is assumed to be in level attitude with only the main wheels in contact with the runway. Side loads of 80% of the vertical

reaction (on one side) acting inward and 60% of the vertical reaction (on the other side) acting outward must be combined with one-half the maximum vertical gust obtained in the level landing conditions. The ground reaction in the nose wheel is assumed zero. These loads are assumed to be applied at the ground contact point and to be resisted by the inertia of the aeroplane. According to the same source, the drag loads may be neglected.

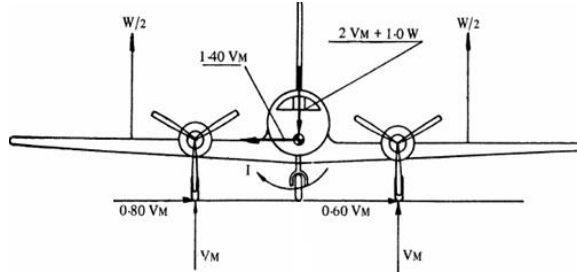


Figure 9 - Side load landing [1].

3.1.5. Three-points landing

The three point landing conditions are usually critical for the nose gear and its support structure, and the main gear landing loads are critical for the two-point landing conditions [5].

3.1.5.1. Three-Point Level Landing Analysis

According to CS 25.479 [1], in the level attitude, the aeroplane is assumed to contact the ground at forward velocity components:

$$V_{L_1} \leq V_{landing} \leq 1.25V_{L_2} \quad (3.28)$$

Where V_{L_1} is equal to V_{S_0} (TAS) at the appropriate landing weight and in SSL conditions. V_{L_2} is equal to V_{S_0} (TAS) at the appropriate landing weight and altitudes in a hot day temperature of 22.8°C (41°F) above standard. The effects of increased contact speed must be investigated if approval of downwind landing exceeding 19km/h (10 knots) is requested.

The equilibrium equations may be found in a similar fashion with the Two-Point Landing Analysis:

$$\sum F_z = 0 \Rightarrow V_{MG_r} + V_{MG_l} + V_{NG} = n_z W - L \quad (3.29)$$

$$\Leftrightarrow n_z = 1 + (V_{MG_r} + V_{MG_l} + V_{NG})/W \quad (3.30)$$

Adopting a similar approach for the force equilibrium in the horizontal direction and assuming that the thrust equals the total drag:

$$\sum F_x = 0 \Rightarrow D_{MG_r} + D_{MG_l} + D_{NG} = n_x W - D + T_{eng} \quad (3.31)$$

$$\Leftrightarrow n_x = (D_{MG_r} + D_{MG_l} + D_{NG} + D - T_{eng})/W \quad (3.32)$$

Finally, for the pitching moment equilibrium:

$$\sum M_{cg} = 0 \quad (3.33)$$

$$\Rightarrow V_{NG}C - D_{NG}E_{NG\alpha} = B(V_{MG_r} + V_{MG_l}) + E_{MG\alpha}(D_{MG_r} + D_{MG_l}) - E_T T_{eng} \quad (3.34)$$

where,

$$E_{NG\alpha} = E - r_{NG} \quad (3.35)$$

$$E_{MG\alpha} = E - r_{MG} \quad (3.36)$$

The variables (r_{MG}) and (r_{NG}) represent main gear wheels rolling axis and nose gear wheels rolling axis, respectively.

3.2. Take-off Landing Gear Analysis

A major concern when talking about landing gear loads arises when the landing gear is retracted. As it is known, in order to minimize noise propagation and aerodynamic forces, most of today's aircrafts retract their landing gears immediately after take-off (Figure 9). Although the nose landing gears are usually retracted without changing its wheel direction, the main gears are commonly retracted inwards, which means that there will be a change in the wheel direction which can generate significant loads on the landing gear and its attaching structure. Indeed, if the wheels are still rotating at high angular speeds this can be a critical design condition for this structure.



Figure 10 - Airbus A320 landing gear retraction after take-off.

In order to overcome this problem, most of today's aeroplanes have brakes on their wheels that act as soon as the planes leave the ground so that when the landing gears are retracted there are not significant inertial forces acting on the structure, which means the gyroscopic moments acting are important. Despite this fact, an approach to compute this moment of force will be presented next.

If the landing gear retraction is considered a rigid body motion about an axis, the sum of moments about this point will be given by [12]:

$$\Sigma M_0 = (\dot{H}_0)_{xyz} + \Omega \times H_0 \quad (3.37)$$

The angular momentum will be given by [12]:

$$\begin{cases} H_x = I_x \omega_x - I_{xy} \omega_y - I_{xz} \omega_z \\ H_y = -I_{yx} \omega_x + I_y \omega_y - I_{yz} \omega_z \\ H_z = -I_{zx} \omega_x - I_{zy} \omega_y + I_z \omega_z \end{cases} \quad (3.38)$$

The reference frame used is the one shown in Figure 10. Notice that it is assumed that the landing gear retraction angular velocity vector is acting at the wheels' geometric centre. In fact only the change in direction of the rotating wheel will actually contribute to the force moment on the landing gear attaching structure, which means this is a plausible assumption.

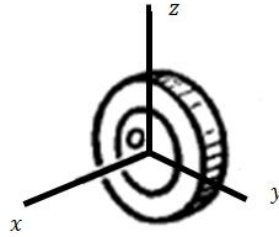


Figure 11 - Reference axis in the wheel.

Finally, and substituting the results shown on equation (3.38) in equation (3.37), and recognizing that $(\Omega = \omega_y)$, and recalling that the cross products of inertia will be zero due to symmetry, the expression to compute the moment will take the following form:

$$\Sigma M_0 = 0 + \omega_y \mathbf{j} \times (I_x \omega_x \mathbf{i} + I_y \omega_y \mathbf{j}) \quad (3.39)$$

$$\Sigma M_0 = -\omega_y I_x \omega_x \mathbf{k} \quad (3.40)$$

3.3. Ground Load Analysis

The ground-handling loads discussed in this chapter are a number of conditions involving ground manoeuvres, braking during landing and take-off, and special conditions such as towing, jacking and tie-down [5]. For static analysis conditions, airloads are assumed zero, and only inertia loads are taken into account [1]. Ground handling conditions are usually defined as taxi conditions, braked-roll conditions, refused take-off conditions, turning conditions, towing and jacking conditions and the tie-down problem.

3.3.1. Static Load Conditions

Static load conditions are defined at a vertical load factor equal to unity with the aeroplane in a three-point static attitude [5]. The main gear loads are:

$$(V_{MGr})_s = W \left(\frac{A}{2C} + \frac{BL_{cg}}{T} \right) \quad (3.41)$$

$$(V_{MGl})_s = W \left(\frac{A}{2C} - \frac{BL_{cg}}{T} \right) \quad (3.42)$$

$$(D_{MGr})_s = (D_{MGl})_s = (S_{MGr})_s = (S_{MGl})_s = 0 \quad (3.43)$$

The main gear loads are:

$$(V_{NG})_s = \frac{WB}{C} \quad (3.44)$$

$$(D_{NG})_s = (S_{NG})_s = 0 \quad (3.45)$$

The subscript ‘s’ in equations (3.41)-(3.45) refers to the static condition. Notice that this static load condition is a particularly relevant feature in the load analysis domain, since many of the yet to be derived equations for non-static conditions will be a function of the respective static load condition.

3.3.2. Taxi, take-off and Landing Roll Conditions

According to CS 25.491 [1], “Within the range of appropriate ground speeds and approved weights, the aeroplane structure and landing gear are assumed to be subjected to loads not less than those obtained when the aircraft is operating over the roughest ground that may reasonably be expected in normal operation.”.

3.3.2.1. Taxi Design Load Factors and Gear Loads

The design load factors used for gear load calculations vary with aeroplane configuration and time period in which the aircraft structure was designed. The load factors as used for rigid loads analysis for various aircrafts are summarized in the Table 2 [13].

Table 2 - Vertical load factor as a function of the landing gear configuration [13].

n_z	Main gear configuration
2.0	Single axle gear
1.7	Multiple axle gears

The regulations do not specifically require a given load factor to be used for design. These numbers feature in AC 25.491-1 [13]. In this Advisory Circular, it is shown as computers became more powerful and dynamic analysis methods became more sophisticated that dynamic effects sometimes resulted in loads that were actually greater than those predicted by

the static criterion. Such a study is out of the scope of the present research, but it must be kept in mind.

The gear reactions will thus be the product of the appropriate design load factor by the static ground reactions at each wheel for the maximum design ramp weight, assuming no wing lift.

3.3.3. Braked Roll Condition

3.3.3.1. Three-Point Braked-Roll

The aeroplane is assumed to be in a level attitude and its loads distributed between the main gears and the nose gear. In accordance with CS 25.493(b)(1) [1] zero pitch acceleration is assumed and zero lift is considered.

The equations for determining the gear loads for braking under these circumstances may be derived from the remaining forces acting on the aeroplane.

The main gear loads will be [5]:

$$V_{MGr} = n_z W \left(0.5 + \frac{BL_{cg}}{T} \right) - 0.50V_{NG} \quad (3.46)$$

$$V_{MGl} = n_z W - V_{NG} - V_{MGr} \quad (3.47)$$

$$D_{MGr} = \mu_{MG} V_{MGr} \quad (3.48)$$

$$D_{MGl} = \mu_{MG} V_{MGl} \quad (3.49)$$

$$S_{MGr} = -0.5S_{NG} \quad (3.50)$$

$$S_{MGl} = 0.5S_{NG} \quad (3.51)$$

Whereas, the nose gear loads will be:

$$V_{NG} = \frac{n_z W (B + E \mu_{MG})}{C + E \mu_{MG}} \quad (3.52)$$

Assuming no nose gear brakes,

$$D_{NG} = 0 \quad (3.53)$$

$$S_{NG} = \frac{[D_{MGl}(BL_{cg} + 0.50T) + D_{MGr}(BL_{cg} - 0.50T)]}{C} \quad (3.54)$$

The friction coefficient is equal to 0.8 or as limited by brake torque and the vertical load factor varies from 1.0 at the design taxi weight and 1.2 at design landing weight, in accordance with CS 25.493 [1].

3.3.4. Two-Point Braked-Roll

According to CS 25.493 (b)(2) [1], the aeroplane is assumed to be in a level attitude with the nose gear off the ground with the resulting pitching moment reacted by angular acceleration. No wing lift may be considered [1]. The equations for determining gear loads for braking conditions in the two-point attitude may be derived from the forces acting on the aeroplane [5].

Accordingly, the nose gear loads will be:

$$V_{NG} = D_{NG} = S_{NG} = 0 \quad (3.55)$$

The main gear loads will be:

$$V_{MGr} = n_z W \left(0.50 + \frac{BL_{cg}}{T} \right) \quad (3.56)$$

$$V_{MGl} = n_z W - V_{MGr} \quad (3.57)$$

$$S_{MGr} = S_{MGl} = 0 \quad (3.58)$$

$$D_{MGr} = \mu_{MG} V_{MGr} \quad (3.59)$$

$$D_{MGl} = \mu_{MG} V_{MGl} \quad (3.60)$$

In accordance with CS 25.493 [1], the friction coefficient will be equal to 0.8, while the load factor will vary from 1.0 at the design ramp weight until 1.2 at the design landing weight. The pitching acceleration will thus be given by the following expression:

$$\ddot{\theta} = - \frac{[Bn_z + E(D_{MGr} + D_{MGl})]}{I_y} \quad (3.61)$$

3.3.5. Nose Gear Loads Due to Sudden Application of Brakes

An aeroplane equipped with a nose gear must be designed to withstand the loads arising from the dynamic pitching motion of the aeroplane due to sudden application of maximum brake force. According to CS 25.493 [1]:

$$V_N = \frac{W_T}{A+B} \left(B + \frac{f\mu A E}{A+B+\mu_f E} \right) \quad (3.62)$$

Where V_N is the nose vertical reaction, W_T is the design take-off weight, A is the Horizontal distance from the CG of the aeroplane to the nose wheel, B is the horizontal distance from the CG of the aeroplane to the main wheel, E is the vertical height of the CG of the aeroplane above the ground, μ_f is the friction coefficient (0.8 according to CS 25.493 [1]) and f is the dynamic response factor (2.0 according to CS 25.493 [1])

3.3.5.1. Reversed Braking

In order to assess this condition, the aeroplane must be in a three-point static ground attitude at unitary load factor, ($n_z = 1$). For aeroplanes with nose wheels, the pitching moment is balanced by rotational inertia.

According to CS 25.507 [1], gear loads due to reversed braking are calculated assuming a drag load applied in the forward direction equal to 0.55 of the vertical load at each wheel with brakes. This drag load need not exceed the load developed by 1.2 times the nominal maximum static brake torque. Therefore, the nose gear loads will be:

$$V_{NG} = n_z V_{NGs} \quad (3.63)$$

$$D_{NG} = S_{NG} = 0 \quad (3.64)$$

The main gear loads are:

$$V_{MGr} = n_z V_{MGr s} \quad (3.65)$$

$$V_{MGl} = n_z V_{MGl s} \quad (3.66)$$

$$D_{MGr} = -\mu_{MG} V_{MGr} \quad (3.67)$$

$$D_{MGl} = -\mu_{MG} V_{MGl} \quad (3.68)$$

$$S_{MGr} = S_{MGl} = 0 \quad (3.69)$$

The pitching acceleration about aeroplane centre of gravity:

$$\ddot{\theta} = -\frac{E(D_{MGr} + D_{MGl})}{I_y} \quad (3.70)$$

3.3.6. Turning condition

The ground-handling conditions involving turning situations may come from:

- A steady turn executed by nose gear steering or differential thrust
- Nose wheel yaw;
- Unsymmetrical braking
- Nose gear steering
- Pivoting about one side of the aeroplane

3.3.6.1. Ground Turning

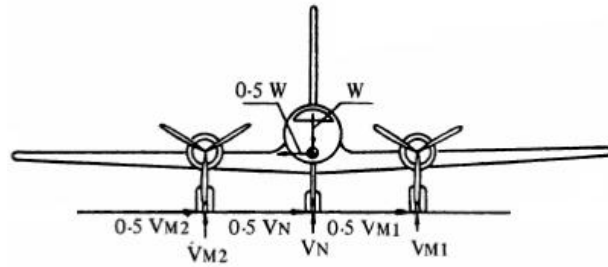


Figure 12 - Ground turning condition [1].

Under this condition, and according to CS 25.495 [1], the aeroplane is assumed to execute a steady state turn by nose gear steering, or by the application of sufficiently differential power, so that the limit load factors applied at the centre of gravity are 1.0 vertically (n_z) and 0.5 laterally (n_y). Additionally, the side ground reaction must be 0.5 of the vertical reaction.

The static load equations for the nose gear loads are:

$$V_{NG} = n_z(V_{NG})_S \quad (3.71)$$

$$D_{NG} = 0 \quad (3.72)$$

$$S_{NG} = -n_y(V_{NG})_S \quad (3.73)$$

The static load equations for the main gear loads are:

$$V_{MGr} = n_z(V_{MGr})_S + n_y WE/T^* \quad (3.74)$$

$$V_{MGl} = n_z(V_{MGl})_S - n_y WE/T^* \quad (3.75)$$

$$D_{MGr} = D_{MGl} = 0 \quad (3.76)$$

$$S_{MGr} = -0.50V_{MGr}^* \quad (3.77)$$

$$S_{MGl} = 0.50V_{MGl}^* \quad (3.78)$$

The subscript 's' refers to the static condition. Notice that the marked with a * equations apply for a left-hand ground turn. For a right-hand ground turn the signs would be reversed in the second term of the mentioned.

3.3.6.2. Nose Wheel Yaw and Steering

Nose wheel yaw is caused by a ground turn such that the nose gear wheels skid, thus producing side loads. According to CS 25.499 [1], a vertical load factor of 1.0 at the aeroplane

centre of gravity, and a side component at the nose wheel ground contact equal to 80% of the vertical ground reaction at that point are assumed.

With the aeroplane at its maximum ramp weight, and its nose gear at any steerable position, CS 25.499 (e) demands that the combined application of full normal steering torque and vertical force equal to 1.33 times the maximum static reaction on the nose gear must be considered in designing the nose gear, its attaching structure as well as the forward fuselage structure.

3.3.6.3. Unsymmetrical Braking

Additionally, by CS 25.499(b) [1], the loads resulting from the use of brakes on one side of the main landing gear, the nose gear, its attaching structure, and the fuselage structure forward of the centre of gravity must withstand the following loads:

- A vertical load factor of 1.0 at the centre of gravity;
- A forward acting load at the aeroplane centre of gravity of 80% times the vertical load acting on one main gear;
- Side and vertical loads at the ground vertical point on the nose gear that are required for static equilibrium;
- A side load factor at the aeroplane centre of gravity of zero.

Nose gear loads:

$$V_{NG} = \frac{n_z W \left[B + E \mu_{MG} \left(0.50 + \frac{BL_{cg}}{T} \right) \right]}{[C + 0.50 E \mu_{MG}]} \quad (3.79)$$

$$D_{NG} = 0 \quad (3.80)$$

$$S_{NG} = \frac{D_{MGr} (BL_{cg} - 0.50T)}{C} < 0.80 V_{NG} \quad (3.81)$$

Main gear loads:

$$V_{MGr} = n_z W \left(0.50 + \frac{BL_{cg}}{T} \right) - 0.50 V_{NG} \quad (3.82)$$

$$V_{MGl} = n_z W - V_{NG} - V_{MGr} \quad (3.83)$$

$$D_{MGr} = \mu_{MG} V_{MGr} \quad (3.84)$$

$$D_{MGl} = 0 \quad (3.85)$$

$$S_{MGr} = -0.50 S_{NG} \quad (3.86)$$

$$S_{MGl} = 0.50S_{NG} \quad (3.87)$$

Notice that these equations were derived upon the assumption of braking on the right gears. The load factors applied to the aeroplane under these conditions are specified in the regulations, as follows:

$$n_z = 1.0 \quad (3.88)$$

$$n_y = 0 \quad (3.89)$$

The forward load factor can be computed from the drag load:

$$n_x = \frac{\mu_{MG}V_{MGr}}{W} \quad (3.90)$$

In equation (3.90) the dynamic friction coefficient (μ_{MG}) is 0.80 for normal tire conditions, except when the main gear brakes are torque limited, in which case a reduced forward acting force at the aeroplane centre of gravity may be used.

Side and vertical loads at the ground contact point on the nose gear are as required for equilibrium. The ratio of the nose gear side load does not need to exceed 0.80.

3.3.6.4. Pivoting

Under this condition the aeroplane is assumed to pivot about one side of the main gear with the brakes on that side locked. According to CS 25.503 [1], the limit vertical load factor is 1.0 and the coefficient of friction is 0.8. Furthermore, the aeroplane is assumed to be in static equilibrium, with the loads being applied at the ground contact points.

The nose gear loads will be:

$$V_{NG} = n_z(V_{NG})_s \quad (3.91)$$

$$D_{NG} = S_{NG} = 0 \quad (3.92)$$

The main gear loads will be:

$$V_{MGl} = n_z(V_{MGl})_s \quad (3.93)$$

$$V_{MGr} = n_z(V_{MGr})_s \quad (3.94)$$

$$D_{MGl} = S_{MGl} = D_{MGr} = S_{MGr} = 0 \quad (3.95)$$

The torque about the locked main gear is defined as [1]:

$$T_{piv} = V_{MGr} \mu_{MG} K_{piv} L_{piv} \quad (3.96)$$

Where, $\mu_{MG} = 0.8$,

$$\begin{cases} L_{piv} = 0.5 F, & 2 - \text{wheel landing gear} \\ L_{piv} = 0.25(F^2 + d^2), & 4 - \text{wheel landing gear} \end{cases} \quad (3.97)$$

$K_{piv} = 1.33$, F is the distance between the wheels on the same axle (in), and d is the distance between axles of the main gear (in).

3.3.7. Towing condition

The design tow loads are specified in the regulations, being a function of the aeroplane gross weight and towing direction. These loads are independent of the aeroplane's centre of gravity position. The towing loads (F_{tow}) are applied parallel to the ground at the landing gear towing fittings. The requirements are established by CS 25.509 [1]. According to it, towing points not on the landing gear but near the aeroplane symmetry plane, the drag and side load components specified for the auxiliary gear apply, whereas when these points are located outboard of the main gear, the main gear drag and side tow load components apply.

The towing load (F_{tow}) is a function of the design take-off weight (W_T), as follows:

$$F_{tow} = \begin{cases} 0.3 W_T, & W_T < 30,000 \text{ lb} \\ \frac{6W_T + 450,000}{70}, & 30,000 \text{ lb} < W_T < 100,000 \text{ lb} \\ 0.15 W_T, & W_T > 100,000 \text{ lb} \end{cases} \quad (3.98)$$

The prescribed towing loads are specified on the Table 3 – CS 25.509 [1]. The side component of the towing load at the main gear must be reacted by a side force at the static ground line of the wheel to which the load is applied. A reaction with a maximum value equal to the vertical reaction must be applied at the wheel to which the load is applied.

Table 3 - CS-25 specifications for towing condition [1].

Tow Point	Position	Load				
		Magnitude	No	Direction		
Main Gear		0.75 F_{tow} per main gear unit	1	Forward, parallel to drag axis		
			2	Forward, at 30° to drag axis		
			3	Aft, parallel to drag axis		
			4	Aft, at 30° to drag axis		
Auxiliary Gear	Swivelled forward	1.0 F_{tow}	5	Forward		
			6	Aft		
	Swivelled aft		7	Forward		
			8	Aft		
	Swivelled 45° from forward		0.5 F_{tow}	9	Forward, in plane of wheel	
				10	Aft, in plane of wheel	
				Swivelled 45° from aft	11	Forward, in plane of wheel
					12	Aft, in plane of wheel

3.3.8. Jacking and Tie-down Provisions

Jacking loads (see Figure 13) refer to the condition under which the aeroplane is supported on several points – which may not coincide with the landing gears' positioning – usually when significant maintenance technical checks take place. According to CS 25.519 [1], the aeroplane must withstand the following limit loads when the aeroplane is supported on jacks.

Table 4 - CS-25 specification for jacking condition.

$n_{horizontal}$	n_z	Condition	
0.33	1.33	Jacking by landing gear at maximum ramp weight	Aeroplane Structure*
0.33	1.33	Jacking by other aeroplane structure	Aeroplane Structure*
0.33	2.0		Jacking pads and local structure

***The point of application depends from aeroplane to aeroplane**

While in preservation, and due to slot constrains in most of the maintenance companies' hangars, the aeroplanes are kept outside, hence being subject to far more severe load conditions due to wind. In order to assure the aeroplane stands still, a number of cables connect the sides of the fuselage or wing to the ground.

Tie-down (see Figure 14) refers to the loads to which the aeroplane structure will be subject due to wind. Several different names have been used to refer to this condition over the years, such as mooring, tethering and picketing.

According to CS 25.519 [1], if tie-down points are provided, the main tie-down points and local structure must withstand the limit loads resulting from a 120km/h horizontal wind from any direction. Although these might be considered ground loads, they can also be included in the miscellaneous loads group. Given the particularity of each of these two analyses the procedure to compute these loads can be significantly different from aeroplane to aeroplane.



Figure 13 - Lockheed Hercules C-130 supported on jacks.



Figure 14 - Tied-down aeroplane.

4. Wing loads

In order to perform the wing loads' analysis some basic assumptions will be made. Several different approaches will be presented and discussed. Notice that although these theories were derived for the wings, they are obviously generalizable for other lifting surfaces, like the horizontal and vertical stabilizers.

The loads on the wing are the sum of the aerodynamic lift and drag forces, as well as concentrated and distributed weight of wing-mounted engines, fuel stored and structural elements. The resulting load factor will vary within the aeroplane's flight envelope already discussed.

4.1. Lift Distribution

4.1.1. Approach 1 – SCHRENK Method

As a consequence of the finite aspect ratio of any wing, the lift distribution will vary along the wingspan, from a maximum near its root to a minimum near its tip. CORKE (2002) [14] has shown that the spanwise lift distribution should be proportional to the shape of the wing planform. In the case of an elliptical planform, the local chord distribution, $c(y)$ given as:

$$c(y) = \frac{4s_w}{\pi b} \sqrt{1 - \left(\frac{2y}{b}\right)^2} \quad (4.1)$$

an analytic spanwise distribution exists, and is given by:

$$L^E(y) = \frac{4L}{\pi b} \sqrt{1 - \left(\frac{2y}{b}\right)^2} \quad (4.2)$$

The analysis of an elliptic planform wing shows that it results in an elliptic spanwise lift distribution. This result is the basis for a semi-empirical method to estimate the spanwise lift distribution on untwisted wings with general trapezoidal shapes. This method has been attributed to SCHRENK (1940) and assumes that the spanwise lift distribution of a general untwisted wing has a shape that is the average between the actual planform chord distribution, and that of the elliptical wing.

For the trapezoidal wing, the local chord length varies along the span as follows:

$$c(y) = c_r \left[1 - \frac{2y}{b}(1 - \lambda)\right] \quad (4.3)$$

Following the elliptical wing the lift distribution may vary likewise the chord length:

$$L^T(y) = L_r \left[1 - \frac{2y}{b}(1 - \lambda) \right] \quad (4.4)$$

The total lift can now be obtained by integrating the lift distribution in the spanwise direction over the span [14]:

$$L = 2L_r \int_0^{b/2} \left[1 - \frac{2y}{b}(1 - \lambda) \right] dy \quad (4.5)$$

$$L_r = \frac{2L}{b(1+\lambda)} \quad (4.6)$$

The approximated spanwise lift distribution is then the local average of the two distributions:

$$\bar{L}(y) = \frac{1}{2} [L^T(y) + L^E(y)] \quad (4.7)$$

It must be noted that the SCHRENK's method herein presented does not provide trustworthy estimates for highly swept wings. In that case, a panel method approach or a computational method is required. This method is also not reliable in the case of wings with aerodynamic torsion, as it is the case of most of today's wings.

In spite of its limitations, this method can be reasonably applied to horizontal stabilizers with low sweep angles, since most of them do not have aerodynamic torsion. It would also be an interesting method to study the *Supermarine Spitfire*³ wing – its elliptical planform geometry, together with the absence of aerodynamic torsion make the formerly discussed approximations valid.

4.1.2. Approach 2 – Joukowski Based Method

The first assumption will be that there is an elliptical spanwise distribution of circulation. Despite being hard to have a distribution like this – as was achieved by the famous *Supermarine Spitfire* – most of the wings currently used try to approximate these distributions, namely commercial aeroplanes, business jets and military cargo aeroplanes, the exception being modern military fighters where performance is always ahead of aerodynamic efficiency. Since the analysis of such aeroplanes goes out of the scope of this work, this was not found to be a problem.

Although *Joukowski* aerofoils will not be used, *Joukowski* theory will be used. This approximation is plausible provided that sharp edged trailing edge's aerofoils are being studied where the *Kutta-Joukowski* condition is met. The reader should bear in mind that the *Kutta-Joukowski* [15] condition demands no infinite velocity discontinuities on the aerofoil trailing edge, which is achieved by imposing a circulation enough to grant that the point that once transformed gives origin to the aerofoil trailing edge is a stagnation point in the

³ WWII most well-known fighter.

generating circle. Notice that the analogous approximation would not be reasonable for blunt edged trailing edge's aerofoils.

BREDERODE (1997) [15], shows that, in perfect fluid analysis of a Joukowski aerofoil, the 2D lift coefficient (C_l) depends on the effective AOA (α_{ef}), on the aerofoil zero lift angle ($-\beta$) and relative thickness (d/c) as follows:

$$C_l = 2\pi \left(1 + 0.77 \frac{d}{c}\right) (\alpha_{ef} + \beta) \quad (4. 8)$$

According to this equation, the aerofoil thickness increases the lift curve slope. However, under real flow conditions, it has been shown experimentally that the lift curve slope is actually slightly smaller due to viscosity. It will be thus assumed that this effect counteracts the former, such that the 2D lift coefficient will be as follows:

$$C_l = 2\pi (\alpha_{ef} + \beta) \quad (4. 9)$$

In order to determine the circulation distribution, the circulation on the wing's symmetry plane must be determined. The relationship between the wing's 3D lift coefficient (C_L) and the circulation on the symmetry plane (Γ_{max}) is the following [17]:

$$\Gamma_{max} = \frac{1}{2} U_\infty \bar{c} C_L \quad (4. 10)$$

Since the free stream velocity (U_∞) and the wing average chord (\bar{c}) are known, the only unknown is the wing's 3D lift coefficient. In the same reference, it is shown the 3D analogy of a 2D Joukowski aerofoil is as follows:

$$C_L = \frac{1}{\frac{1}{2\pi} + \frac{1}{\pi\Lambda}} (\alpha_{wing} + \beta_{wing}) \quad (4. 11)$$

Where Λ is the wing aspect ratio, α is the wing AOA and β is the symmetrical of the wing's zero lift angle. Recalling the assumption of the elliptical wing circulation spanwise distribution, the spanwise circulation can be obtained from the following expression:

$$\Gamma(y) = \Gamma_{max} \sqrt{1 - \left(\frac{2y}{b}\right)^2} \quad (4. 12)$$

After performing the wing spanwise discretization, the aim is to determine the lift coefficient at each spanwise station. Since the spanwise circulation and chord are already known, the following equation can be used to relate the spanwise circulation with the local lift coefficient.

$$C_l(y) = \frac{\Gamma(y)}{\frac{1}{2} U_\infty c(y)} \quad (4. 13)$$

Even though this approach is more accurate than that of SCHRENK's, being applicable to a broaden number of wing configurations, it must be noticed that it is only applicable to

situations where there are no flaps or ailerons deflections, since it is assuming a zero lift angle constant for the whole wing. As the purpose of this analysis is to estimate wing load distribution in extreme cases, the goal is to assess the wing loads with flaps and ailerons deflected, which would enable the use of this second approach. However, in the case of a wing with an arbitrary shape without ailerons or flap deflection this is the simplest and most adequate method.

Note that the wing twist will not be taken into account. However, and since common wings have negative twist from the wing root to its tip, this results will be conservative in the way they will cause an overload in the wing tip, with a consequent increase on the local shear force and bending moment at the wing-fuselage joints.

4.1.3. Approach 3 – Joukowski Based Modified Method

A method to generalize Joukowski's to the case when flaps and/or ailerons may be deflected will now be discussed. In order to simplify the analysis herein presented the situation of a wing with deflected ailerons but without flaps' deflection will be considered.

$$C_{L_w} = \frac{1}{\frac{1}{2\pi} + \frac{1}{\pi A}} (\alpha_w + \beta_w) \quad (4.14)$$

The lift coefficient and wing aspect ratio are assumed to be known. In order to estimate the wing AOA, its zero lift angle must be estimated. To do that, a linear weighted average will be used:

$$\beta_w = \frac{S_{ail}}{S_w} \beta_{ail} + \frac{S_{clean}}{S_w} \beta_{clean} \quad (4.15)$$

From these two equations the wing AOA can be estimated. However, this AOA is a virtual angle, since it does not coincide with the clean aerofoil part of the wing nor the aileron's deflected area. In order to determine the AOA of the wing section with ailerons and the clean aerofoil, the two following equations can be used (refer to Figure 15):

$$\alpha_w = \frac{S_{ail}}{S_w} \alpha_{ail} + \frac{S_{clean}}{S_w} \alpha_{clean} \quad (4.16)$$

$$\alpha_{aileron} - \alpha_{clean} = \arctan \left[\frac{x_2 \sin(\delta_{ail}^{max})}{x_1 + x_2 \cos(\delta_{ail}^{max})} \right] \quad (4.17)$$

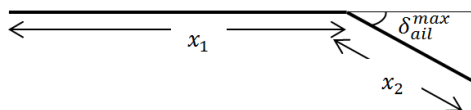


Figure 15 - Chordwise fractions (downwards deflected aileron)

Since the AOA of each wing section is now known, it is possible to estimate the lift coefficient that would act the wing in the case of a totally clean wing as well as in the case of a wing with ailerons deflected along its total span. These two lift coefficients are virtual lift coefficients but will make possible to compute the circulation distribution in the two cases, which, once appropriately combined can indeed provide a realistic result. Accordingly:

$$C_{L_{ail}} = \frac{1}{\frac{1}{2\pi} + \frac{1}{\pi\lambda}} (\alpha_{ail} + \beta_{ail}) \quad (4.18)$$

$$\Gamma_{ail}^{max} = \frac{1}{2} U_{\infty} \bar{c} C_{L_{ail}} \quad (4.19)$$

$$C_{L_{clean}} = \frac{1}{\frac{1}{2\pi} + \frac{1}{\pi\lambda}} (\alpha_{clean} + \beta_{clean}) \quad (4.20)$$

$$\Gamma_{clean}^{max} = \frac{1}{2} U_{\infty} \bar{c} C_{L_{clean}} \quad (4.21)$$

Finally, the spanwise distribution of circulation can be determined from a weighted average of the two spanwise circulation distributions already derived (where the reader should note that the elliptical circulation distribution has been assumed). This will be done by using a *Hermite* polynomial function Reddy (2006) [18], as follows:

$$\Gamma(y) = \Gamma_{clean}(y) \cdot f(y) + \Gamma_{aileron}(y) [1 - f(y)] \quad (4.22)$$

Assuming that the ailerons are attached to the wing tips, this *Hermite* function will be zero at the wing tip and one close to the root. This function will assure that no discontinuities in the spanwise circulation occur, thus making this method more realistic. Using the relation between local lift coefficient and circulation:

$$C_l(y) = \frac{\Gamma(y)}{\frac{1}{2} U_{\infty} c(y)} \quad (4.23)$$

Between the three methods presented this is the most realistic. The reasoning developed for the case of a wing with aileron can be extended for the case of a wing with ailerons and flaps. The *Hermite* functions [18] to weight the spanwise circulation distribution are important to avoid circulation discontinuities and must be carefully chosen to generate plausible results.

4.2. Drag Distribution

Once the spanwise lift coefficient distribution has been determined, the total drag coefficient (C_D) at each wing section obtained from the formerly mentioned discretization procedure can be determined, being the sum of the aerofoil drag coefficient plus the lift induced drag coefficient. Accordingly:

$$C_D = C_{d_{aerofoil}}(\gamma) + C_{D_i}(\gamma) \quad (4.24)$$

$$C_d = C_{d_{aerofoil}}(\gamma) + \frac{[C_L(\gamma)]^2}{\pi A} \quad (4.25)$$

4.3. Pitching Moment Coefficient

The reader should note that the aerodynamic centre of the lifting surfaces has been used as the reference point in what refers to the pitching moment determination. Despite being recognized as a key point for aerodynamicists, the aerodynamic centre is an irrelevant point for engineers working in the fields of structures that rather work with the wing pressure centre, which is the point where the pitching moment is null.

In the present work since the pressure centre depends on the wing AOA, whereas the aerodynamic is a wing property (independent of the AOA), this has been chosen as the reference point.

Using the usual convention of aerodynamic texts, the nose up pitching moment is taken as positive. BREDERODE (1997) [15] shows that the pitching moment in the aerodynamic centre – assuming the aerodynamic centre is placed as $\frac{1}{4}$ chord of the aerofoil as it is common – is given by:

$$C_{M_{ac}}(\gamma) = C_{M_c}(\gamma) - \frac{C_L}{4}(\gamma) \quad (4.26)$$

$$C_{M_{ac}}(\gamma) = \frac{\pi}{2} [\alpha_{ef}(\gamma) + \lambda] - \frac{\pi}{2} [\alpha_{ef}(\gamma) + \beta(\gamma)] \quad (4.27)$$

The variable (λ) is the angle of attack that creates a null pitching moment relative to the aerofoil's centre. In the case of a Joukowski aerofoil this angle of attack is zero. Expression (4.26) is thus a generalization of Joukowski expression, derived in [5], applicable to all kind of aerofoils.

It must be noticed that the aerofoil's centre refers to its mid-chord section. In reality, this is only true for zero thickness and camber aerofoils (flat plate), but it is a reasonable approximation provided that the aerofoils under study do not have high thicknesses or cambers, as the ones that are expected to be analysed herein.

4.4. Compressibility effects

The stagnation density of a moving perfect gas is given by the following isentropic relation [12]:

$$\frac{\rho_0}{\rho} = \left(1 + \frac{\gamma-1}{2} M^2\right)^{\frac{1}{\gamma-1}} \quad (4.28)$$

For air at usual operating conditions ($\gamma = 1.4$), the difference between the stagnation and static densities is less than 5% for Mach numbers below 0.32, thus, the compressibility

effects are usually not accounted for when performing aerodynamic analysis at Mach numbers lower than this. Since the local maximum velocity over an aerofoil is approximately three times the free-stream velocity, the entire flow may be considered incompressible without significant loss of accuracy for Mach numbers around 0.1. Within the above mentioned conditions, it is valid to use the Bernoulli equation [19], as follows:

$$p_0 = p + \frac{1}{2}\gamma M^2 p \quad (4. 29)$$

Since the generic aeroplane under study is assumed to fly at subsonic speed, namely medium to high subsonic regime – where the compressibility effects become a meaningful contribution – some way to correct the incompressible theory results obtained already derived must be determined.

4.4.1. Subsonic Compressibility Correction Methods

Subsonic compressibility correction methods relate the subsonic compressible flow past a particular aerofoil to the incompressible flow past a second aerofoil that is geometrically related to the former by means of an affine⁴ transformation.

An affine transformation, by definition, changes all the coordinates in a given direction by a uniform ratio. These methods generate the so-called similarity laws' expressions [19][20]. There are four different methods that may be applied, namely the *Gotherl's* rule, the *Prandtl-Glauert* rule, *Laitone's* rule and the *Karman-Tsien* rule.

The elegance of the compressibility correction methods lies in the fact that compressible flow aerofoil characteristics can be predicted by modifying the incompressible data obtained from either the theoretical methods already described or from low-speed wind tunnel tests. They are applicable for two-dimensional, inviscid, isentropic, irrotational, subsonic flow past thin aerofoils at low AOA.

⁴ This term was firstly used for the first time in 1748 by Leonhard Euler, when he stated that «*deux courbes images l'une de l'autre par une telle transformation présentent entre elles une certaine affinité*», to mean that there was some relation («*affinité*» in french) between two curves.

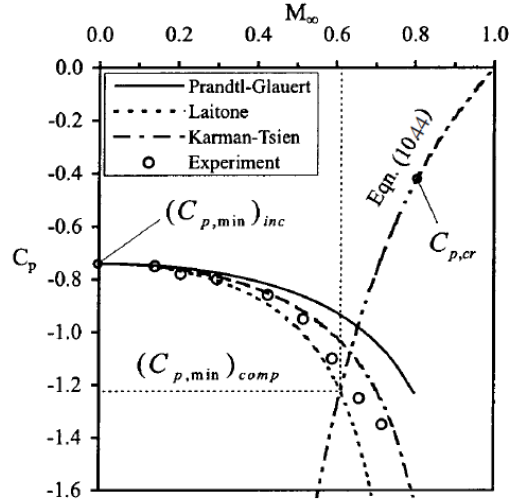


Figure 16 – Comparison between the similarity laws and experimental data [19].

A discussion of the advantages and disadvantages of each of these four methods was presented by DAVIES (2002) [4]. Due to its simplicity – and despite being the least accurate of the methods presented in Figure 16 – the *Prandtl-Glauert* rule will be the adopted.

Let β_{comp} be the Prandtl-Glauert compressibility factor:

$$\beta_{comp} = \sqrt{1 - M_{\infty}^2} \quad (4.30)$$

Prandtl-Glauert method presents a number of expressions that relate the relevant variables in incompressible and compressible flow regimes, in such a way that the theory is extendable to the three-dimensional flow field under study.

These equations are useful and may be used in subsonic flow as well as supersonic flow – provided that the compressibility factor is redefined⁵. Plus, these expressions only relate the aerodynamic coefficient for two different Mach numbers, either in subsonic regimes or supersonic regimes. This means, neither it is possible to forecast the supersonic coefficients from the subsonic nor the contrary. Furthermore, these expressions are not applicable under transonic and hypersonic speeds, which means that by using them the flow field is assumed to be below the transonic flow threshold (roughly $M=0.85$). Accordingly [20]:

$$C_{p_{comp}} = \frac{C_{p_{inc}}}{\sqrt{1 - M_{\infty}^2}} = \frac{C_{p_{inc}}}{\beta_{comp}} \quad (4.31)$$

$$\lambda_{comp} = \lambda_{inc} \quad (4.32)$$

$$\Lambda_{comp} = \frac{\Lambda_{inc}}{\beta_{comp}} \quad (4.33)$$

$$\varphi_{comp} = \arctan[\beta \cdot \tan(\varphi_{inc})] \quad (4.34)$$

⁵ $\beta_{comp} = \sqrt{M_{\infty}^2 - 1}$

$$\left(\frac{t}{c}\right)_{inc} = \left(\frac{t}{c}\right)_{comp} \quad (4.35)$$

$$c_{comp} = c_{inc} \quad (4.36)$$

$$b_{comp} = \frac{1}{\beta_{comp}} b_{inc} \quad (4.37)$$

Finally, the expressions that relate the lift and induced drag coefficients under incompressible and compressible flow regime can be presented:

$$C_{L_{comp}} = \frac{C_{L_{inc}}}{\beta_{comp}} \quad (4.38)$$

$$C_{D_{comp}}^i = \frac{C_{D_{inc}}^i}{\beta_{comp}} \quad (4.39)$$

Notice that the form drag is assumed to be the same regardless the Mach number, whereas the pitching moment coefficient will be influenced by the change in the lift coefficient.

4.5. Symmetrical Manoeuvres

The symmetrical manoeuvre requirements are analysed to determine the necessary parameters for wing loads calculations. These parameters are:

- Aeroplane Load Factor, n_z ;
- Pitching Acceleration about the centre of gravity;
- Pitching Rate;
- Wing reference AOA;
- Inertia parameters due to operating empty weight (OEW) and fuel;
- Airspeed and Altitude (i.e. dynamic pressure).

The wing spanwise load distribution may be considered the sum of the following increments:

- Basic Lift – The lift distribution at AOA=0, $\{L_0\}$;
- Additional Lift – The lift distribution due to AOA, $\{L_\alpha\}\alpha_w$;
- The Lift distribution due to aeroelastic effect of inertia due to N_z , $\{L_n\}n_z$;
- The Lift distribution due to pitching velocity, $\{L_{\dot{\theta}}\}\dot{\theta}$;
- The Lift distribution due to aeroelastic effect of inertia due to pitching acceleration, $\{L_{\ddot{\theta}}\}\ddot{\theta}$;
- The Lift distribution due to speedbrakes (e.g. spoilers), $\{L\}_{sp}$;
- The Basic Lift and Additional Lift increments apply to either flaps up or down analysis (included in the first two terms);

According to Lomax (1996) [5], these contributions may be summarized in the following equation:

$$L = L_0 + L_\alpha \alpha_w + L_n n_z + L_{\dot{\theta}} \dot{\theta} + L_{\ddot{\theta}} \ddot{\theta} + L_{sp} \quad (4.40)$$

Aeroelasticity effects are supposed to be included in all the terms of equation (4.40) and that's why there is no explicitly aeroelasticity term on the equation. In the scheme shown in Figure 17, the algorithm used to perform a symmetrical manoeuvre wing analysis is shown.

4.5.1. Basic Lift and Additional Lift

These two lift contributions shall be computed from the expressions already derived for the calculation of an elliptical lift distribution for a rigid wing. The basic lift refers to the lift generated by the wing at zero AOA, while the additional lift accounts for the lift due to AOA.

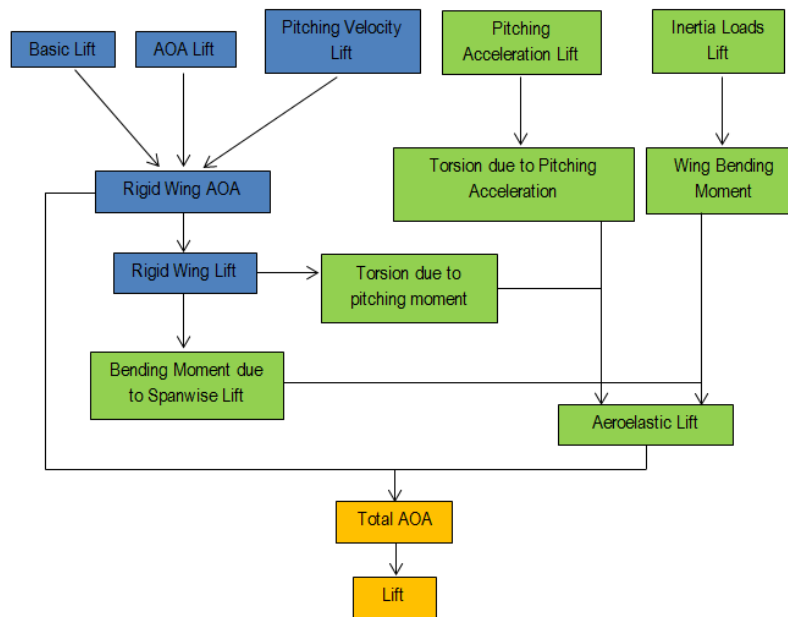


Figure 17 - Wing lift sources scheme.

4.5.2. Lift distribution due to pitching velocity

In general, steady state manoeuvre conditions produce the maximum design wing loads under symmetrical manoeuvre. The lift distribution due to pitch velocity arises because there will be an additional vertical velocity component between the free and the wing leading edge that will eventually cause an increment in the AOA. This effect is a function of the spanwise position. For such flight conditions where pitching acceleration is zero and performing a balance of forces:

$$\frac{v_\infty^2 W}{Rg} = n_z W - W \quad (4.41)$$

$$\Leftrightarrow \frac{V_{\infty} \dot{\theta}}{g} = n_Z - 1 \quad (4.42)$$

$$\Leftrightarrow \dot{\theta} = \frac{n_Z - 1}{V_{\infty}} g \quad (4.43)$$

Furthermore, the pitching velocity with the AOA increment it causes can be related. On Figure 18, it is apparent that a nose down pitching velocity results in an increased local AOA whereas a nose up pitching velocity has the opposite effect of the former.

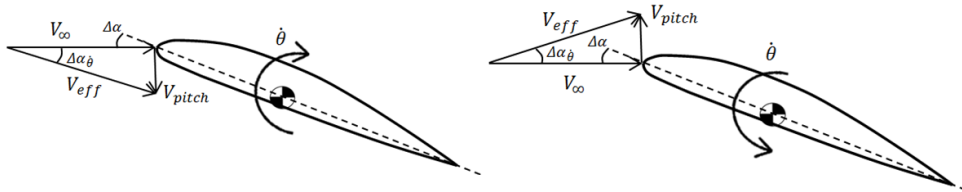


Figure 18 - Pitching velocity induced lift.

Looking at the spanwise effect of the pitching velocity induced AOA, and recalling that the pitching velocity is relative to the aeroplane centre of gravity, it is possible to compute the pitch induced velocity at the leading edge of the wing in order to determine the AOA increment.

$$V_{pitch} = \left[\frac{(n_Z - 1)g}{V_{\infty}} \right] \left(x_{cg} - x_v + \frac{c}{4} \right) \quad (4.44)$$

Where, c is the local chord x_v and is the distance from the wing root leading edge to the local aerodynamic centre ($0.25c$). Thus the induced pitching velocity will always vary along the span provided that the wing sweep is different from zero. Finally, it is possible to compute the AOA due to pitch velocity.

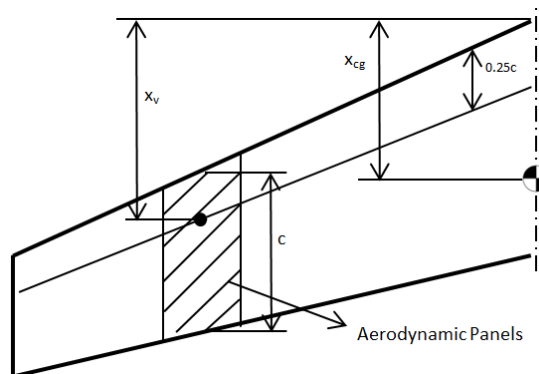


Figure 19 - Pitching velocity lift scheme.

$$\{\Delta\alpha\}_{\dot{\theta}} = \arctan\left(\frac{V_{pitch}}{V_{\infty}}\right) \quad (4.45)$$

4.5.3. Lift distribution due to pitching acceleration

The pitching acceleration generated by the elevator surface deflection will transmit a pitching moment, which will be named torsion:

$$\Sigma M = I_y \ddot{\theta} \quad (4.46)$$

Where, M is the pitching moment (torsion) applied to the aeroplane pitching axis, I_y is the aeroplane moment of inertia and $\ddot{\theta}$ is the pitching acceleration.

4.5.4. Lift distribution due to aeroelastic effect of inertia

Aeroelasticity will be an important contribution for lift. Indeed, due to aeroelasticity there will be an additional wing twist along the wingspan, which will cause the local AOA to change. Additionally, the wing will bend due to the difference in its acting forces. In the case of the symmetrical manoeuvre, the two limit cases will happen for the maximum (Figure 20) and minimum (Figure 21) load factors. For the first case the wing will bend upwards force will be greater than its own weight and centrifugal forces, while for the second the wing will bend downwards as the negative lift force generated, together with the wing weight will be greater than the wing's centrifugal force [21][22].

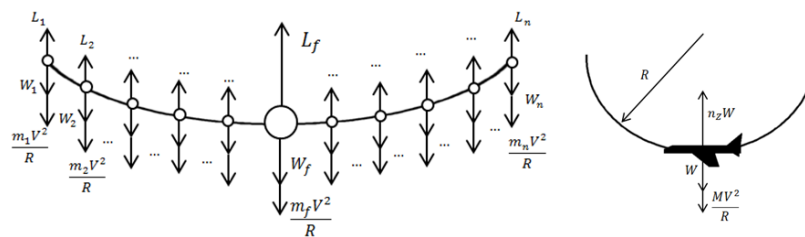


Figure 20 - Positive load factor symmetric manoeuvre.

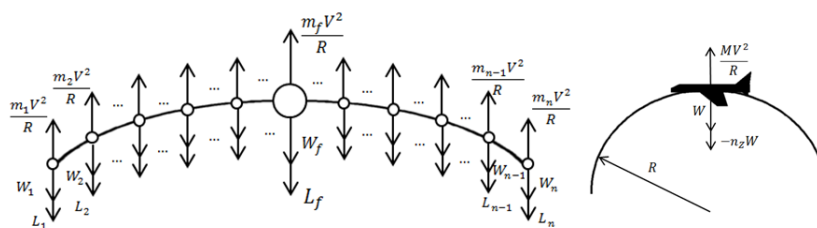


Figure 21 - Negative load factor symmetric manoeuvre.

4.5.5. Lift distribution due to Spoilers

The spoilers' purpose is to reduce lift, thus contributing to a structural relief of the wing from the wing section lift generation viewpoint, provided that they are working at positive load factors. However, when working at negative load factor, the spoilers' will no longer have a relieving effect, on the contrary, the spoilers will actually contribute to an additional bending

moment (bending the wings downwards), becoming a critical design situation that must be accounted for. Furthermore, the increased wing drag forces and torsion caused by the spoilers' deflection will, whichever the load factor, contribute to an additional bending moment that must also be determined.

These comments apply to both ground spoilers and flight spoilers, the former being used to brake the aeroplane during landing while the latter are used differentially to enhance the aeroplane's rolling performance relative to the case when only the ailerons are deflected.

The spoilers' load distribution may be obtained directly from the hinge moment capability of the spoilers' actuators. For the in-flight conditions with the spoilers extended, two distributions are assumed, each producing the same hinge moment defined by the extension capability of the spoilers' actuators. The condition whereby P_1 at the spoiler's leading edge produces the largest airload. The relationship between chordwise pressure and spoiler hinge moment can be obtained by moment of forces equilibrium. Accordingly:

$$P_1 = \frac{6M_{sp_hinge_ext}}{(S.c)_{sp}} \quad (4.47)$$

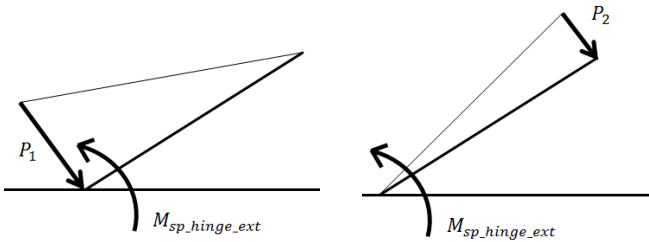
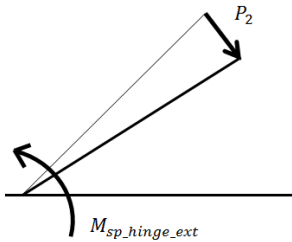
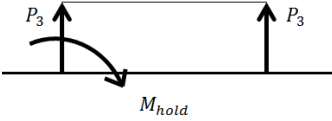
The aft loaded condition will design the spoiler trailing edge structure and has been selected to provide adequate structure to withstand buffeting that may occur at maximum spoiler deflection. Therefore:

$$P_2 = 0.5P_1 \quad (4.48)$$

The spoiler hold-down condition must be considered in design of the hold-down mechanism and related spoiler structure. Assuming a pressure distribution as shown in the Table 5 and by performing the moment of forces equilibrium with respect to the hinge axis, one can calculate the chordwise pressures:

$$P_3 = \frac{2M_{sp_hinge_hold}}{(S.c)_{sp}} \quad (4.49)$$

Table 5 - Pressure distribution over a spoiler.

Spoilers extended		Spoilers retracted
		
$P_1 = \frac{6M_{sp_hinge_ext}}{(S.c)_{sp}}$	$P_2 = 0.5P_1$	$P_3 = \frac{2M_{sp_hinge_hold}}{(S.c)_{sp}}$

For simplicity, and in order to keep on a conservative track, it will be assumed that under positive load factor flight conditions, no spoilers' deflection and consequently no wing lift relief occurs. Secondly, and in order to simplify a bit further the analysis, the extreme case

when the spoiler's deflection result in a total loss of lift of the spanwise portion where these lifting surfaces are acting will be considered.

The maximum moment that the hinge can withstand must be known, which can be done using the aeroplane's manufacturer's manuals. As soon as this is known, the pressures can be determined. Furthermore, from the pressure the additional drag due to extended flap is as follows (refer to Figure 22):

$$D_{sp} = \frac{P_1 S_{sp}}{2} \cos(\alpha_{sp}) \quad (4.50)$$

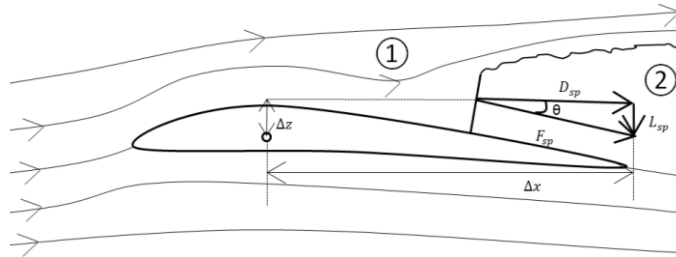


Figure 22 - Spoiler scheme.

A last word to the additional torsion due to spoiler deflection, which will be the algebraic sum of the moment with flaps retracted with the maximum hinge moment due to spoiler deflection.

4.5.6. Lift distribution due to Aeroelastic Effect

The effects of aeroelasticity are not usually determined without a large amount of calculations. These calculations must be based on estimated stiffness of the structure. Additionally, the structural deflection is hard to determine accurately. Thus, it is common practise to neglect aeroelastic effects or make simple assumptions on its calculation, as long as these approximations are found not to put at risk the final results. The simplest method is to estimate the angle of attack change from structural deflection and then calculate the load increment caused by this situation.

Aeroelasticity will encompass two contributions, namely, the spanwise deflection due to pure structural bending and wing chordwise deflection due to torsion. However, and performing an aeroelastic analysis to assess its influence on lift generation these two effects must be accounted for. The expression to obtain the wing chordwise deflection due to torsion can now be presented. If the elastic axis⁶ (also known as shear centre) is taken as reference:

$$d\theta = \frac{T}{GJ} dy \Rightarrow \theta_A - \theta_B = \int_B^A \frac{T}{GJ} dy \quad (4.51)$$

The change on the AOA on the strip due to a combined effect of wing bending and torsion can be obtained from the following expression:

⁶ It is the point of a section where a shear force can be applied without inducing any torsion.

$$\Delta\alpha_{FLEX} = \theta \cdot \cos(\Lambda) - \phi \cdot \sin(\Lambda) \quad (4.52)$$

From the previous expression, it can easily be understood that changes in aerodynamic forces due to structural deflection on a straight wing are mainly due to torsional loads whereas bending load deflection will become increasingly important as sweep increases while the former deflection will lose its relevance. Furthermore, it can be stated that, the bending induced deflection on an aft swept wing tends to decrease the bending moment in contrast with what happens for a swept forward wing – this is the reasoning that justifies why swept forward wings are more susceptible to divergence at high speeds.

4.6. Rolling Manoeuvres

The rolling manoeuvre analysis [5] makes use of the following parameters:

- Aeroplane Load Factor, (n_z) and resulting flight wing loads;
- Maximum Roll Velocity, ($\dot{\phi}$);
- Maximum Roll Acceleration, ($\ddot{\phi}$);

The wing spanwise load distribution [5] may be considered the sum of the following increments:

- Symmetrical Loads Increments;
- Spanwise Load Distributions During Rolling Manoeuvres;
- Rolling Manoeuvre Load Factors.

The lateral control surfaces' deflection is a function of the pilot control wheel angle. Spoilers usually have got a delay in the system and are only used when the control wheel is above a specified limit.

4.6.1. Symmetrical Load Increments

Wing loads for symmetrical load increments must be computed (in accordance with CS-25.349 (a)) for load factors of zero and two-thirds of the positive manoeuvring load factor during roll. In the case of aircraft configurations with unsymmetrical operation of lateral control devices like ailerons and spoilers, a correction must be found to maintain the design load factor during the roll.

Rolling conditions must be considered in both the clean wing configuration and for the case when speedbrakes are being used. The spoilers are operated differentially such that the contribution to roll may be from reduction of spoilers on one wing versus extension on the other wing.

4.6.2. Spanwise Load Distributions during Rolling Manoeuvres

Lateral control devices and roll damping include the contribution of aeroelasticity, provided that a flexible wing analysis is performed, as it is the case. The ailerons' deflection

will cause an increased loading in the outboard wing section moving upwards and a decrease in the moving downwards wing. Attention must also be given to the possibility of having spoilers acting on the half wing moving down.

4.6.3. Rolling Manoeuvre Load Factors

Load factors in steady roll acting outboard of both wings must be combined with the symmetrical manoeuvre load factors. The total load factor that the structure will withstand will be the symmetrical load factor – which is the load factor acting on the aeroplane's CG, (flight envelope [1][2] – plus the load factor caused by the rolling acceleration.

$$n_z = n_{z\ sym} + \frac{ma}{mg} = n_{z\ sym} + \frac{R\ddot{\phi}}{g} \quad (4. 53)$$

Where (y) is the wing spanwise position coordinate. Now, if the symmetrical responses on each wing are considered (and assuming left wing up):

$$n_z = n_{z\ sym} + y\ddot{\phi}/g \text{ (Left Wing)} \quad (4. 54)$$

$$n_z = n_{z\ sym} - y\ddot{\phi}/g \text{ (Right Wing)} \quad (4. 55)$$

From the force equilibrium in the spanwise direction, the load factor due to centrifugal acceleration can be derived from the quotient between the centrifugal force and

$$n_Y = \frac{F_c}{W} = \frac{\frac{mV^2}{y}}{mg} = \frac{V^2}{yg} \quad (4. 56)$$

Accordingly:

$$n_Y = \frac{y\dot{\phi}^2}{g} \quad (4. 57)$$

The reader should notice that the load factor derived acts outboard on both wings, on the contrary of what happened in the case of the vertical load factor contributions.

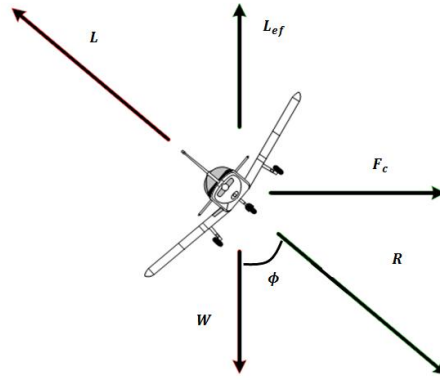


Figure 23 - Force equilibrium diagram in a coordinated turn.

4.7. Yawing Conditions

The lateral manoeuvre and lateral gust requirements involve design conditions that are critical for the empennage and for the fuselage. In general, the wing structure is not critical for these kind of conditions, except for the attachment of wing/nacelles located outboard of the wing or other external stores located on the wing like bombs or missiles [5]. According to LOMAX (1996) [5], the aerodynamic moments on an aeroplane about its rolling axis will be:

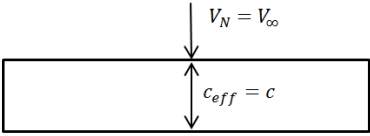
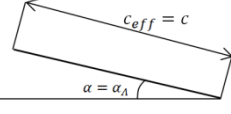
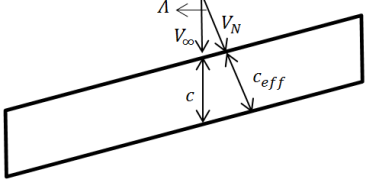
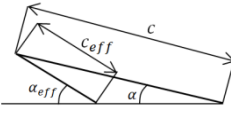
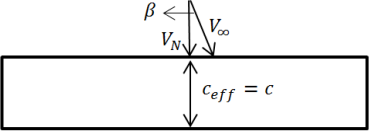
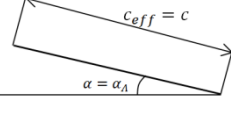
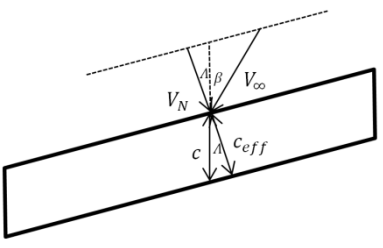
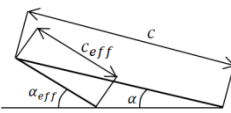
$$C_l = C_{l_\beta}\beta + C_{l_\phi}\dot{\phi} + C_{l_\psi}\dot{\psi} + C_{l_{sp}} + C_{l_{ail}} + C_{l_{rud}} \quad (4. 58)$$

The yawing manoeuvres are assumed to be accomplished with the wings held in a level flight attitude; hence the roll rate ($\dot{\phi}$) is assumed to be zero. Furthermore, if the sideslip angle is maximum for the condition being investigated, the yaw rate ($\dot{\psi}$) will also be zero. Finally, it can be assumed that the net rolling moment coefficient is zero, which complies with a flat manoeuvre; the former expression is simplified as follows:

$$C_{l_\beta}\beta + C_{l_{sp}} + C_{l_{ail}} + C_{l_{rud}} = 0 \quad (4. 59)$$

In order to determine the additional aerodynamic contributions due to yaw, what happens when the wing sweep is different from zero must be studied. It is clear from Table 6 that the geometric local chord (c), will be different from the equivalent streamwise chord ($c \cdot \sec(A)$). This fact will make the lift coefficient curve slope to vary with the AOA. If the contribution of the sideslip angle is now included, the obtained results are listed on Table 6. Notice that only the normal component of the free stream velocity and the correspondent effective chord will actually contribute to the lift generation. The velocity component along the spanwise direction is not relevant for the current calculations.

Table 6 - Sweep and sideslip angles influence on life generation.

Sweep/Sideslip combination	Effective Chord	Variables
		$V_N = V_\infty$ $c_{eff} = c$ $\alpha_{eff} = \alpha$
		$V_N = V_\infty \cdot \cos(\Lambda)$ $c_{eff} = c \cdot \cos(\Lambda)$ $\alpha_{eff} = \alpha$
		$V_N = V_\infty \cdot \cos(\beta)$ $c_{eff} = c$ $\alpha_{eff} = \alpha$
		$V_N = V_\infty \cos(\beta \pm \Lambda)$ $c_{eff} = c \cdot \cos(\Lambda)$ $\alpha_{eff} = \arcsin\left(\sin(\alpha) \cdot \frac{1}{\cos(\Lambda)}\right)$

+ Refers to the left wing
 - Refers to the right wing
 (Rearward sweep assumed)

Notice that in the schemes presented in Table 6 has been assumed that the wings had constant chord. It is noticeable that, given the constant spanwise component of the flow velocity and the relative increase on the upper surface and decrease on the lower surface will result in three dimensional effects acting on the fluid. This fluid behaviour depends on the wing sweep angle [23][24]. In the case of a rearward swept wing the flow moves outboard in the lower surface and inboard in its upper surface (Figure 24). The contrary happens in the case of a forward swept wing (Figure 25). Notice that this reasoning does only apply to the fluid behaviour outside the boundary layer.

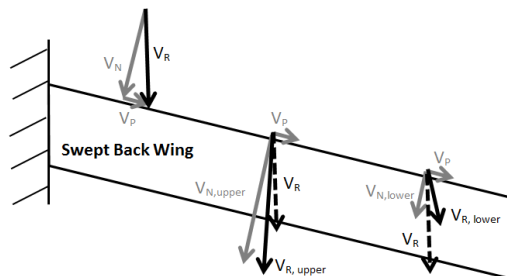


Figure 24 - Swept back wing airflow [23].

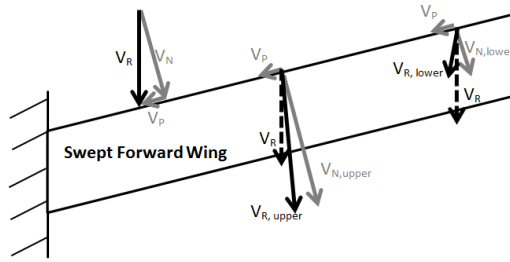


Figure 25 - Swept forward wing airflow [23].

Furthermore, knowing the effective sweep angle, the equivalent streamwise chord at each point can be determined. Looking at Table 6, it is easy to understand how it varies. Recalling the theoretical definition of lift curve slope in 2D for perfect fluid [16] (refer to Figure 26):

$$(C_{l\alpha})_{theory} = 2\pi \left[1 + \frac{0.77t}{c \cdot \sec(A)} \right] \quad (4. 60)$$

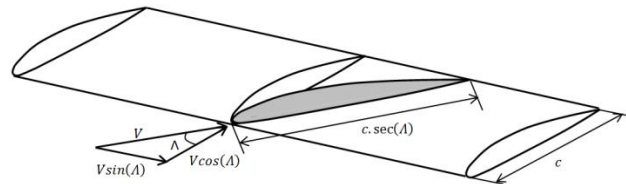


Figure 26 - Swept back wing influence on effective values of the normal airflow and spanwise chord.

However, it should be noticed that, as already discussed, the lift curve slope increase with aerofoil thickness will be counter-acted by the viscosity associated with real flow. Thus, the theoretical lift curve slope may still be regarded as a constant equal to (2π) . The usual source of data for aerofoils and wings is USAF datcom, using the same approach used for the symmetrical manoeuvres calculations, thus:

$$C_{l\alpha} = \frac{1.05}{\beta_{slip}} (C_{l\alpha})_{theory} \quad (4. 61)$$

$$C_{L\alpha} = \frac{1}{\frac{1}{\pi A} + \frac{1}{2\pi \beta_{slip} \frac{1.05}{\beta_{slip}}}} \quad (4. 62)$$

Since there is no spanwise pressure data available from wind-tunnel, flight test measurements, nor CFD analysis, an approximate way to estimate the wing loads under yawed flight developed by LOMAX (1996) [5] will be presented next. Accordingly:

- 1) Estimate the rolling moment due to sideslip for the airplane for tail-off.
- 2) Assume no contribution of rolling moment due to body or external stores on the wing

$$(C_{l\beta}\beta_{slip})_{wing} = (C_{l\beta}\beta_{slip})_{tail-off} \quad (4.63)$$

- 3) Assume that the distribution of loads on the left and right wings are represented by the sweep parameters.

$$\Lambda_{\beta lw} = \Lambda_{0.25} + \beta_{slip} \text{ (Left wing)} \quad (4.64)$$

$$\Lambda_{\beta rw} = \Lambda_{0.25} - \beta_{slip} \text{ (Right wing)} \quad (4.65)$$

The left and right wing increments are as follows:

$$R_{lw} = \frac{\left(\frac{\beta_{slip} C_{L\alpha}}{k}\right)_{lw}}{\left(\frac{\beta_{slip} C_{L\alpha}}{k}\right)_{baseline}} ; R_{rw} = \frac{\left(\frac{\beta_{slip} C_{L\alpha}}{k}\right)_{rw}}{\left(\frac{\beta_{slip} C_{L\alpha}}{k}\right)_{baseline}} \quad (4.66)$$

The incremental airload may be incremented in the following way:

$$\{L_{\beta_{slip}}\}_{lw} = R_{lw}(L_{\alpha})_{sym}R_{cor} \quad (4.67)$$

$$\{L_{\beta_{slip}}\}_{rw} = R_{rw}(L_{\alpha})_{sym}R_{cor} \quad (4.68)$$

$(L_{\alpha})_{sym}$ is the symmetrical flight shear, moment, or torsion in symmetrical 1-g flight net loads. The remaining variables are:

$$R_{cor} = \frac{(C_{l\beta})_{wind\ tunnel\ data}}{(C_{l\beta})_{uncorrected}} \quad (4.69)$$

$$(C_{l\beta})_{uncorrected} = \frac{2C_{L\alpha}y_{cp}(R_{lw}-R_{rw})}{b} \quad (4.70)$$

$C_{L\alpha}$ is the lift curve slope, y_{cp} is the spanwise centre of pressure for symmetrical airload, b the wingspan and the subscripts lw and rw refer to left and right wing, respectively. Finally, the net loads in yawed flight can be determined using the previously discussed assumptions in the following manner:

$$\{L\}_{net\ lw} = \{L\}_{sym} + \{L_{\beta}\}_{lw} + \{L_{ail}\}_{lw} \quad (4.71)$$

$$\{L\}_{net\ rw} = \{L\}_{sym} + \{L_{\beta}\}_{rw} + \{L_{ail}\}_{rw} \quad (4.72)$$

5. Horizontal Tail Loads

The loads acting on the horizontal tail of any aircraft require careful considerations since they affect the design of a significant part of the aircraft structure, namely the horizontal tail stabilizer and elevator, the body structure aft of the pressure bulkhead and horizontal tail support structure, the aft fuselage monocoque structure, the fuselage centre section structure as well as the stabilizer actuator.

The procedures used throughout the aerodynamic analysis of the horizontal tail are analogous to the ones already used for the wing load analysis and will thus not be presented again.

5.1. Horizontal Tail Arrangement

Three different horizontal stabilizer arrangements may be used [25]:

- Integral Stabilizer with Elevator (e.g. *Airbus A320*) – In this configuration the stabilizer deflects as a whole to ensure that as the centre of gravity shifts forward or rearward throughout the flight the aeroplane remains balanced with the elevator in its neutral position. This adjustment is usually done by the automatic pilot. The elevator works whenever the pilot wants to perform a pitch-up or pitch-down manoeuvre.
- Integral Stabilizer without Elevator (e.g. *F-16*) – In this configuration the whole stabilizer works to balance force moments and to manoeuvre the aeroplane with respect to its pitch axis. Despite this Structural Loads Handbook focus being Large Aeroplanes (CS 25) – this stabilizer configuration not being common among these aircrafts – it will be analysed since it is the simplest configuration.
- Non-Integral Stabilizer with Elevator and Tabs (e.g. *Lockheed C-130*) – In this configuration the stabilizer as a whole does not move. Instead, the tab deflection ensures the balance of forces and moments about the CG. Once again, the elevator deflection is used to manoeuvre about the pitch axis.

Moreover, each of these three arrangements can – at least theoretically – be used either in a conventional tail configuration or in a T-tail configuration [26]. Both situations are thus analysed, since the goal is to widen the range of applicability of the methods herein presented.

5.2. Equilibrium Equations

The equations for horizontal tail load and pitching moment are a function of the stabilizer's AOA and elevator angle as follows [5]:

$$L_t = L_{\alpha_s} \alpha_s + L_{\delta_e} \delta_e + L_c \quad (5.1)$$

$$M_t = M_{\alpha_s} \alpha_s + M_{\delta_e} \delta_e + M_c \quad (5.2)$$

where L_t and M_t are the horizontal tail lift and pitching moment about its aerodynamic centre, L_{α_s} and M_{α_s} are the tail load and pitching moment due to unit stabilizer angle of attack (α_s), L_{δ_e} and M_{δ_e} are the tail load and pitching moment due to unit elevator deflection (δ_e) and L_c and M_c are the tail load and pitching moment due to unit built in camber.

The horizontal tail AOA α_s may be defined as a function of wing AOA (in the case of a non-integral stabilizer), the curvilinear flight increment due to pitching velocity, and fuselage flexibility terms together with the initial trim setting of the stabilizer, as follows [5]:

$$\alpha_s = (1 - \varepsilon_{\alpha w}) \alpha_w - \varepsilon_0 + \frac{180 \cdot l_t g (n_z - 1)}{\pi \cdot V_t^2} + \left(\frac{d\alpha_s}{dn_z} \right) n_z + \left(\frac{d\alpha_s}{dL_t} \right) L_t + \left(\frac{d\alpha_s}{dM_t} \right) M_t \quad (5.3)$$

The increment due to wing AOA is modified by the wing downwash at the horizontal stabilizer:

$$\Delta \alpha_s = \alpha_w - \varepsilon_{\alpha w} \alpha_w - \varepsilon_0 = (1 - \varepsilon_{\alpha w}) \alpha_w - \varepsilon_0 \quad (5.4)$$

The increment due to curvilinear lift in a steady state manoeuvre is:

$$\Delta \alpha_s = \frac{180}{\pi} \dot{\theta} l_t / V_t \text{ [DEG]} \quad (5.5)$$

$$l_t = x_t + (0.25 - c.g) c_w \quad (5.6)$$

$$\dot{\theta} = \frac{g(n_z - 1)}{V_t} \text{ [Rad. s}^{-1}\text{]} \quad (5.7)$$

Finally, it is possible to compute the horizontal tail balancing tail load (BTL), as shown in equation (5.9).

$$BTL = L_t - M_t / x_t \quad (5.8)$$

The previously presented equations can be rearranged and represented in matrix form as shown in equation (5.10), for the condition when the elevator angle of attack is unknown. In the case when the elevator angle is known, the matrix in equations (5.9) and (5.10) loses its last column and row and the first two terms on the right-hand side of the system of equations shown below become, $L_c + L_{\delta_e} \delta_e$ and $M_c + M_{\delta_e} \delta_e$, respectively [5].

$$\begin{bmatrix} 1 & 0 & -L_{\alpha_s} & -L_{\delta_e} \\ 0 & 1 & -M_{\alpha_s} & -M_{\delta_e} \\ x_t & -1 & 0 & 0 \\ b_1 & b_2 & 1 & 0 \end{bmatrix} \begin{bmatrix} L_t \\ M_t \\ \alpha_s \\ \delta_e \end{bmatrix} = \begin{bmatrix} L_c \\ M_c \\ BTL \cdot x_t \\ c_1 \end{bmatrix} \quad (5.9)$$

Where,

$$b_1 = -\left(\frac{d\alpha_s}{dL_t}\right) \quad (5.10)$$

$$b_2 = -\left(\frac{d\alpha_s}{dM_t}\right) \quad (5.11)$$

$$c_1 = (1 - \epsilon_{\alpha_w})\alpha_w - \epsilon_0 + \frac{180 \cdot l_t g (n_z - 1)}{\pi \cdot V_t^2} + s + \left(\frac{d\alpha_s}{dn_z}\right) n_z \quad (5.12)$$

5.3. Balanced Manoeuvre Analysis

Assuming the aeroplane to be in equilibrium with null pitching acceleration, the manoeuvring conditions A through I on the manoeuvring envelope (see: CS 25.333 (b)) must be investigated.

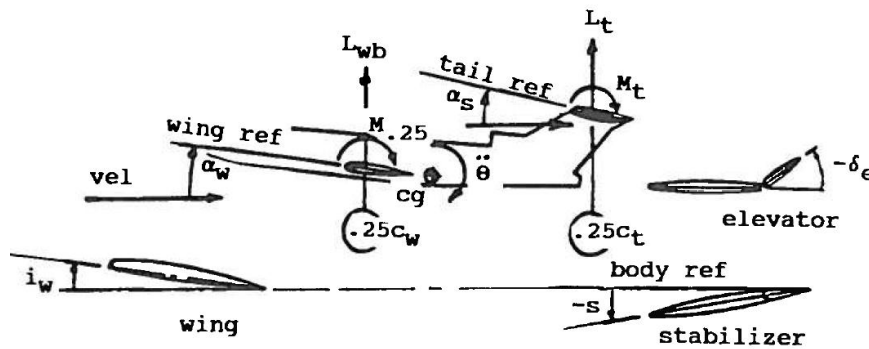


Figure 27 - Sign convention [5].

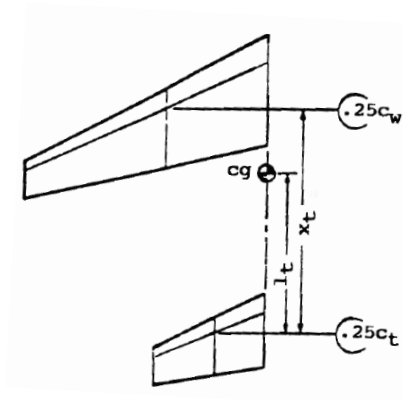


Figure 28 – Horizontal tail geometric parameters [5].

Neglecting the drag terms, and by writing force and moment equilibrium, it is possible to obtain the following relations [5]:

$$L + L_t = n_z W \quad (5.13)$$

$$x_a = (CG - 0.25)c_w \quad (5.14)$$

$$C_{L_a} = \frac{n_z W}{q S_w} \quad (5.15)$$

$$M_{0.25} = C_{M0.25} q S_w c_w \quad (5.16)$$

$$L_t = \frac{[(CG-0.25)C_{L_a} + C_{M0.25}]q S_w c_w}{x_t} + \frac{M_t}{x_t} + \frac{T_{eng} z_e}{x_t} + \frac{n_x W z_A}{x_t} \quad (5.17)$$

Neglecting the last term which is clearly smaller than the others and making the further simplification of considering the tail's pitching moment negligible in face of the wing's pitching moment:

$$L_t \approx \frac{[(CG-0.25)C_{L_a} + C_{M0.25}]q S_w c_w}{x_t} + \frac{T_{eng} z_e}{x_t} \quad (5.18)$$

From the tail geometry the tail's lift coefficient is readily know, which means the respective angle of attack may be computed which enables the computation of the remaining aerodynamic variables – drag and pitching moment. However, the assumption of neglecting the drag force acting on the stabilizer is not reasonable in the case of a T-tail aeroplane, in which case a more accurate solution is given by:

$$L_t \approx \frac{[(CG-0.25)C_{L_a} + C_{M0.25}]q S_w c_w}{x_t} + \frac{T_{eng} z_e}{x_t} + \frac{D_t z_d}{x_t} \quad (5.19)$$

5.4. Abrupt Pitching Manoeuvres

Making the assumption that the manoeuvres are purely symmetrical and that airspeed and altitude are held constant, one can derive the equations of motion for translation along the z-axis and rotation about the y-axis.

$$\ddot{Z} = Z_\alpha \Delta\alpha + Z_{\dot{\alpha}} \dot{\alpha} + Z_{\dot{\theta}} \dot{\theta} + Z_{\delta_e} \delta_e \quad (5.20)$$

$$\ddot{\theta} = M_\alpha \Delta\alpha + M_{\dot{\alpha}} \dot{\alpha} + M_{\dot{\theta}} \dot{\theta} + M_{\delta_e} \delta_e \quad (5.21)$$

In [5], it is shown that:

$$\ddot{Z} = V(\dot{\alpha} - \dot{\theta}) \quad (5.22)$$

Combining equations (5.21) to (5.23):

$$\dot{\alpha} = \frac{Z_{\alpha}\Delta\alpha + (V - Z_{\dot{\theta}})\dot{\theta} + Z_{\delta_e}\delta_e}{V - Z_{\dot{\alpha}}} \quad (5.23)$$

$$\Delta n_z = -\frac{V}{g}(\dot{\alpha} - \dot{\theta}) \quad (5.24)$$

5.4.1. Abrupt Unchecked Elevator Conditions

One of the manoeuvring pitching conditions is the so-called maximum pitching control displacement at design manoeuvring speed. In accordance with CS 25.331 [1] the aeroplane is assumed to be flying in steady level flight and the cockpit pitch control is suddenly moved to obtain extreme nose-up pitching acceleration. The maximum elevator deflection used to be limited by pilot force [1], thus being a function of the aeroplane's velocity; however, with the advent of commercial jet aircraft using advanced control systems, the maximum control surface deflection is no longer limited by control surface force but rather by the maximum hinge moment available from the control system [5].

Furthermore, during initial certification of some commercial aircrafts before the 1960s, horizontal tail loads were computed assuming an instantaneous application of elevator, neglecting aeroplane response, such that ($\Delta\alpha_s = 0$). Thus, the resulting tail loads and pitching moment were calculated on a conservative basis. Given the tools being used in these estimates, herein the adopted procedure will be the same.

5.4.2. Checked Manoeuvre Conditions

The other pitching manoeuvre condition to be investigated is the checked manoeuvre condition between design manoeuvring speed and design dive speed. Herein, nose up checked manoeuvres must be analysed in which the positive limit load factor is achieved. As a separate condition, nose down checked pitching manoeuvre must be analysed in which a minimum load factor of zero is achieved.

According to CS 25.331, whose requirements are significantly different from the ones of FAR 25.331 up to this point, the elevator motion is defined by equation (5.26).

$$\delta_e = \delta_{e0} \sin \omega t; \quad 0 \leq t \leq t_{max} \quad (5.25)$$

Where δ_{e0} is the maximum elevator deflection, δ_e is the elevator deflection at a generic time, $t_{max} = 3\pi/2\omega$, and ω is the circular frequency of the control deflection taken equal to the undamped natural frequency of the short period rigid mode of the aeroplane, provided it is greater than $\omega \geq \pi V/2V_A$.

Additionally, in both manoeuvres, the elevator motion may be scaled down in such a way that it is granted the maximum design load factor and the zero load factor in the nose up

and nose down pitch manoeuvres. Conversely CS 25.331 [1] establishes that, whenever the limit load factors are not attained, the following pitch control must be used:

$$\begin{cases} \delta_e(t) = \delta_{e0} \sin \omega t & 0 \leq t \leq t_1 \\ \delta_e(t) = \delta_{e0} & t_1 \leq t \leq t_2 \\ \delta_e(t) = \delta_{e0} \sin[\omega(t + t_1 - t_2)] & t_2 \leq t \leq t_{max} \end{cases} \quad (5.26)$$

where:

$$\begin{cases} t_1 = \pi/2\omega \\ t_2 = t_1 + \Delta t \\ t_{max} = t_2 + \pi/\omega \end{cases} \quad (5.27)$$

Δt , being the minimum time interval to allow the prescribed load factor to be achieved in the initial direction, but it need not exceed five seconds.

Furthermore, aeroplane loads that occur beyond the time when normal acceleration at the CG goes to zero for the nose up pitching manoeuvre and when the time when normal acceleration at the CG goes to the maximum available load factor for the nose down pitching manoeuvre do not need to be taken into account.

By deflecting the elevator an angular pitching acceleration proportional to the difference between the pitching moments that the tail generates relative to the aeroplane's CG in a balanced 1g flight and in the deflected elevator condition. The superscript n refers to the time step on equations (5.29) through (5.31). At time step (n) the pitching acceleration will be given by:

$$\ddot{\theta}^n = \frac{M_{t_{unbal}}^n - M_{t_{bal}}^n}{I_{yy}} \quad (5.28)$$

The angular parametric equations of motions that relate the aeroplane's pitch angle, velocity and acceleration at time step (n) are given by:

$$\begin{cases} \theta^n = \theta^{n-1} + \dot{\theta}^n t^n + \frac{\ddot{\theta}^n}{2} t^{n2} \\ \dot{\theta}^n = \dot{\theta}^{n-1} + \ddot{\theta}^n t^n \end{cases} \quad (5.29)$$

Accordingly, and since this is a time-dependent problem:

$$\alpha_s^{n+1} = \alpha_s^n + \theta^n \quad (5.30)$$

By knowing the elevator deflection and angle of attack at time step ($n + 1$), it is possible to compute the loads and moments acting the horizontal tail at that time step. The cycle ends when the previously defined conditions are reached.

The reader is invited to investigate reference [27] for further information on the subject.

6. Vertical Tail Loads

Vertical tail loads affect the design of a significant part of the aeroplane structure, thus requiring a careful study. The structures affected by vertical tail loads are the vertical tail itself and its rudder, the aft body structure, the horizontal tail structure if the tail is mounted up the fin and the fuselage centre section and the centre fuselage section.

The conditions that will determine the maximum loads acting on the structure are the yawing conditions (either pilot induced or engine out) as well as the lateral gust condition. Generally, conditions such as rolling manoeuvres are usual not critical for the vertical tail structure except possibly for structural configurations with fin mounted horizontal tails – a situation that is not covered in this study.

6.1. Rudder Manoeuvre Requirements

At speeds from V_C to V_D , the following manoeuvres must be considered. In computing the tail loads, the yawing velocity may be assumed zero (CS 25.351) and the manoeuvres described in Table 7 must be investigated.

Table 7 - Manoeuvres do be investigated [1].

Manoeuvre I	With the aeroplane in unaccelerated flight at zero yaw, it is assumed that the rudder control is displaced to the maximum deflection defined in CS 25.351(a)
Manoeuvre II	With the rudder deflected as specified in CS 25.351(a)(1), it is assumed that the aeroplane yaws to the resulting sideslip
Manoeuvre III	With the aeroplane yawed to the static sideslip angle corresponding to the rudder deflection defined in CS 25.351(a)(1), it is assumed the rudder is returned to neutral

In Manoeuvre I the sideslip angle is null and the rudder deflection is maximum (as prescribed in the aeroplane's flight manual).

In Manoeuvre II the rudder will be assumed to deflect to its maximum which is a conservative assumption (see CS 25.351), and the sideslip angle will also be maximum.

Finally, in Manoeuvre III the rudder is not deflected and the steady sideslip angle (β_{ss}) will be the following:

$$\beta_{ss} = \frac{-C_{n\delta_r} + C_{l\delta_r} C_{n\delta_w} / C_{l\delta_w}}{C_{n\beta} - C_{l\beta} C_{n\delta_w} / C_{l\delta_w}} \delta_r \quad (6. 1)$$

The stability derivatives presented on equation (6.1) relate the rudder deflection, wing sideslip angle and the wing's control surface deflection with the rolling moment and yawing moment, respectively: $C_{n_{\delta_r}}$, $C_{l_{\delta_r}}$, $C_{l_{\beta}}$, $C_{n_{\beta}}$, $C_{l_{\delta_w}}$ and $C_{n_{\delta_w}}$.

6.2. Vertical Tail Loads for Yawing Manoeuvre

The equations of motion for yawing manoeuvres are defined by [5]:

$$\begin{bmatrix} \frac{I_z}{qS_w b_w} & -C_{n_{\delta_w}} & 0 \\ -\frac{I_{xz}}{qS_w b_w} & -C_{l_{\delta_w}} & 0 \\ 0 & -C_{y_{\delta_w}} & \frac{MV_T}{qS_w} \end{bmatrix} \begin{bmatrix} \ddot{\psi} \\ \delta_w \\ \dot{\beta} \end{bmatrix} = \begin{bmatrix} C_{n_{e_o}} + C_{n_{\delta_r}} \delta_r + C_{n_r} \dot{\psi} + C_{n_{\beta}} \beta \\ C_{l_{\delta_r}} \delta_r + C_{y_r} \dot{\psi} + C_{l_{\beta}} \beta \\ C_{y_{\delta_r}} - \left[\frac{MV_T}{qS_w} - C_{y_{\delta_r}} \right] \dot{\psi} + C_{y_{\beta}} \beta \end{bmatrix} \quad (6.2)$$

Using the generalized load parameter \mathcal{L} , vertical tail loads can be calculated from unit solution data:

$$\mathcal{L}_{net} = \mathcal{L}_{\alpha_v} \alpha_v + \mathcal{L}_{\delta_r} \delta_r + \mathcal{L}_{in} n_{yvt} \quad (6.3)$$

Where \mathcal{L}_{α_v} is the vertical tail load, moment or torsion due to fin angle of attack = 1.0 deg; \mathcal{L}_{δ_r} is the vertical tail load, moment or torsion due to rudder = 1.0 deg; \mathcal{L}_{in} is the vertical tail load, moment or torsion due to inertia $n_{yvt} = 1.0$.

The fin angle of attack may be defined by the following expression:

$$\alpha_v = -\beta + \Delta\alpha_{v_{bb}} \quad (6.4)$$

The relation between fin angle of attack and aeroplane sideslip angle is the following:

$$\alpha_v = \sigma - \beta = \left(1 - \frac{d\sigma}{d\beta}\right) (-\beta) \quad (6.5)$$

, where σ is the sidewash angle. The change in vertical tail angle of attack due to aft body lateral bending may be determined with equation (6.6), L_v being the force and T_v the torsion (neglecting lateral loads due to inertia) [5]:

$$\Delta\alpha_{v_{bb}} = \left(\frac{d\alpha_v}{dL_{av}}\right)_{bb} L_v + \left(\frac{d\alpha_v}{dT_{av}}\right)_{bb} T_v \quad (6.6)$$

6.3. Vertical Tail Loads on Engine-Out Condition

The aeroplane must be designed for the unsymmetrical loads resulting from the failure of the critical engine. Turbo-propeller aeroplanes must be designed for the following conditions:

- At speeds between V_C and V_D , the loads resulting from power failure because of fuel flow interruption are considered to be limit loads.

- At speeds between V_C and $V_{C'}$, the loads resulting from the disconnection of the engine compressor from the turbine or from loss of the turbine blades are considered to be ultimate loads.

The time history variation of the thrust decay and drag build-up occurring as a result of the prescribed engine failures as well as the pilot's corrective action must also be taken in two account but are out of the scope of the present work.

Two conditions may be considered when solving the steady-state engine-out problem, one with the maximum sideslip angle with zero rudder and the other with the required rudder to balance the engine-out condition with zero sideslip. The amount of yawing moment due to engine-out may be determined from equation (6.7), where T is the thrust, D_{eo} is the drag and a_{eo} is the engine out lift curve slope for engine out conditions.

$$C_{n_{eo}} = \frac{(T+D_{eo})a_{eo}}{qS_w b_w} \quad (6.7)$$

The steady state equations for engine-out condition are the following:

$$\begin{bmatrix} C_{y\beta} & C_{y\delta_w} & C_{y\delta_r} \\ C_{n\beta} & C_{n\delta_w} & C_{n\delta_r} \\ C_{l\beta} & C_{l\delta_w} & C_{l\delta_r} \end{bmatrix} \begin{bmatrix} \beta_{eo} \\ \delta_w \\ \delta_r \end{bmatrix} = \begin{bmatrix} C_L \phi \\ -C_{n_{eo}} \\ 0 \end{bmatrix} \quad (6.8)$$

Not only shall the loads due to manoeuvres I, II and III be assessed, but also the loads due to zero rudder and no slip engine out conditions.

6.3.1. Engine-Out with Zero Rudder

If the assumption is made that the rudder is held neutral, then the steady sideslip angle will be the following [5]:

$$\beta_{eo} = \frac{C_{n_{eo}}}{C_{n\beta} - C_{l\beta} C_{n\delta_w} / C_{l\delta_w}} \quad (6.9)$$

6.3.2. Engine-Out with Zero Sideslip

If the assumption is made that the sideslip is zero, then the rudder required to balance an engine-out condition may be determined the following expression [5]:

$$\delta_{r_{eo}} = \frac{-C_{n_{eo}}}{C_{n\delta_r} - C_{l\beta} C_{n\delta_w} / C_{l\delta_w}} \quad (6.10)$$

6.4. Concluding Remarks

In order to estimate all the coefficients involved in the equations formerly derived, the reader should search on reference [27]. The formerly discussed flight conditions under which vertical tail loads must be investigated can be summarized in the Table 8.

Table 8 - Summary scheme with all the conditions to be investigated.

Flight Condition	Scheme
Manoeuvre I	
Manoeuvre II	
Manoeuvre III	
Engine-Out (delta_r = 0)	
Engine-Out (beta = 0)	

So as to determine the steady sideslip angle as well as the rudder deflection for zero sideslip its stability derivatives must be known. To estimate these variables USAF Datcom [27] is recommended as it provides several analytical expressions combined with approximate correlations that have proven to give trustworthy result.

The aerodynamic analysis of the vertical tail adopts the same reasoning, methods and assumptions already discussed for the case of the wing.

7. Fuselage Loads

Albeit being objectively simple to calculate, body monocoque⁷ loads determination has evolved through the years [5]. The approach has been changing, primarily due to the increased capability of computers to handle large amounts of data. Before 1970, monocoque loads were classically determined using stress analysis beam theory to calculate the bending stresses and shear flow at a given body station. Nowadays, finite element method analysis takes the lead.

The study of the wing, empennage and landing gear loads has already taken place. Body monocoque loads for static load conditions are found from the combination of these loads with fuselage's aerodynamic, pressurization and inertia loads. The applicable legislation provides the pressurization loads as a function of the limit aircraft operating altitudes. The outmost challenge is thus to determine the airloads acting the fuselage, since there are neither wind-tunnel nor a CFD program to determine the pressure distribution field around it. Finally, and by combining these loads with the loads that the wings and stabilizers are also transmitting to the fuselage it will be possible to determine the maximum loads acting at each point of the fuselage.

7.1. Wing, Empennage and Landing Gear Loads

Having already presented the procedure to compute the maximum loads acting on the wings, empennage and landing gears, it is just a matter of applying those loads on the connections between these parts and the fuselage section to determine the most extreme load situation in the fuselage.

7.2. Pressurization Loads

The pressure cabin has been the source of some spectacular disasters directly attributed to fatigue in aircraft. The contribution to the failure of the fuselage shells are:

- Cut-outs in shell structures, which create high local stresses;
- Cut countersink rivets adjacent to the edge of the cut-out compounds the stress concentration effects;
- Aluminium materials with high yield to ultimate strength ratios are prove to rapid tearing at low stress levels.

According to CS 25.365, the aeroplane structure must be strong enough to withstand the flight loads combined with pressure differentials loads from zero up to the maximum relief

⁷ Monocoque is a construction technique that supports structural load by using an external skin, as opposed to using an internal frame that is covered with a non-load-bearing skin.

valve setting. This relieving valve works as a safety device that enables a decrease in the cabin pressure whenever the pressure difference between the fuselage's outer and inner skins exceeds a given admissible threshold for a particular fuselage.

In the case of a pressurized cabin landing, these must be combined with the landing loads. The aeroplane must be capable of withstanding pressure differential loads corresponding to the maximum relief valve setting multiplied by a factor of 1.33, not accounting for other loads.

Available on aeroplanes flight manuals is the so-called Pressurization Chart that provides guidance on the difference between inner and outer skin pressure for each aeroplane operating altitude.

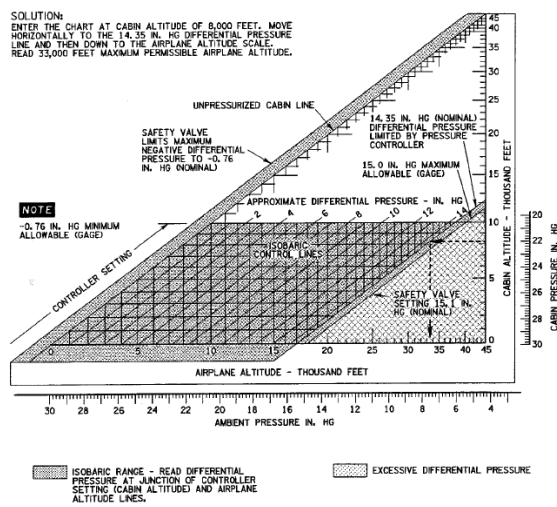


Figure 29 - Lockheed C-130H Pressurization Chart [28].

The critical loading conditions arise when no pressure difference is felt or when the maximum admissible pressure difference is reached, which corresponds to the relief valve setting. A typical pressurization chart is shown in Figure 29.

The hoop and longitudinal tension stresses in the fuselage skin (Figure 30), neglecting the stress concentration due to skin cut-outs, may be computed by the following expressions, where f_{HT} is the hoop tension, f_{LT} is the longitudinal tension, R is the fuselage skin and th is its skin thickness:

$$f_{HT} = \frac{\Delta p \cdot R}{th} \quad (7.1)$$

$$f_{LT} = \frac{\Delta p \cdot R}{2th} \quad (7.2)$$

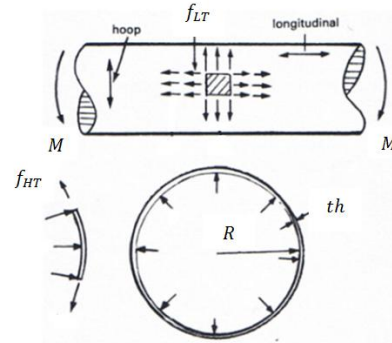


Figure 30 - Hoop and longitudinal tension stresses [29].

7.3. Fuselage Airloads

7.3.1. Approach

One of the major challenges of this research was to find a plausible way of estimating the pressure distribution around the fuselage due to airloads [30]. In order to do this, and since in fuselage sections 1, 2 and 4 (Figures 31 and 32) there are not meaningful interferences with the wing or the stabilizers the forces acting on each section will be assumed to be an algebraic sum of the contribution of the longitudinal axisymmetric flow together with the cross flow contribution due to sideslip, AOA or gusts. In what concerns to fuselage sections 3 and 5, it will be assumed that the lifting surfaces will not enable the cross flow, the only contributions being the longitudinal axisymmetric flow along with the elliptical distribution of lift from the wings and horizontal stabilizer upon the fuselage.

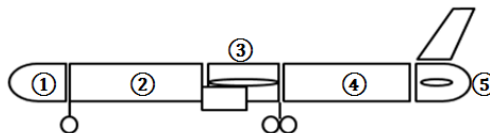


Figure 31 - Different fuselage sections considered – side view.

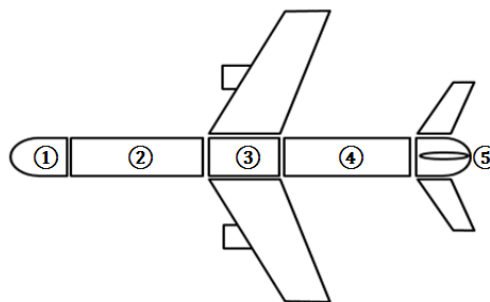


Figure 32 - Different fuselage sections considered – top view.

Despite knowing that by decoupling the airflow hitting the fuselage in its normal and tangential components, the fuselage drag would not be very realistic, it was found to be the only means by which these loads could easily be computed in a conservative fashion. Indeed, in reality, this flow is highly three-dimensional with the tangential airflow component delaying the boundary layer of the normal airflow component separation (see chapter on Future Work).

These effects, together with the pressure loads due to pressure differences on each side of the fuselage skin will complete the aerodynamic contribution of the fuselage. The cross flow acting on the fuselage will contribute to the fuselage bending while the lengthwise stream will tend to increase or decrease the outer pressure, thus changing the local pressurization loads acting at each fuselage cross section.

7.3.2. Fuselage Cross Flow

7.3.2.1. Lateral Force

Assuming no vorticity (cylinder twist) there will only be a drag coefficient associated with the cross flow on the cylinder. There will be a stagnation point – a point where the pressure reaches its peak – which is followed by the boundary layer development under favourable pressure gradient, and hence acceleration until the free stream flow velocity [31]. However, as the rear of the cylinder relative to the cross flow is approached, the pressure must begin to increase. Hence, there is a maximum in the pressure distribution after which the boundary layer is under the influence of an adverse pressure gradient (Figures 33 and 34).

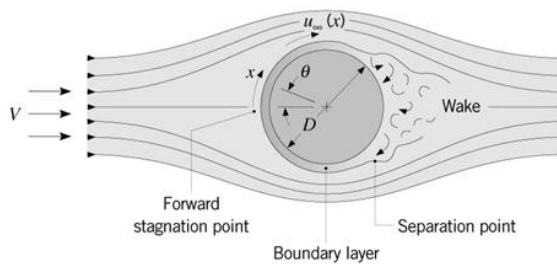


Figure 33 - Schematic of the cross flow around a cylinder [31].

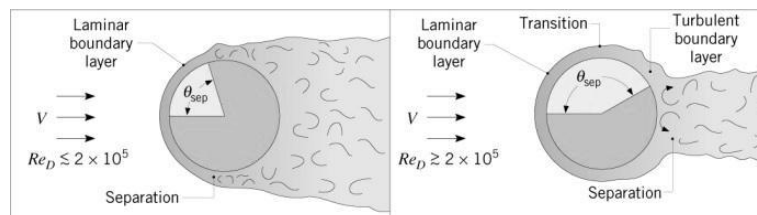


Figure 34 - Possible cross flow configurations around the cylinder [31].

In order to determine the drag coefficient (C_D), and, consequently, the drag force the Reynolds number based on the characteristic dimension (cylinder diameter) (Re_ϕ) must be determined. Indeed, the plot of Figure 35 shows how these two variables are related.

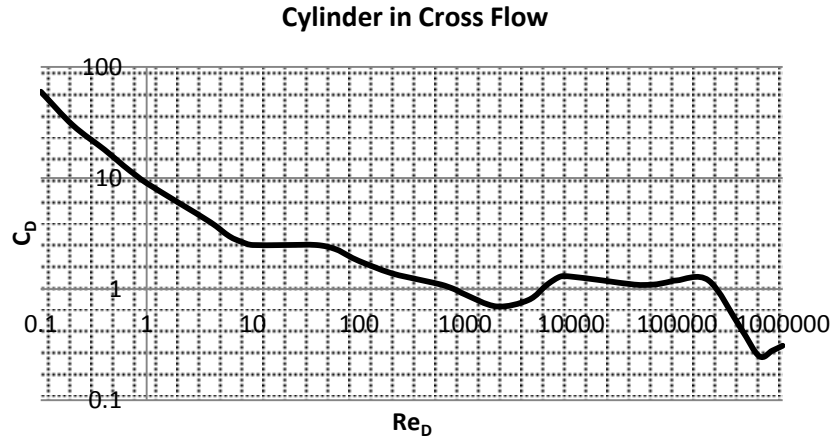


Figure 35 - Experimental relation between the Drag coefficient and the Reynolds number in a cylinder under cross flow [31].

The Reynolds number and drag coefficient are defined in the following manner:

$$Re_\phi = \frac{\rho V \phi}{\mu} \quad (7.3)$$

$$C_D = 2 \frac{F_D}{A_f \rho V^2} \quad (7.4)$$

The variable A_f on equation (7.4) refers to the fuselage's lateral wet area [31].

As stated before this cross flow will only occur at AOA and/or sideslip and different from zero and in the event of gusts. The most critical situation arises from the combination of the maximum AOA, maximum sideslip angle and maximum gust. In such case, the velocity perpendicular to the cylinder may be computed as follows:

$$V_\perp = U_\infty \sqrt{\sin^2 \alpha + \sin^2 \beta} + V_{gust} \quad (7.5)$$

Notice that in the previous equation it has been assumed that the gust was acting on the same direction of the resultant normal components of the AOA and sideslip angle, which comprises the worst case scenario.

7.3.2.2. Pressure Coefficient Distribution

In order to determine the pressure coefficient distribution around the fuselage a cylinder given by a doublet (source and sink) under uniform cross flow assuming potential flow will be considered [15]. This assumption is rather conservative, since the potential flow minimum

pressure coefficient is always smaller than the real minimum. Furthermore, the greater the Reynolds number, the smaller will be the difference between the actual value and the potential flow approximation.

The stream function due to this combination is:

$$\psi_{str} = \frac{\mu}{2\pi r} \sin \theta - V_{\perp} y \quad (7.6)$$

It is shown [23] that the velocity anywhere on the surface of the cylinder is given by:

$$U = 2 \cdot V_{\perp} \cdot \sin \theta \quad (7.7)$$

Making use of Bernoulli's equation⁸ it is possible to determine the pressure p acting on each point of the cylinder's surface as follows:

$$p_{\infty} + \frac{1}{2} \rho V_{\infty}^2 = p + \frac{1}{2} \rho (2 \cdot V_{\perp} \cdot \sin \theta)^2 \quad (7.8)$$

$$C_p^{lat} = 1 - 4 \sin^2 \theta \quad (7.9)$$

From the equation (7.9) it is clear that the pressure coefficient is never less than -3. This limit represents a local pressure drop. Together with the pressure drop due to longitudinal flow – to be discussed next – it will be possible to determine the maximum operational altitude of the aeroplane.

7.3.3. Pressure Distribution on a Body of Revolution in an Uniform Stream

One of the methods to address this problem is the vortex distribution method, applicable to axisymmetric flow, in which the velocity flow field is obtained directly as the solution of an integral equation. However, a much more rapidly computed method (using slender-body theory [32]) gives interesting results, provided that the slender body approximation is valid [32]. The pressure distribution is derived from Bernoulli's equation, which can be written in the form:

$$\frac{p-p_{\infty}}{\rho} = V \cdot \nabla \phi' - \frac{1}{2} (\nabla \phi')^2 \quad (7.10)$$

where ϕ' is the perturbation velocity potential, V is the velocity vector of the free stream relative to the body. For a slender body subject to axisymmetric flow it is shown [32] that on or near its surface:

$$C_p^{long} = \frac{p-p_{\infty}}{\frac{1}{2} \rho U_{\infty}^2} = -2 \frac{u'}{U_{\infty}} - \left[\frac{s'(x)}{2\pi r} \right]^2 + O[r^4 \log(r)] \quad (7.11)$$

⁸ Incompressible flow Bernoulli equation is used because of the low cross flow velocities involved

In particular, the pressure coefficient on the surface of a slender spheroid [32] is:

$$C_p^{long} = \left(\frac{t}{c}\right)^2 \left[\frac{4x^2}{c^2 - 4x^2} + 2 - \log\left(\frac{4c^2}{t^2}\right) \right] \quad (7.12)$$

Where t is the maximum thickness, the longitudinal distance x is measured from the body centre and c is the fuselage length. It is shown that there is a reasonably good agreement between the exact results and the slender-body theory approximation, especially when the body has got a high aspect ratio, as theoretically forecasted.

On the contrary of what has been done in the cross flow acting the fuselage, where it was assumed that that contribution was only meaningful in the fuselage sections 1, 2 and 4, now the fuselage must be treated as a whole, since the lengthwise flow acts it all.

7.4. Combined Loads on the Fuselage

From the pressurization chart (Figure 29), it is known the maximum static pressure difference that a particular fuselage withstands. However this does not automatically enable the computation of the maximum operating altitudes of the aircraft because the aerodynamic effects do also contribute to change the local static pressure in the outer side of the fuselage. This means that the operating altitude will end up being smaller than the one computed without accounting for the aerodynamics of the fuselage.

The maximum inner fuselage static pressure is specified in the legislation (p_{in}). The relief valve setting pressure difference (Δp) is available on the aircraft flight manual. From these two the minimum outer static skin pressure can be determined. Finally, after computing the maximum dynamic pressure around the fuselage it is possible to determine the stagnation or total pressure ($p_{0\infty}$), which will be the same everywhere, since the flow is regarded as isentropic.

$$p_{out} = p_{in} - \Delta p \quad (7.13)$$

$$p_{0\infty} = p_{out} + \frac{1}{2}\rho(U_\infty^2 C_p^{long} + V_\perp^2 C_p^{lat}) \quad (7.14)$$

The static pressure in the undisturbed flow region will coincide with the stagnation pressure, since the dynamic pressure is null. Using ISA's expression to determine the aircraft ceiling:

$$H_{max} = \frac{T_0}{0.0065} \left[\left(\frac{p_{0\infty}}{p_0} \right)^{\frac{1}{5.2561}} + 1 \right] \quad (7.15)$$

Depending on the type of fuselage section being addressed, different loads may be present. Nevertheless all sections will be subject to shear stresses, bending moments, torsion

as well as pressurization loads. Table 9 identifies the causes of each type of loading for each fuselage section. Notice that it has been assumed that the wings were connected to fuselage section 3 (F3), the main landing gear is attached to the wings and the nose landing gear is attached to fuselage section 1 (F1).

Table 9 - Different loads acting on each fuselage section.

Fuselage		Type of Loads		
Section	Shear Stress	Bending Moment	Torsion	Pressurization
F1	Nose gear, β_{slip} , α , F2	Nose gear, β_{slip} , α , F2	Nose gear, F2	Working on all fuselage sections (depending on altitude)
F2	β_{slip} , α , F1, F3	β_{slip} , α , F1, F3	F3	
F3	Wing, β_{slip} , α , F2, F4	Wing, β_{slip} , α , F2, F4	Wing, F2, F4	
F4	β_{slip} , α , F3, F5	β_{slip} , α , F3, F5	F3, F5	
F5	Tails, β_{slip} , α , F4	Tails, β_{slip} , α , F4	Tails	

8. Miscellaneous loads analysis

The term «miscellaneous loads» refers to loads required to design non-primary aircraft structure, thus encompassing a wide range of aeroplane components and systems. Now that the major structural component loads due to gust, manoeuvre and ground conditions load considerations must be given to everything the aeroplane, either inside or outside. Indeed, the structural failure of minor components can prove fatal.

The number of items to be covered is so large that it is not possible to discuss them all herein. The following is a partial list of types of miscellaneous loads:

- Ground handling;
- Control surface;
- Doors;
- Pressure;
- Nose;
- Fluid system;
- Seat and floor;
- Auxiliary Power Unit;
- Environmental Control System;
- Jacking and mooring;
- Fixed leading edge;
- Engine and gear;
- Antenna;
- Ram air turbine;

A great number of new structures and mechanisms are placed in the cockpit when OGMA performs aircraft upgrades and/or modifications. Hence, a careful study of all the possible loadings acting on the cockpit gains particular relevance in the current work. The maximum and minimum load factors at the aeroplane CG must be combined with the load factors due to pitching, yawing and rolling acceleration.

9. Results – Case Study

In order to test the *Microsoft Excel*® workbooks throughout this study, the *Lockheed C-130* will be studied. An Instructions Manual⁹ has been created to facilitate the user's task when handling those workbooks. The reader is encouraged to study it before looking at the results obtained to be aware of its architecture, inputs, outputs and read chapter 1 to 8 to know the assumptions that underlie each result.

9.1. Presentation of the Lockheed C-130

The C-130 (Figure 36) was not only chosen for its historical relevance, but also for representing the bulk of the military work at OGMA. Indeed, OGMA, *Indústria Aeronáutica de Portugal*, SA, manages the French Air Force C-130 fleet also working for many other clients like the Portuguese Air Force, the Belgian Air Component, the U.S. Air Force, the Spanish Air Force the Algerian Air Force, the Libyan Air Force, the Moroccan Air Force, the Tunisian Air Force, among many other African Air Forces.



Figure 36 - Lockheed C-130H (Portuguese Air Force).

The C-130 is not a single aircraft, but rather a family of aircrafts. The *Lockheed C-130* family is without a single doubt one of the most remarkable family of military aircrafts ever built. Since the flight of its first prototype in 1954 in California 40 different models of this aircraft have been built. Today, the C-130 is operated in more than 50 countries worldwide and is about to commemorate a record of 54 years in service. The C-130 is seen as one of the most versatile aircrafts ever built with very good performances.

Despite being a military aircraft – which means the certification authority is the respective Air Force – the results presented next were obtained making use of EASA's CS-25. It is not uncommon that the Air Forces demand the design organizations to follow several specifications for civilian aeroplanes.

⁹ See appendix E

9.2. Lockheed C-130 Specifications

In order to make use of the Microsoft Excel® workbooks developed throughout this study, a number of inputs variables must be known¹⁰. In the Tables 10-14 it is possible to find the most relevant parameters of the C-130H.

Table 10 - C-130H external dimensions [33].

External Dimensions	SI units	US units
Overall Length	30.33 m	99.5 ft
Overall Height	11.66 m	38.25 ft
Wheel Track	4.34 m	14.25 ft

Table 11 - C-130H Aerodynamic and Engines data [28].

Other Variables	
Wing root aerofoil	NACA 64A318
Wing tip aerofoil	NACA 64A412
Horizontal tail aerofoil	NACA 23012 (Modified)
Vertical tail aerofoil	NACA 64A015
Engines	(4x) ALLISON T56-A-7 GAS TURBINE, MODEL NO. 501- D8

In order to determine the zero lift angle of each of the C-130H aerofoils, several 2D aerofoil simulations were ran on XFLR5. Given that this commercial software is regarded as very accurate for low Reynolds [40] number analysis – and given the relatively low C-130 cruise speed – it was found to be an acceptable way of estimating the zero lift angle of each of its aerofoils⁶.

Table 12 - C-130H performance data [28].

Performance	SI units	US units
Empty Weight	34,274 kg	75,562 lbs
MTOW	70,305 kg	155,000 lbs
MLW	58,965 kg	130,000 lbs
Maximum Operating Altitude	10,668 m	35,000 ft

¹⁰ See appendix C

Table 13 - C-130H main materials density [34].

Materials Density	SI units	US units
7075 Aluminium Alloy	2,795.7 kg/m ³	0.101 lbs/in ³
2024 Aluminium Alloy	2,768.0 kg/m ³	0.100 lbs/in ³
316 Stainless Steel	8,000.0 kg/m ³	0.289 lbs/in ³

Since a significant portion of data concerning a military aeroplane as the C-130 is classified information, it was impossible to have an exact weight distribution along the wing, horizontal tail and vertical tail spanwise stations as well as along the fuselage's lengthwise positions. However, as the aeroplane's MTOW, structural weight and fuel weight are known, some estimates could be obtained¹¹.

The results obtained from these estimated are summarized on Table 14.

Table 14 - Weight Estimates [28].

	Weight (kg)	Weight (lbs)
Maximum Take-off Weight	70,300	155,000
Empty Weight	34,400	75,800
Payload	28,100	62,000
Fuel weight	7,800	17,200
Weight/Engine	900	1,984
Wing weight* (Including engines)	7,000	15,500
Horizontal tail weight*	1,400	3,000
Vertical tail weight*	730	1,600
Fuselage weight* (including landing gears)	16,250	35,800
* Estimates		

9.3. Results

The mass discretization and the loadings that may act on each point of the aeroplane in the limit manoeuvring conditions have been estimated. The shear, bending and torsion for each aeroplane part studied will now be plotted – wing, fuselage, horizontal tail and vertical tail.

¹¹ See appendix C

9.3.1. Landing Gear Loads

9.3.1.1. Landing Loads

The landing gear loads due to landing have already been discussed. The maximum loads are presented on Table 15. The reader should note that these values are highly dependent on the spring constant (k) and on the damping coefficient (C). Unfortunately, it was impossible to find out the true values for the landing gear for the C-130H, which means the following values are not comparable with the ground loads to determine the actual maximum loads acting on the landing gear system.

Table 15 - Maximum Loads due to landing impact on each landing gear.

Landing Gear	Variable	Maximum Value [N]
Nose Gear	V_z	3.28×10^5
	V_x	1.24×10^5
	V_y	1.99×10^5
Main Gear (Right)	V_z	1.70×10^6
	V_x	5.74×10^5
	V_y	5.23×10^5
Main Gear (Left)	V_z	1.70×10^6
	V_x	5.74×10^5
	V_y	5.23×10^5

9.3.1.2. Ground Loads

After having computed the values for all the possible ground loads to which the landing gear may be subject to, it is possible to obtain the loads summarized on Table 16.

Table 16 - Maximum ground loads acting on the landing gears.

Landing Gear	Variable	Maximum Value [N]
Nose Gear	V	3.85×10^5
	D	0
	S	2.17×10^5
Main Gear (Right)	V	4.26×10^5
	D	2.79×10^5
	S	6.81×10^4
Main Gear (Left)	V	4.26×10^5
	D	2.79×10^5
	S	6.81×10^4

Notice that the values for the left and right main gears are the same since it has been assumed that the aeroplane's CG coincides with its plane of symmetry.

9.3.2. Wing Loads

As discussed in Chapter 2, the critical wing limit loading conditions are the ones referring to the minimum and maximum load factors at each design speed (PHAA, PLAA, NHAA and NLAA). Each stringer and longeron is thus designed for the maximum tension or compression of each of these conditions. It is usually common place to neglect other conditions since the structure withstands almost all intermediate loadings provided it bears these limit loads.

In the *Microsoft Excel*® workbooks developed¹² the user is just required to input the speed at which he wants to evaluate the limit loading conditions, and the *Microsoft Excel*® workbooks do automatically calculate the maximum and limit load for each velocity. Notice that each velocity corresponds to a different value of the wing angle of attack – PHAA and NHAA at manoeuvring speed (V_A) and PLAA and NLAA at design dive speed (V_D).

The plots presented below refer to the loadings in the wing's half-wingspan. As expected the maximum wing loadings are found at the wing root, while both the shear forces and bending moment are null at its free tips.

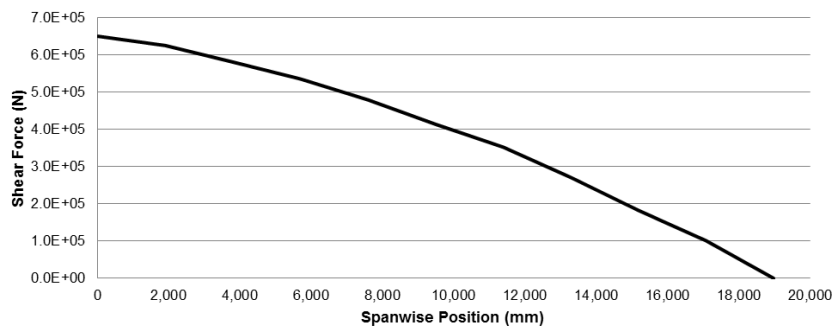


Figure 37 - Wing maximum shear force on the vertical plane – ($n_z = n_{z_{max}}$).

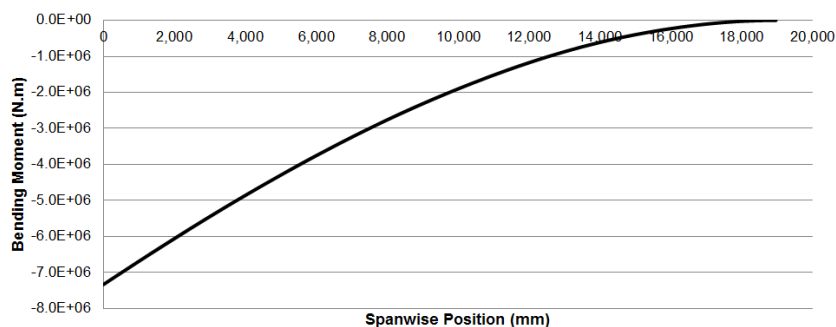


Figure 38 - Wing maximum bending moment on the vertical plane – ($n_z = n_{z_{max}}$).

¹² See appendixes D and E

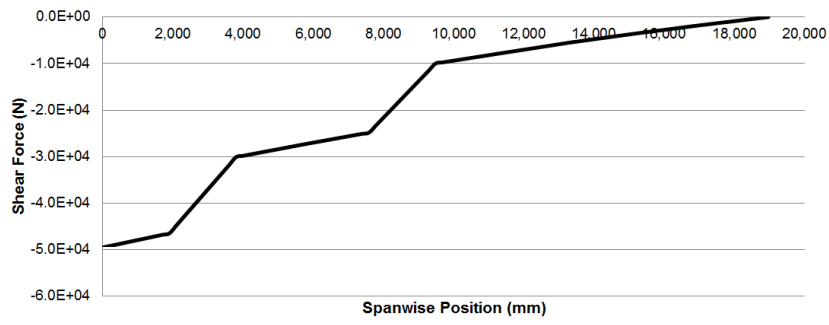


Figure 39 - Wing maximum shear force on the vertical plane – static ground condition.

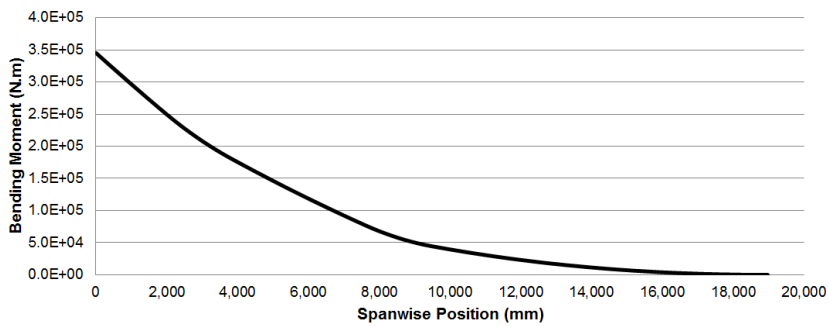


Figure 40 - Wing maximum bending moment on the vertical plane – static ground condition.

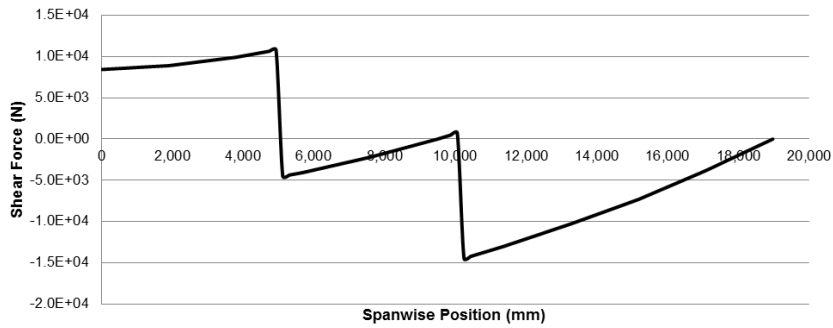


Figure 41 - Wing maximum shear force on the horizontal plane - ($n_z = n_{z_{max}}$).

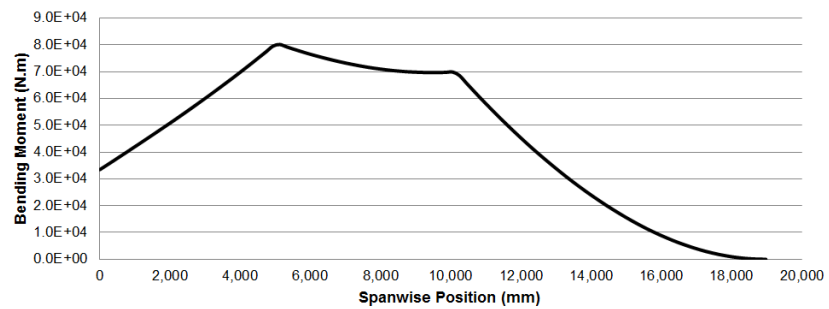


Figure 42 - Wing maximum bending moment on the horizontal plane ($n_z = n_{z_{max}}$).

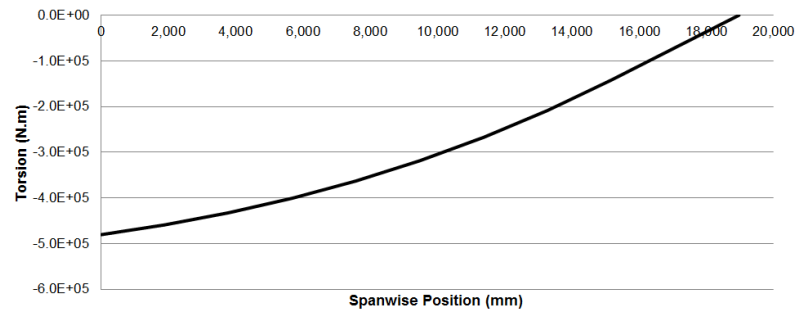


Figure 43 - Wing maximum pitching moment (torsion) – ($n_z = n_{z_{max}}$).

9.3.3. Horizontal Tail Loads

In accordance with what was discussed in Chapter 5, the horizontal tail loads have been determined. After performing the estimates for the spanwise load distributions for each of the conditions under study, the maximum and minimum values for the lift, drag and moment are plotted next.

The plots presented below refer to the loadings in the horizontal tails' half-wingspan. The plots are similar to the ones presented for the wing except that there are no discontinuities due to engine weight or propulsive force.

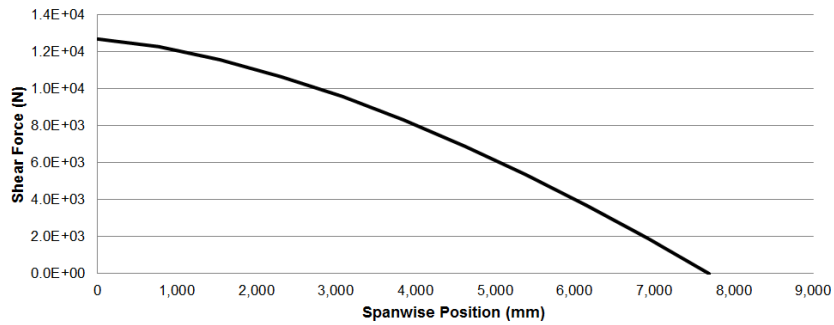


Figure 44 - Horizontal tail maximum shear force on the vertical plane.

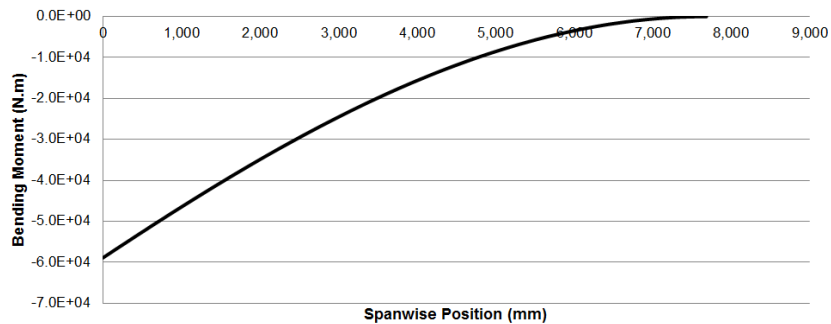


Figure 45 - Horizontal tail maximum bending moment on the vertical plane.

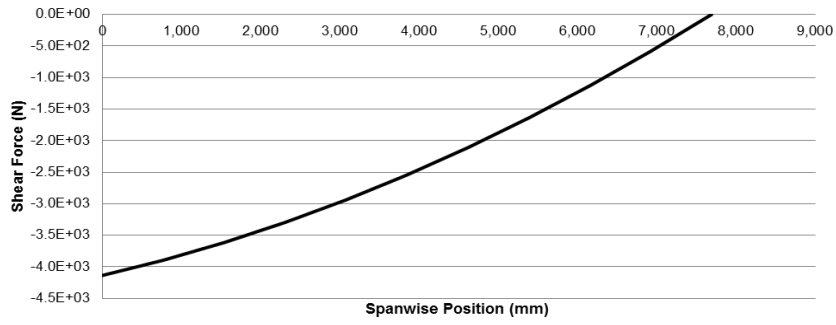


Figure 46 - Horizontal tail maximum shear force on the horizontal plane.

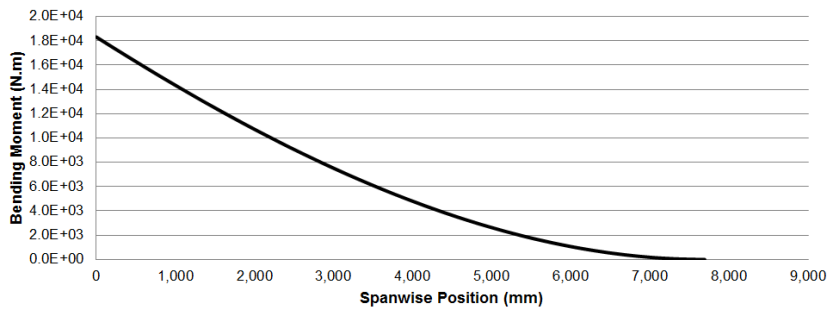


Figure 47 - Horizontal tail maximum bending moment on the horizontal plane.

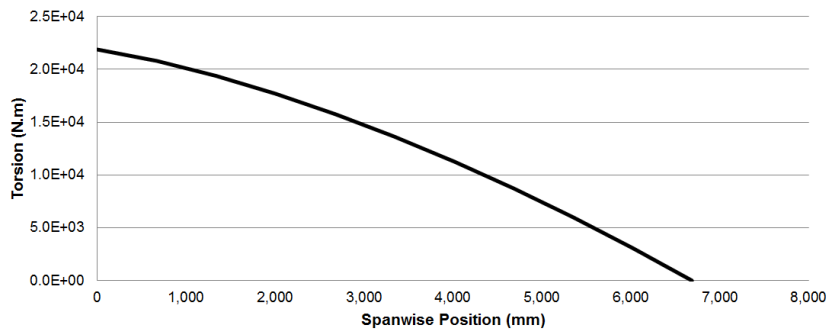


Figure 48 - Horizontal tail maximum torsion.

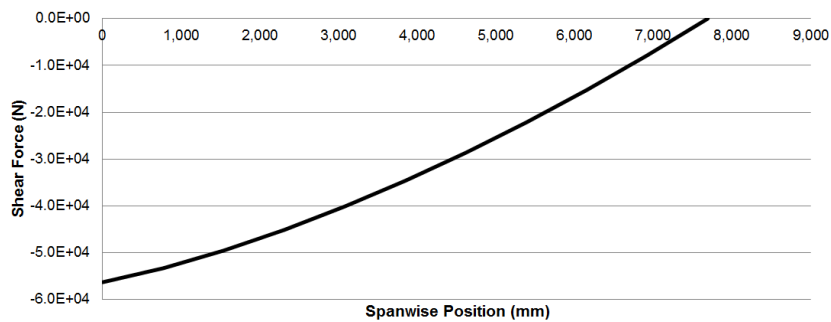


Figure 49 - Horizontal tail minimum shear force in the vertical plane.

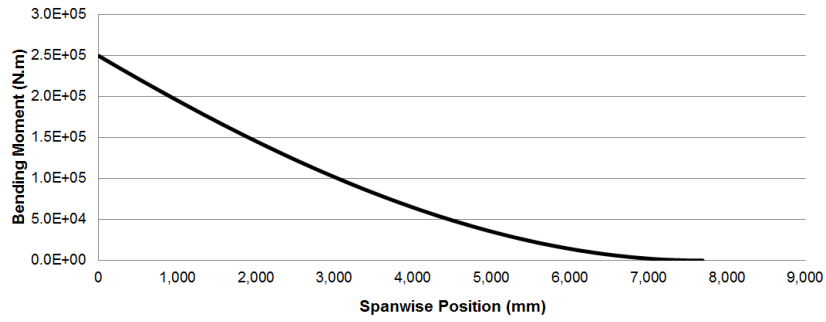


Figure 50 - Horizontal tail minimum bending moment in the vertical plane.

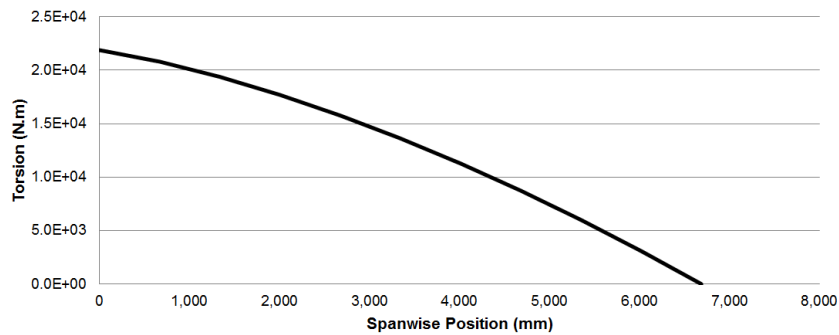


Figure 51 - Horizontal tail minimum torsion.

9.3.4. Vertical Tail Loads

As discussed in Chapter 6, the vertical tail loads must be computed for Manoeuvres I, II and III [1], as well as for the engine-out conditions, both with zero rudder deflection and zero sideslip angle. After performing the estimates for the spanwise load distributions for each of these five conditions, the maximum values for the lift, drag and moment are plotted next. In the particular case of the vertical tail, and due to its symmetry, the maximum values are the same regardless of the rudder deflection direction. These plots presented refer to the maximum spanwise load distribution in the normal plane, where only the side lifting force generated by the rudder deflection is accounted for.

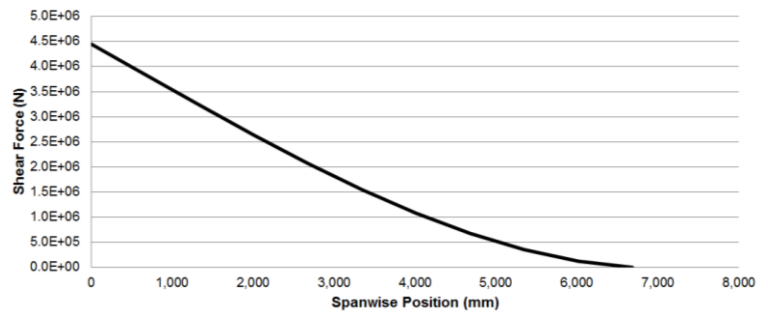


Figure 52 - Vertical tail maximum shear force in the normal plane (spanwise distribution).

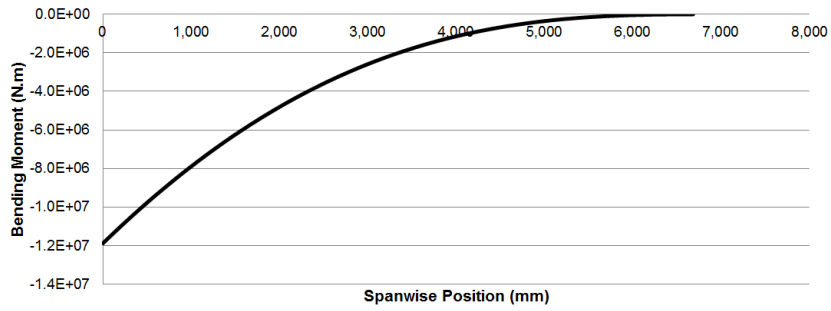


Figure 53 - Vertical tail maximum bending moment in the normal plane (spanwise distribution).

The plot with the spanwise shear force and bending moment on the vertical plane oriented along the undeflected vertical stabilizer chord direction are shown. The drag force is the only force acting in this direction.

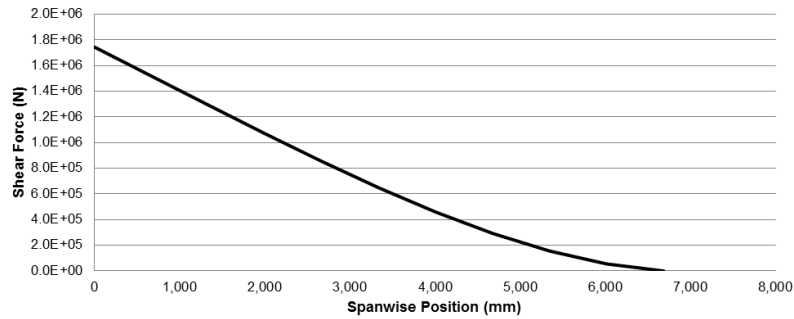


Figure 54 - Vertical tail maximum shear force in the vertical plane (spanwise distribution).

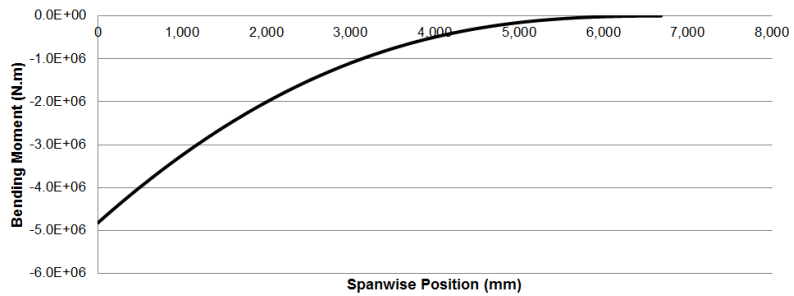


Figure 55 - Vertical tail maximum bending moment in the vertical plane (spanwise distribution).

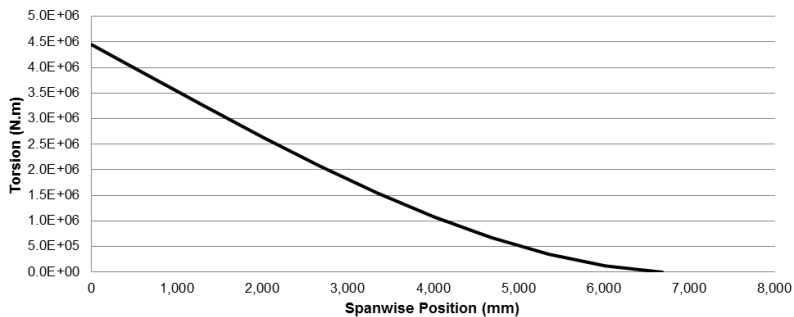


Figure 56 - Vertical tail maximum torsion (spanwise distribution).

9.3.5. Fuselage Loads

The maximum and minimum load factors conditions already presented for the wing are important limit loading conditions for the fuselage as well. Of particular relevance for the fuselage loading are the empennage loads. Indeed, the limit load conditions for the horizontal and vertical tail can prove to be design conditions for the fuselage. The maximum pressurization loads can easily be determined from the aeroplane's flight manual pressurization chart. In what refers to torsion, the critical conditions will arise in a 1-point landing condition or when the aeroplane banks, depending on the landing gear positioning relative to the fuselage structure. For the C-130H under study it is not clear which of these two is the critical condition for the fuselage torsion, once the main landing gear is attached to the fuselage, which results in a smaller moment in the 1-point landing condition than in the case of a wing-mounted main landing gear.

The reader should note that much more loading combinations can be studied and plotted in order to determine the actual critical loads, which will work as important design drivers. Figure 57 shows the shear force distribution along the fuselage length for a unitary load factor. It's perceptible that the structural weight acts downwards, as well as the horizontal tail (to have a balanced aeroplane), while the wing generates a lift force equal to the sum of the structural weight, fuel and payload plus the downwards vertical force generated by the horizontal tail. Notice that the boundary conditions of free tips – zero shear force – is met.

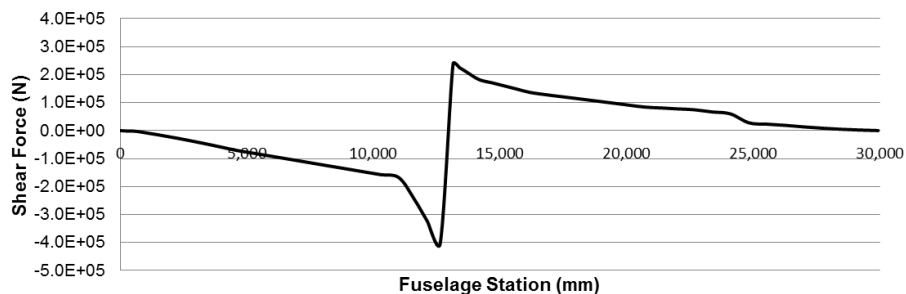


Figure 57 – Fuselage shear force in level flight (lengthwise distribution).

Figure 58 plots the fuselage lengthwise bending moment distribution is shown. Once again, idealizing the fuselage as beam (free at its tips) demands zero bending moment at its tips (as verified). Furthermore, it becomes clear that the fuselage central section will withstand the higher loads.

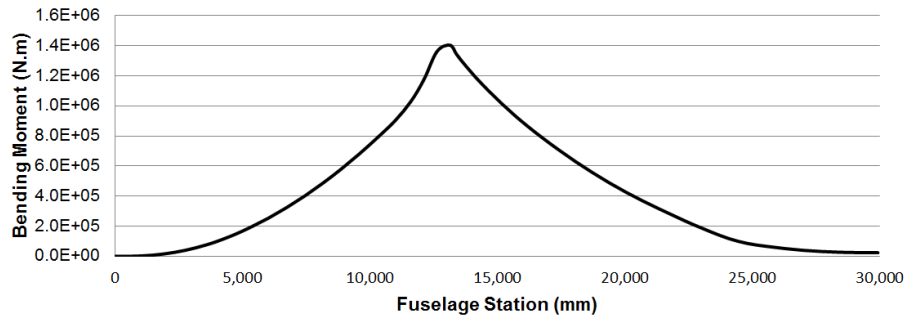


Figure 58 - Fuselage bending moment in level flight (lengthwise distribution).

Using a similar approach, it is possible to determine the shear force and bending moment distribution in flight conditions involving higher loads – maximum and minimum admissible load factors.

9.4. Validation

Although the purpose of this master thesis was to work with loads without working with stresses, it must be noticed that the best means to validate the results presented so far is to determine the maximum tensile stresses working on the C-130 structure to evaluate if these values were in the order of magnitude of the tensile stress of its materials.

Some simple equations – with conservative assumptions – relating the bending moment and the maximum tensile stress were used [22]. The results were found to be within the expected range of the order of magnitude of the 2024 and 7075 aluminium alloys tensile stresses and below these values, as required ($\sigma_{UTS} \approx 215MPa$ for the 2024 and $\sigma_{UTS} \approx 400MPa$ for the 7075).

10. Conclusions and Future Work

10.1. Conclusions

Structural loads analysis is an everyday procedure for design companies all over the world. Not only the aircrafts' manufacturer companies, but also companies operating design modifications on aeroplanes. In order to enhance the methods to perform structural load analysis analytical methods capable of providing trustworthy estimates have been presented. With these methods the Loads Engineers can validate computational data in a faster way, at the same time all the load analysis process becomes more reliable, which can ultimately lead to lower costs and more productivity.

The generic set *Microsoft Excel*® workbooks developed throughout a six month curricular internship at *OGMA, Indústria Aeronáutica de Portugal, SA* enables determining the static loads acting on most of the aircraft to which the company's Engineering, Design and Modifications Office works with, namely the *Lockheed Hercules C-130, Lockheed Orion P3, Embraer 134/145* and all *Airbus A320 family*. So as to ease the handler's use of the *Microsoft Excel*® workbooks developed, an Instructions Manual is attached to this report. Reading this manual as well as the current report is a request for anyone wanting to work with these workbooks.

In order to perform a first real test of these methods, a case study was performed. This was done by inputting the geometry, mass properties and operating conditions of the Hercules C-130H. The results presented were found to be both qualitatively correct from the graphics observation and quantitatively plausible. On the one hand, the respect of the boundary conditions and the correct algebraic sign of each variable corroborate the qualitative agreement of the solutions. On the other hand, the stress analysis checks performed mean that these results are assuredly not far from the real ones. A more detailed validation would require the use of computational fluid dynamics and/or finite element method softwares.

10.2. Future Work

10.2.1. Improve the Fuselage's Aerodynamics

To perform a comprehensive study of the complex flow structure around the fuselage therefore computing in a more accurate way the drag acting on it instead of decoupling the flow in its normal and tangential components as was herein done is surely the best enhancement of the *Microsoft Excel*® workbooks developed so far.

10.2.2. Miscellaneous Loads Analysis

Now that the major structural component loads have been covered load considerations must be given to everything in the aeroplane, either inside or outside. Indeed, the structural failure of minor components can prove to be fatal. The number of items to be covered is so large that it is almost impossible to number them all herein. The following is a partial list of types of miscellaneous loads:

- Engine loads;
- APU loads;
- Load factor distribution;
- Pressurized cabin loads;
- Maximum angular rates and accelerations;
- Gyroscopic loads;
- Emergency landing conditions;
- Fuel pressures;
- Landing gear doors loads;
- Dorsal fin loads;
- Auxiliary aerodynamic surfaces loads;
- Structural ditching provisions

10.2.3. Dynamic Analysis

In order to make this tool complete, it must also encompass a dynamic analysis. Given that the mass discretization implementation has already been completed, this work can be used to perform the below listed analysis making this work a rather robust and full-bodied tool.

- Continuous Turbulence Design Criteria (CS-25/FAR-25);
- Free vibration;
- Modal analysis;
- Aeroelasticity;
- Flutter.

10.2.4. Stress Analysis

Another interesting step following the current work is to adopt a simplified stress analysis which is always the step that comes after any load analysis.

The most common method is to assume that every aeroplane main structural component, (e.g. fuselage, wings, stabilizers) are beams and that all the shear stresses are carried by their walls (skin), while the normal stresses due to structural bending are carried by

concentration of areas that represent stringers and spar flanges called booms. See reference [22]. It must be noticed however that this structural idealization is a function of the already known loads acting on each main component.

10.2.5. Final Statement

The author of this work is available to share information and introduce any interested student to pursue any of the formerly mentioned future working plans. The Instructions Manual (appendix E of this report) may also help on the *Microsoft Excel*® workbooks architecture's understanding.

References

- [1] **Certification Specifications for Large Aeroplanes (CS-25) – Subpart C – Structure**, European Aviation Safety Agency, 2009.
- [2] **Federal Aviation Regulations for Large Airplanes (FAR-25) – Subpart C – Structure**, Federal Aviation Administration, 2011.
- [3] SULEMAN, Afzal, **Acetatos de Projeto Aeroespacial**, Instituto Superior Técnico – Universidade Técnica de Lisboa, 2010.
- [4] DAVIES, Mark, **The Standard Handbook for Aeronautical and Astronautical Engineers**, McGraw-Hill, 2002.
- [5] LOMAX, Ted L.; **Structural Load Analysis for Commercial Transport Aircraft: Theory and Practice**, AIAA, 1996.
- [6] CUNHA, Filipe; **Acetatos de Estruturas Aeroespaciais**, Instituto Superior Técnico – Universidade Técnica de Lisboa, 2008.
- [7] SULEMAN, Afzal, **Folhas de Estruturas Aeroespaciais**, Instituto Superior Técnico – Universidade Técnica de Lisboa, 2006.
- [8] JOHNSON, Wally; JAMES, E. Locke; **Aircraft Structural Loads: Requirements Analysis, Testing & Certifications**, University of Kansas, 2005.
- [9] MAIA, Nuno; MONTALVÃO, Júlio; **Vibrações e Ruído**, Instituto Superior Técnico – Universidade Técnica de Lisboa, 2011.
- [10] BEARDS, C.E.; **Structural Vibration: Analysis and Damping**, ARNOLD, 1996.
- [11] HARRIS, Cyril M.; PIERSOL, Allan G., **Harri's Shock and Vibration Handbook**, McGraw Hill, 2002.
- [12] BEER, Ferdinand; JOHNSTION, Russel; EISENBERG, Elliot; **Vector Mechanics for Engineers – Dynamics**, 2004.
- [13] **Advisory Circular 25.491-1**, U.S. Department of Transportation, Federal Aviation Administration, 2000.
- [14] CORKE, Thomas C.; **Design of Aircraft**, Prentice Hall, 2002.
- [15] BREDERODE, Vasco de, **Fundamentos de Aerodinâmica Incompressível**, Edição do Autor, Instituto Superior Técnico – Universidade Técnica de Lisboa, 1997.
- [16] GUTFINGER, Chaim; PNUELI, David; **Fluid Mechanics**, Cambridge University Press, 1997.
- [17] EÇA, Luís de; **Acetatos de Aerodinâmica I**, Instituto Superior Técnico – Universidade Técnica de Lisboa, 2010.
- [18] ANDERSON, John D.; **Modern Compressible Flow with Historical Perspective**, McGraw-Hill, 2003.
- [19] PEREIRA, J. C. Fernandes; **Aerodinâmica II, Volume 2**, Engenharia Aeroespacial, Instituto Superior Técnico – Universidade Técnica de Lisboa, 2011.
- [20] REDDY, J. N.; **An Introduction to the Finite Element Method**, McGraw-Hill International Edition, 2006.

- [21] BISPLINGHOFF, Raymond L.; Holt Ashley and Robert L. Halfman, **Aeroelasticity**, DOVER, 2003.
- [22] MEGSON, **Aircraft Structures for Engineering Students**, Fourth Edition, ELSEVIER, 2006.
- [23] OBERT, Ed; **Aerodynamic Design of Transport Aircraft**, Technical University of Delft, 2009.
- [24] WEISSINGER, J. ; **The Lift Distribution of Swept Back Wings**, NACA Technical Memorandum No. 1120 (translation from Uber die Auftriebsverteilung von Pfeilflugeln Forschungsbericht No. 1553), 1947.
- [25] STINTON, Barrol, **The Anatomy of the Aeroplane**, BSP, 1966.
- [26] STINTON, Barrol, **The Design of the Aeroplane**, BSP, 1983.
- [27] ETKIN, Bernard; **Dynamics of Flight – Stability and Control**, JOHN WILEY & SONS, INC, 1996.
- [28] **Flight Manual – Hercules C-130H Model**, Lockheed, 2004.
- [29] NIU, Michael; **Airframe Structural Design**, Hong Kong Conmilit Press LTD, 2006.
- [30] MULTHOFF, H.; **Aerodynamics of the Fuselage**, NACA Technical Memorandum No. 1036, (Luftfabrtforschung Vol. 18, No. 2-3, March 29, 1941 Verlag von R. Oldenbourg, Munchen und Berlin), 1941.
- [31] LAVINE, Bergman; DEWITT, Incropera; **Fundamentals of Heat and Mass Transfer**, Sixth Edition, WILEY, 2006.
- [32] THWAITES, Bryan; **Incompressible Aerodynamics – An Account of the Theory and Observation of the Steady Flow of Incompressible Fluid Past Aerofoils, Wings and Other Bodies**, DOVER PUBLICATIONS, INC, 1960.
- [33] **Structural Repair Instructions – Hercules C-130**, Technical Manual, Lockheed, 2005.
- [34] **Metallic Materials Properties Development and Standardization (MMPDS)**, U.S. Department of Transportation, Federal Aviation Administration, 2003.
- [35] LAGE, Yoann Eras; **Análise Estrutural à Asa de uma aeronave Lockheed Martin C-130H**, Dissertação de Mestrado em Engenharia Aeroespacial, Instituto Superior Técnico, 2009.
- [36] **T56-A-15LFE MAINTENANCE MANUAL**, Rolls-Royce, 2003.
- [37] HILL, Philip; PETERSON, Carl; **Mechanics and Thermodynamics of Propulsion**, PEARSON, 1992.
- [38] **XFLR5 – Analysis of foils and wings operating at low Reynolds number**, 2009.
- [39] BEER, Ferdinand; DEWOLF, John; JOHNSTON, Russell; MAZUREK, David; **Mechanics of Materials**, McGraw Hill, 2011.
- [40] LOURENÇO, Bernardo; **Damage Tolerance Design**, Dissertação de Mestrado em Engenharia Aeroespacial, Instituto Superior Técnico, 2010.
- [41] GUSTON, Bill; **The Cambridge Aerospace Dictionary**, Cambridge University Press, 2004.

Appendix A. EASA CS-25 Inertial Loads

Table C. 1 - EASA Certification for Large Aeroplanes (CS 25) Load factors specifications [1].

Type of Load	Direction	LOAD FACTORS					
		Limit	× Safety	Ultimate	× Special	Static Test	Critical Static Test
Manoeuvring	Forward	–	–	–	–	–	–
	Down	A	1.5	1.5 A	–	1.5 A	1.5 A
	Side	–	–	–	–	–	–
	Up	B	1.5	1.5 B	–	1.5 B	1.5 B
	Rear	C	1.5	1.5 B	–	1.5 B	–
Gust	Forward	–	–	–	–	–	–
	Down	D	1.5	1.5 D	–	1.5 D	–
	Down*	E	1.5	1.5 E	–	1.5 E	1.5 E
	Side	F	1.5	1.5 F	–	1.5 F	1.5 F
	Up	G	1.5	1.5 G	–	1.5 G	–
	Rear	–	–	–	–	–	–
Ground	Forward	H	1.5	1.5 H	–	1.5 H	1.5 H
	Down	I	1.5	1.5 I	–	1.5 I	–
Ultimate Inertia Loading for Emergency Landing Condition (CS 25.561)	Forward	Already Prescribed as Ultimate		9.0g	–	–	–
	Down			6.0g	–	–	–
	Side**			3.0g	–	–	–
	Side***			4.0g	–	–	–
	Up			-3.0g	–	–	–
	Rear			1.5g	–	–	–
Ultimate Inertia Loading for Emergency Landing Condition For Seat, Litter & Berth Attachment to Aircraft Structure (CS 25.561)	Forward	Already Prescribed as Ultimate		9.0g	1.33	12.0g	12.0g
	Down			6.0g	1.33	8.0g	8.0g
	Side**			3.0g	1.33	4.0g	4.0g
	Side***			4.0g	1.33	5.3g	5.3g
	Up			-3.0g	1.33	-4.0g	-4.0g
	Rear			1.5g	1.33	2.0g	2.0g

* For locations aft of fuselage
 ** Airframe
 *** Seats and attachments
 Constants 'A' to 'I' are a function of the aeroplane under study.
 'g' refers to the gravitational acceleration.

Appendix B. Landing Gear Shock

A. Overdamped System ($\xi > 1$)

In the case when the damping force is dominant, the roots of the equilibrium equation will be:

$$s_{1,2} = -\omega_n \xi \pm \sqrt{\xi^2 - 1} \quad (\text{B. 1})$$

The solution will be of the form:

$$x(t) = e^{-\xi \omega_n t} (C_1 e^{\omega_n \sqrt{\xi^2 - 1} t} + C_2 e^{-\omega_n \sqrt{\xi^2 - 1} t}) \quad (\text{B. 2})$$

Using Euler's formulas for the hyperbolic cosine and sine:

$$\cosh(y) = \frac{e^{-y} + e^y}{2} \quad (\text{B. 3})$$

$$\sinh(y) = \frac{e^{-y} - e^y}{2i} \quad (\text{B. 4})$$

$$x(t) = e^{-\xi \omega_n t} \left[A_1 \cosh(\omega_n \sqrt{\xi^2 - 1} t) + A_2 \sinh(\omega_n \sqrt{\xi^2 - 1} t) \right] \quad (\text{B. 5})$$

After applying the initial conditions for the displacement and velocity, the expression becomes:

$$x(t) = e^{-\xi \omega_n t} \left[x(0) \cosh(\omega_n \sqrt{\xi^2 - 1} t) + \frac{\dot{x}(0) + \xi \omega_n x(0)}{\omega_n \sqrt{\xi^2 - 1}} \sinh(\omega_n \sqrt{\xi^2 - 1} t) \right] \quad (\text{B. 6})$$

B. Underdamped System ($\xi < 1$)

If the inertial and spring forces proof dominant over the damping force, the roots of the equilibrium equations will be.

$$s_{1,2} = -\omega_n \xi \pm i \omega_n \sqrt{1 - \xi^2} \quad (\text{B. 7})$$

The solution will be of the form:

$$x(t) = e^{-\xi \omega_n t} (C_1 e^{i \omega_n \sqrt{1 - \xi^2} t} + C_2 e^{-i \omega_n \sqrt{1 - \xi^2} t}) \quad (\text{B. 8})$$

Using Euler's formulas for the cosine and sine:

$$\cos y = \frac{e^{-iy} + e^{iy}}{2} \quad (\text{B. 9})$$

$$\sin y = \frac{e^{-iy} - e^{iy}}{2i} \quad (\text{B. 10})$$

$$x(t) = e^{-\xi \omega_n t} \left[A_1 \cos(\omega_n \sqrt{1 - \xi^2} t) + A_2 \sin(\omega_n \sqrt{1 - \xi^2} t) \right] \quad (\text{B. 11})$$

After applying the initial conditions, this expression becomes:

$$x(t) = e^{-\xi \omega_n t} \left[x(0) \cos(\omega_n \sqrt{1 - \xi^2} t) + \frac{\dot{x}(0) + \xi \omega_n x(0)}{\omega_n \sqrt{1 - \xi^2}} \sin(\omega_n \sqrt{1 - \xi^2} t) \right] \quad (\text{B. 12})$$

C. Critically Damped System ($\xi = 1$)

In this case, the roots of the equilibrium equation will be:

$$s_{1,2} = -\frac{c}{2m} \quad (\text{B. 13})$$

The solution will be of the form:

$$x(t) = C_1 e^{-\omega_n t} + C_2 t e^{-\omega_n t} \quad (\text{B. 14})$$

After applying the initial conditions (see subsection 3.1.1), this expression becomes:

$$x(t) = e^{-\omega_n t} [x(0)(1 + \omega_n t) + \dot{x}(0)t] \quad (\text{B. 15})$$

Appendix C. Lockheed Martin C-130H – Specifications

Table C. 2 – Performance [35].

Performance	SI units	US units
V_C	151.9 m/s	498.4 ft/s
V_D	227.9 m/s	747.6 ft/s

Table C. 3 - Engine Data [28] [36]

Engines	SI units	US units
Inboard engine (y_1)	4,978.4 mm	196.0 in
Inboard engine (z_1)	3,890 mm	153.0 in
Outboard engine (y_2)	10,160.0 mm	400.0 in
Outboard engine (z_2)	4,093 mm	161.1 in
Propulsive Force/Engine*	15,453 N	3,474 lbf
Engine Dry weight	836 kg	1844 lb
Propeller Diameter	4.11 m	13.5 ft
Number of Engines	4	4
*Estimate for design cruise speed [37]		

Table C. 4 - Wing data [33].

Wing Variables	SI units (multiples and submultiples)	US units
Wing Root Incidence	5.236×10^{-2} rad	3.0°
Wing Tip Incidence	0.0 rad	0.0°
Wingspan	40,437 mm	1592 in
Wing Area	162,162,256.3 mm ²	251,352.0 in ²
Aspect Ratio	10.1	10.1
Wing Root Chord	4,876.8 mm	192.0 in
Wing Tip Chord	2,540.0 mm	100.0 in
Spanwise Initial Taper	5,588.0 mm	220.0 in
Max Flap Deflection	+0.628 rad	+ 36°
Inboard Flap Chord	1460.5 mm	57.5 in
Outboard Flap Chord	1257.3 mm	49.5 in
Max Aileron Deflection	+0.262 rad/-0.436 rad	+ 15° /- 25°
Aileron Chord Percentage	28%	28%
Min Aileron Spanwise Position	14,427 mm	568 in
Max Aileron Spanwise Position	20,219 mm	796 in

Table C. 5 - Horizontal Tail data [33].

Horizontal tail Variables	SI units	US units
Horizontal tail incidence	-3.054×10^{-2} rad	$-1^{\circ}45'$
Horizontal tail span	16,052.8 mm	632.0 in
Horizontal tail Area	50,632,156.0 mm ²	78,48 in ²
Horizontal tail Aspect Ratio	5.02	5.02
Horizontal tail Root Chord	4,643.12 mm	182.8 in
Horizontal tail Tip Chord	1,724.7 mm	67.9 in
Max Elevator Deflection	+0.262 rad/-0.698 rad	+15 ^o /-40 ^o
Elevator Chord Percentage	36.4%	36.4%
Min Elevator Spanwise Position	1295.4 mm	51.0 in
Max Elevator Spanwise Position	8,026.4 mm	316 in

Table C. 6 - Vertical Tail data [33].

Vertical tail Variables	SI units	US units
Vertical tail span	7036.0 mm	277.0 in
Vertical tail Area	28,950,710.0 mm ²	44,874 in ²
Vertical tail Aspect Ratio	1.81	1.81
Vertical tail Root Chord	6,350.0 mm	250.0 in
Vertical tail Tip Chord	1,879.6 mm	74.0 in
Max Rudder Deflection	+0.611 rad/-0.611 rad	+35 ^o /-35 ^o
Rudder Chord Percentage	25%	25%
Min Rudder Spanwise Position	0 mm	0 in
Max Rudder Spanwise Position	7036 mm	277.0 in

Table C. 7 - Fuselage data [33].

Fuselage Variables		SI units	US units
Fuselage Section 1	Length	4,229.4 mm	165.6 in
	Nose Gear Position (from section 1 front)	3,495.0 mm	137.6 in
	Front diameter	0 mm	0 in
	Rear diameter	4,127.5 mm	162.5 in
	Diameters offset	589.3 mm	23.2 in
Fuselage Section 2	Length	7,137.4 mm	281.0 in
	Diameter	4,127.5 mm	162.5 in
Fuselage Section 3	Length	5,080.0 mm	200.0 in
	Main Gear Position (from section 3 front)	1,145.5 mm	45.1 in
	Diameter	4,127.5 mm	162.5 in
Fuselage Section 4	Length	6,553.2 mm	258.0 in
	Diameter	4,127.5 mm	162.5 in
Fuselage Section 5	Length	7,307.6 mm	287.0 in
	Front diameter	4,127.5 mm	162.5 in
	Rear diameter	140.97 mm	5.55 in
	Diameters offset	2,032 mm	80.0 in

Table C. 8 - Aircraft weight as percentage of the MTOW (source: Airframe Structural Design, Michael Niu, 2006) [29].

Aeroplane Group	Wing (%)	Fuselage (%)	Tail (%)	Edges (%)	Landing Gear (%)	Nacelle Pylon (%)
Light single propeller engine	9.0-11.0	7.0-11.0	2.0-2.8	1.1-2.0	4.5-7.0	1.1-2.1
Light twin propeller engines	9.0-11.0	7.0-8.5	1.9-2.5	1.2-1.8	4.5-6.5	3.5-4.5
Executive Jet	9.0-10.0	7.7-12.0	1.8-3.0	1.0-2.5	3.0-4.4	1.8-2.6
Turbo propeller 2 to 4 engines	7.5-10.0	7.0-14.0	1.7-3.0	0.7-1.8	3.5-5.0	1.0-4.1
Jet transport 2 engines	10.0-14.0	10.0-13.0	1.8-2.8	1.4-2.3	3.3-4.5	1.2-2.3
Jet transport 3 engines	9.0-11.0	10.0-12.0	2.1-2.8	1.3-1.9	3.8-4.7	1.5-2.4
Jet transport 4 engines	8.5 -12.0	6.5-10.0	1.5-2.5	0.7-1.0	3.4-4.2	1.3-2.2

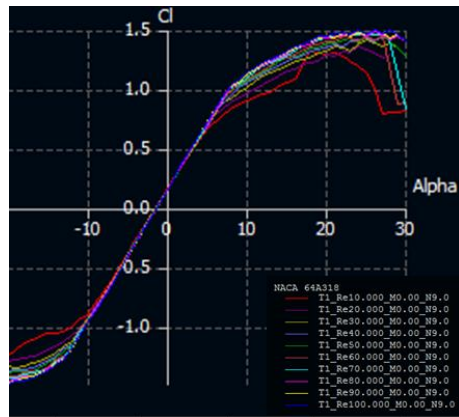


Figure C. 1 – NACA 64A318 (C-130 wing root) aerofoil lift coefficient versus AOA (XFLR5) [38].

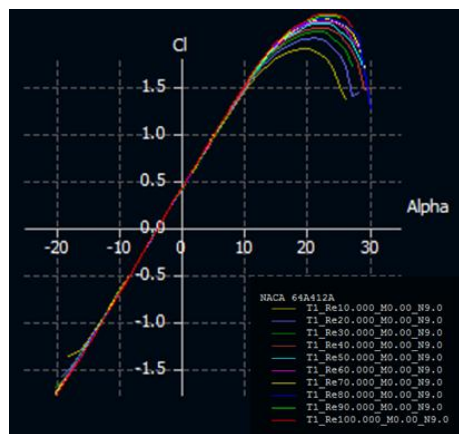


Figure C. 2 – NACA 64A412 (C-130 wing tip) aerofoil lift coefficient versus AOA (XFLR5) [38].



Figure C. 3 – NACA 23012 (C-130 horizontal tail) inverted aerofoil lift coefficient versus AOA (XFLR5) [38].

It was not needed to perform an analogous analysis for the vertical tail aerofoil once it is a symmetric aerofoil, which means its zero lift angle will be null.

Appendix D. Theoretical Background – Shear, Bending and Torsion Plots

A. Shear Force and Bending Moment

A brief review of the physical expressions that enable us to relate the loads applied to the structure with its shear force and bending moment. Let us perform the equilibrium of forces represented on Figure (C.1) [39].

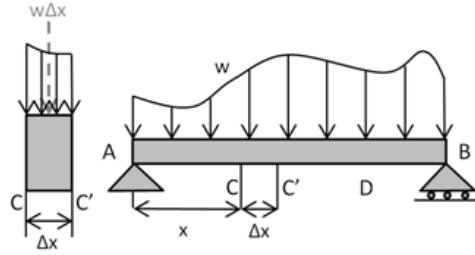


Figure D. 1 - Shear force determination scheme [39].

$$+\uparrow \sum F_y = 0: V - (V + \Delta V) - w\Delta x = 0 \quad (C. 1)$$

$$\Delta V = -w\Delta x \Rightarrow \frac{dV}{dx} = -w \quad (C. 2)$$

$$V_D - V_C = -\int_{x_C}^{x_D} w dx \quad (C. 3)$$

It should be noted that equation (C.3) is not valid at a point where a concentrated load is applied or when concentrated loads are applied between points C and D. Hence, this equation is only valid between successive distributed loads. Returning to the free body diagram shown and writing that the sum of moments about C' is zero:

$$+\uparrow \sum M_{C'} = 0: M - (M + \Delta M) - V\Delta x + w\Delta x \frac{\Delta x}{2} = 0 \quad (C. 4)$$

$$\Delta M = V\Delta x - \frac{1}{2}w(\Delta x)^2 \Rightarrow \frac{dM}{dx} = V \quad (C. 5)$$

$$M_D - M_C = \int_{x_C}^{x_D} V dx \quad (C. 6)$$

, where the area under the shear curve is considered positive when the shear is positive and negative otherwise. Notice that this equation is valid even when concentrated loads are applied between points C and D, provided the shear curve has been properly drawn.

In order to determine the beam lengthwise deflection the expression by which this variable can be related with the distributed loading acting on the body will be presented:

$$EI \frac{d^4 y}{dx^4} = -w(x) \quad (C. 7)$$

$$EI y(x) = - \int dx \int dx \int dx \int w(x) dx + \frac{1}{6} C_1 x^3 + \frac{1}{2} C_2 x^2 + C_3 x + C_4 \quad (C. 8)$$

The four constants of integration found in equation (C.8) can be determined from the boundary conditions. The wing will be treated as a cantilever beam, with zero displacement and rotation at its root and zero moment and shear force at its tip.

B. Torsion Plot

Once the spanwise torsion (T) has been determined along each beam (fuselage, wing, horizontal and vertical stabilizer) length, and provided that the beam's shear modulus (G) and polar moment of inertia (J) are known, it is possible to determine the unitary twist angle [21][22].

$$d\theta = \frac{T}{GJ} dy \quad (C. 9)$$

$$\Rightarrow \theta_A - \theta_B = \int_B^A \frac{T}{GJ} dy \quad (C. 10)$$

Appendix E. Instructions Manual

A. Abstract

The purpose of this Instructions Manual is to guide someone interested in using the *Microsoft Excel*® workbooks developed in a master thesis devoted to aeroplanes structural loads analysis from a collaborative work between *Instituto Superior Técnico* (Technical University of Lisbon) and OGMA, *Indústria Aeronáutica de Portugal, SA*.

The set of *Microsoft Excel*® workbooks developed throughout this research assess all in flight, ground, take-off and landing conditions for a generic aeroplane for each point of its main structural subsets – fuselage, wing, horizontal-stabiliser, vertical-stabiliser and landing gears. Finally, the loads are combined to obtain the limit loads at each point, enabling the plot of the limit shear force, bending moment and torsion loads at each point of the aeroplane.

B. Disclaimer

The use of the *Microsoft Excel*® workbooks developed throughout this work requires careful knowledge of the reasons and consequences that underlie each assumption, which can only be made by an integral and careful study of its report.

Despite the fact that all the assumptions follow a conservative approach, these workbooks are not expected to be a design tool by themselves, but rather a way to validate computational outputs obtained by other means, namely by finite element method or computational fluid dynamics. The author refuses any responsibility in an inadequate use of the tools developed.

C. Architecture

C.1. Colour codes

In order to facilitate the use of the *Microsoft Excel*® workbooks developed throughout this work, a set of different colours has been adopted. In the Table E.1, the user can get familiarized with the meaning of each colour.

INPUTS	Identifies all the data that varies from aeroplane to aeroplane and that must be inputted by the user
OUTPUTS	Identifies all the output data from the aeroplane under study
LEGISLATION	Identifies input data which is predefined in the legislation (CS 25, Subpart C – Structure)
MTOW (N)	Most of the variables are identified in grey cells
F_{max} (N)	Key output variables are identified by green letters in black cells
50	A number in a grey cell is a number that the user must not change, which means it depends on previously user inputted data or on applicable legislation
V-Tail	Identifies to what a group of variables refers to
Notes	Identifies any relevant notes in each excel spread sheet

Figure E. 1 - Microsoft Excel® workbooks colour codes.

NOTE: White cells may refer to variables that the user is required to input if they appear below an «INPUTS» label or to outputs that the user mustn't change if they appear below an «OUTPUTS» label.

D. System of Units

In the main folder the user can find a document named «**System of Units**». In this document it is possible to choose the system of units. It is possible to work with the International System of Units (SI) or with the U.S. Customary Units (US). For SI units the user enters <1> on cell E3, for US units, the user must enter number <2> on the same cell.

INPUT								
SYSTEM OF UNITS IN USE		1	<Enter 1 for IS> <Enter 2 for US>					
Symbol	Name	Symbol	Name	Conversion		Notes		
INTERNATIONAL SYSTEM OF UNITS (IS)		U.S. COSTUMARY UNITS (US)		IS/US	US/IS			
Time	s	second	s	second	1.0000	1.0000	t	Time
Length	m	meter	ft	foot	0.3048	3.2808	H	Altitude
	mm	millimeter	in	inch	25.4000	0.0394	c, S, b	wing chord, area and wingspan
Velocity	m/s	meter per second	ft/s	feet per second	0.3048	3.2808	V	Velocity
Acceleration	m/s ²	meter per square second	ft/s ²	feet per square second	0.3048	3.2808	a	Acceleration
Mass	kg	kilogram	slug	slug	14.5900	0.0685	m	Mass
Pressure	Pa	Pascal	lb/in ²	pound per square inch	6.90E+03	1.45E-04	p/a/r	Pressure/Normal and Shear Stress
Density	kg/mm ³	kilogram per cubic millimeter	slug/in ³	slug per cubic inch	0.0010	1051.1266	p	Material Density
Force	N	Newton	lb	pound	4.4480	0.2248	F	Force
Temperature	K	Kelvin	°R	Rankine	0.5556	1.8000	T	Temperature
Energy	J	Joule	ft.lb	foot pound	1.3560	0.7375	E	Energy

Figure E. 2 - System of Units choice.

NOTE: For simplicity, in some cases, distances are asked in mm (SI) or in (US) instead of SI or US units, since these units are also used on the aeroplane flight manuals. In these cases the *Microsoft Excel*® workbooks do automatically take this into account in order to provide all outputs in SI or US units.

E. Atmospheric Variables

AIR PROPERTIES - TROPOSPHERE			
INPUTS			
M (AIR) (kg/kmol)	28.8	R (J/kmol.K)	8.314
ALTITUDE (m)	11,000	R (J/kg.K)	288.3
		g (m/s ²)	32.2
INPUTS		OUTPUTS	
ISA ATMOSPHERE (TROPOSPHERE h<11000m)			
Reference Values		Actual Values	
T0 (K)	288.2	T (K)	216.7
P0 (Pa)	101,325	P (Pa)	22,630.6
p0 (kg/m ³)	1.225	p (kg/m ³)	0.362
		a (m/s) Soud Speed	295.700

Figure E. 3 - Atmospheric Properties.

In the main folder the user can find a document named «**Atmospheric Variables**». In this document it is possible to input the maximum operating altitude of the aircraft under study in the previously chosen system of units. The *Microsoft Excel*® spread sheet will automatically compute the local pressure, air density and temperature which will serve as input of all the other *Microsoft Excel*® workbooks built.

F. Flight Envelope

In the main folder there is a folder called «**Flight Envelope**» where the user can find a workbook with the same name. Herein, the user is required to input a set of parameters (see Figure E.4) so that the manoeuvring flight envelope and the gust envelope are plotted and combined in the flight envelope with the same name.

INPUTS			
INPUTS		CS-25	MEANING
MTOW (N)	700,000.0	Maximum Takeoff Weight	
S (mm ²)	162,000,000.0	Wing Projected Area	
C _{lmax} (flaps down)	2.6	C _{nmax} wing-flaps down	3D Positive lift coefficient before stall (flaps down)
C _{lmax} (flaps up)	1.34	C _{nmax} wing-flaps up	3D Positive lift coefficient before stall (flaps up)
C _{lmin} (flaps up)	-1.34	-C _{nmax} wing-flaps up	3D Negative lift coefficient before stall (flaps up)
n _{max} (flaps down)	2.1		Upper load factor limit (flaps down)
n _{max} (flaps up)	2.5	Must be greater than 2.5 and smaller than 3.8 (= (24000/(MTOW/4.448+10000)))	Upper load factor limit (flaps up)
n _{min} (flaps up)	-1.0	Mustn't be less than -1.0	Lower load factor limit (flaps up)
VS1 (m/s) (flaps down)	100.0		1-g stallin speed (EAS)
VS1 (m/s) (flaps up)	133.4		1-g stallin speed (EAS)
VC (m/s)	250.0		Design Cruise Speed (EAS)
VD (m/s)	375.0		Design Dive Speed (EAS)
ρ (kg/m ³)	1.200		

Figure E. 4 - Inputs for the manoeuvring flight envelope

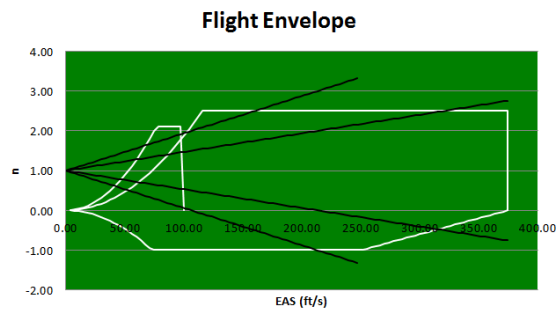


Figure E. 5 - Example plot of the manoeuvring envelope and gust envelope

The last spread sheet of this workbook determines the critical loading conditions that must be evaluated in the upcoming workbooks devoted to the analysis of each aeroplane component.

G. Mass Discretization

The most time-consuming step of data inputting is to introduce data about each part of the aeroplane with the exception of rivets, screws, bolts and other parts of the same size and weight. Notice however that this task only has to be carried out once for each different aeroplane. So, as soon as the user inputs all the relevant data for a particular aeroplane, this particular step can be skipped.

There is a folder inside the main one called «**Weight Distribution (Discretized)**» where the user can find 10 *Microsoft Excel*® workbooks. There is one for each main aircraft component (wings, horizontal tail, vertical tail), except for the fuselage that is divided in 5

portions, one for each *Microsoft Excel*® workbook another for the fuel positioning and the final sheet is for the aircraft as a whole.

In the workbook called «**Wing**» the user is required to input the geometry and/or weight of the following parts:

- Stringers & Spars;
- Panels;
- Systems & Other Geometries;
- Wing mounted landing-gear (if any);
- Fuel tanks (if any);
- Overall wing dimensions and layout.

In the workbook called «**Hor Stabilizer**» the user is required to input the geometry and/or weight for the following parts:

- Stringers & Spars;
- Panels;
- Systems & Other Geometries;
- Overall horizontal stabilizer dimensions and layout.

In the workbook called «**Ver Stabilizer**» the user is required to input the geometry and/or weight for the following parts:

- Stringers & Spars;
- Panels;
- Systems & Other Geometries;
- Overall vertical stabilizer dimensions and layout.

In the workbooks called «**Fuselage Section i**», **i** being a number between 1 and 5, 1 referring to the fuselage nose, 5 to the fuselage tail boom, 3 to the central section and 2 and 4 to the intermediate sections the user is required to input the weight and/or dimensions following parts for each of the five sections:

- Panels;
- Frames;
- Stringers & Longerons;
- Systems & Other Geometries;
- Passengers (if any);
- Cargo;
- Engines (if mounted on the fuselage on the appropriate fuselage section)
- Main gear (if mounted on the fuselage on the appropriate fuselage section);
- Nose Gear (on the appropriate fuselage section);

- Fuel tanks (if there is any fuel tank on the fuselage);
- Overall section dimensions.

In the workbooks called «**Fuel**» the user has to input the mass distribution of fuel, either on the wing or on the fuselage.

In the workbooks called «**Aircraft**» the user does not have to enter any data and can find several plots that provide an idea about the mass discretization of the aeroplane under study as well as determining its gravity centre.

EXACT RESULTS				
OUTPUTS				
Data	Geometric Centre			Mass
Variables	X (mm)	Y (mm)	Z (mm)	W (N)
Panels	2749.01	0.00	0.00	1052.29
Frames	2749.01	0.00	0.00	1517.30
Stringers&Longerons	2114.70	0.00	0.00	453.54
Systems&Other Geometries	0.00	0.00	0.00	0.00
Passengers	0.00	0.00	0.00	0.00
Cargo	0.00	0.00	0.00	0.00
Fuselage Engines	0.00	0.00	0.00	0.00
Fuselage Main Landing Gear	0.00	0.00	0.00	0.00
Fuselage Nose Landing Gear	3495.00	0.00	0.00	862.93
Fuel&Fuel Tanks	0.00	0.00	0.00	0.00
SECTION ASSEMBLY PROPERTIES	2840.63	0.00	0.00	3886.06
DISCRETIZED RESULTS (APPROXIMATE SOLUTION)				
INPUTS				
Fuselage Section Length (mm)	4229.4	Number of mass points		10
Fuselage Section Front Diameter (mm)	0	Fuselage Front and Rear		589.3
Fuselage Section Rear Diameter (mm)	4127.5			
NOTE	Number of mass points must be lower than 10 and greater than			
OUTPUTS				
Data	Geometric Centre			Mass
Mass Point number	x (mm)	y (mm)	z (mm)	W (N)
1	211.47	0.000	0.000	32.17
2	634.41	0.000	0.000	138.80
3	1057.35	0.000	0.000	185.51
4	1480.29	0.000	0.000	232.22
5	1903.23	0.000	0.000	278.35
6	2326.17	0.000	0.000	325.67
7	2749.11	0.000	0.000	372.38
8	3172.05	0.000	0.000	419.09
9	3594.99	0.000	0.000	465.80
10	4017.93	0.000	0.000	512.54
Discretized Body	X (mm)	Y (mm)	Z (mm)	W (N)
	2862.64	0.00	0.00	3886.06
Discretization errors (%)	0.78	0.00	0.00	0.00

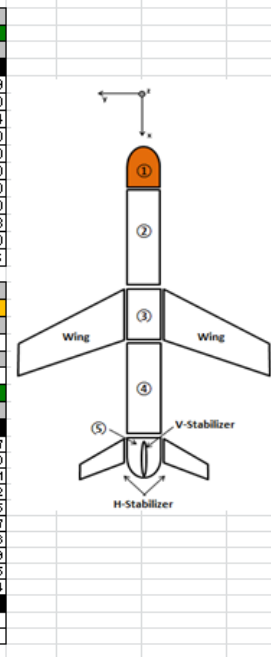


Figure E. 6 - Discretized weight data last sheet (fuselage section 1).

NOTE: For simplicity, the user can skip this point, and input directly the mass discretization on the output data sheet (Figure E.6).

H. Specific Load Analysis

H.1. Landing Gear Loads

H.1.1. Landing Loads

In the folder named «**Landing Loads**» there is a Microsoft Excel® workbook with the name «**Landing Gear Loads**» where the user is required to **input** the following data:

- Maximum Take-off Weight (MTOW) per landing gear, depending on being in a 1, 2 or 3-point landing condition;

- Maximum Landing Weight (MLW) per landing gear, depending on being in a 1, 2 or 3-point landing condition;
- Gear spring constant;
- Gear damping constant.

This *Microsoft Excel*® workbook provides the following **outputs**:

- Undamped natural frequency;
- Critical Damping Constant
- Damping coefficient;
- Damped natural frequency;
- Oscillation period;
- Maximum vertical force;
- Shear in x, y and z directions.

NOTE: In this workbook, the above mentioned outputs are calculated for the 1-Point landing, 2-Points landing, Side load landing and 3-Points landing, each of these for both the Maximum Landing Weight and Maximum Take-off Weight, in accordance with CS 25.473.

NOTE			
* All the aeroplane weight is supposed to be acting on a single gear			
1-POINT LANDING			
INPUTS			
MLW (kg)*	59000	MTOW (kg)*	70300
K - Spring Constant (kg/s ²)*	59000	K - Spring Constant (kg/s ²)*	20000
C - Damping Constant (kg/s)*	20000	C - Damping Constant (kg/s)*	20000
x0 (m)	-1	x0 (m)	-1
LEGISLATION (CS-25)			
(MLW) - Limit Descent Velocity (m/s)	3.05	(MTOW) - Limit Descent Velocity (m/s)	1.83
OUTPUTS			
MLW		MTOW	
Type of system	Underdamped	Type of system	Underdamped
ω (Undamped) (rad/s)	1.000	ω (Undamped) (rad/s)	0.53
Cc - Critical Damping Constant (kg/s)	118000	Cc - Critical Damping Constant (kg/s)	74993
ζ (Damping coefficient)	0.169491525	ζ (Damping coefficient)	0.27
(MLW) - Fmax (N)	1439946	(MTOW) - Fmax (N)	1281980
Vz (N)*	1.44E+06	Vz (N)*	1.28E+06
Vx (N)*	3.60E+05	Vx (N)	3.20E+05

Figure E. 7 - Typical inputs and outputs on the landing gear load analysis.

H.1.2. Ground Loads

In the folder named «**Ground Loads**» there is a Microsoft Excel® workbook with the same name where the user is required to **input** the following data:

- Horizontal distance from CG of the aeroplane to the nose wheel;
- Horizontal distance from CG of the aeroplane to the main wheel;
- Vertical height of the CG of the aeroplane above the ground;
- Distance between left and right main gears;
- Lateral distance from CG to aeroplane's centre line (positive towards the right wing);

- Dynamic Friction Coefficient (Refer to applicable legislation);
- Dynamic Response Factor (Refer to applicable legislation);
- Aeroplane's second moment of the area relative to the Y-axis;
- Maximum Take-off Weight (Refer to aeroplane flight manual);
- Maximum Taxi Weight (Refer to aeroplane flight manual);
- Maximum Landing Weight (Refer to aeroplane flight manual);
- Choose between single axle main gear or multiple axle gear;
- Distance between the wheels on the same axle;
- Distance between axles of the main gear (leave blank if single axle main gear).

INPUTS		
Variable	Value	Notes
A (mm)	15000	Horizontal distance from CG of the aeroplane to the nose wheel
B (mm)	8000	Horizontal distance from CG of the aeroplane to the main wheel
C (mm)	23000	A+B
E (mm)	3000	Vertical height of the CG of the aeroplane above the ground
T (mm)	7000	Distance between left and right main gears
BLcg (mm)	0	Lateral distance from CG to aeroplane's centre line (positite towards the right wing)
μ	0.8	Dynamic Friction Coefficient (Refer to applicable legislation)
f	2	Dynamic Response Factor (Refer to applicable legislation)
ly (kg.mm ²)	1.00E+09	Aeroplane's second moment of the area relative to the Y-axis
MTOW (N)	75000	Maximum Take-off Weight (Refer to aeroplane flight manual)
MTW (N)	75000	Maximum Taxi Weight (Refer to aeroplane flight manual)
MLW (N)	60000	Maximum Landing Weight (Refer to aeroplane flight manual)
Main Gear Configuration	1	Enter <1> for single axle main gear or <2> for multiple axle gear
F (mm)	1200	Distance between the wheels on the same axle
d (mm)	1500	Distance between axles of the main gear (leave blank if single axle main gear)

Figure E. 8 - Input data sheet for the landing gear

The **outputs** of that *Microsoft Excel*® workbook refer to the following ground loads:

- Static load condition;
- Taxi, take-off & landing;
- 3 point braking;
- 2 point braking;
- Sudden braking;
- Ground turning;
- Nose gear yaw and steering;
- Unsymmetrical braking;
- Pivoting;
- Towing;

H.2. Wing Loads

In the folder named «**Wing Loads**» there is a Microsoft Excel® workbook with the name «**0. Wing Input Data**» where the user is required to **input** the following data:

- Aerofoils characteristics;
- Wing geometric data;
- Control surfaces and high lift devices limit deflections;
- Maximum spoiler's hinge moment;
- Operating velocity and air density.

FLAPS		SPOILERS (INBOARD-Braking)		SPOILERS (OUTBOARD-Rolling)	
Minimum Spanwise Position (mm)	2050	Minimum Spanwise Position (mm)	0	Minimum Spanwise Position (mm)	0
Maximum Spanwise Position (mm)	5500	Maximum Spanwise Position (mm)	0	Maximum Spanwise Position (mm)	0
% Chord	25	Spoiler Average Chord (mm)	0	Spoiler Average Chord (mm)	0
Maximum Flap Deflection (DEG)	15	Max Extended Hinge Moment (N.mm)	0	Max Extended Hinge Moment (N.mm)	0
Additional Wing Chord (mm) FOWLER FLAP **	50	Max Retracted Hinge Moment (N.mm)	0	Max Retracted Hinge Moment (N.mm)	0
β (DEG)	4	Maximum Spoiler Deflection (DEG)	0	Maximum Spoiler Deflection (DEG)	0
AILERONS		Vert Dist from Wing MAC to Spoiler Drag	0	Vert Dist from Wing MAC to Spoiler	0
Minimum Spanwise Position (mm)	15000	Horiz Dist from Wing MAC to Spoiler Drag	0	Horiz Dist from Wing MAC to	0
Maximum Spanwise Position (mm)	19000	CLEAN AEROFOIL			
% Chord	28	β clean (DEG)	2		
Maximum Flap Deflection (DEG)	25				
β (DEG)	3				

Figure E. 9 - Several inputs for the wing

This *Microsoft Excel*® workbook provides a number of outputs that will serve as inputs of the workbooks named «**1.1 Symmetrical Loading (nz max)**», «**1.2 Symmetrical Loading (nz min)**», «**1.3 Symmetrical Loading (Flaps Down)**». Each of these three *Microsoft Excel*® workbooks will provide different values for the wing lift, drag and pitching moment. Thereafter, the results are combined in a workbook named «**MAXIMUM LOADS**», which presents the critical in-flight loading for the wing.

H.3. Horizontal-Tail Loads

In the folder named «**Horizontal tail Loads**» there is a Microsoft Excel® workbook with the name «**0. Horizontal tail Input Data**» where the user is required to **input** the following data:

- Aerofoils characteristics;
- Horizontal stabilizer geometric data;
- Elevator limit deflections;
- Operating velocity and air density.

This *Microsoft Excel*® workbook provides a number of outputs that will serve as inputs of the workbooks named «**1.1 Convent Tail – Balanced Manoeuvre**», «**1.2 T-Tail – Balanced Manoeuvre**», «**2.0 Unchecked Manoeuvre**» and «**3.0 Checked Manoeuvre** ». Each of these excel workbooks will provide different values for the horizontal tail lift, drag and pitching moment. Thereafter, the results are combined in a workbook named «**MAXIMUM LOADS**», which presents the critical in-flight loading for the horizontal stabilizer, which values will be used to plot the horizontal stabilizer spanwise shear force, bending moment and torsion.

H.4. Vertical Tail Loads

In the folder named «**Vertical tail Loads**» there is a *Microsoft Excel*® workbook with the name «**0. Vertical tail Input Data**» where the user is required to input the following data:

- Aerofoils characteristics;
- Vertical stabilizer geometric data;
- Rudder limit deflections;
- Operating velocity and air density.

This *Microsoft Excel*® workbook provides a number of outputs that will serve as inputs of the workbooks named «**1. Manoeuvres I, II and III**», «**2. Engine-Out Conditions**» and «**3. Engine-Out Conditions**». Each of these *Microsoft Excel*® workbooks will provide different values for the vertical tail lift, drag and pitching moment. Thereafter, the results are combined in a workbook named «**MAXIMUM LOADS**», which presents the critical in-flight loading for the vertical stabilizer, which values will be used to plot the horizontal stabilizer spanwise shear force, bending moment and torsion.

H.5. Fuselage Loads

In the folder named «**Fuselage Loads**» there is a *Microsoft Excel*® workbook with the name «**0. Fuselage Loads Input Data**» where the user is required to input the following data:

- Fuselage geometric data;
- Maximum fuselage incidence relative to the free stream velocity;
- Operating velocity and air density.

This *Microsoft Excel*® workbook computes the aerodynamic forces acting on the fuselage. Finally, this data is combined with the loads from the wings, horizontal tail, vertical tail and landing gears attached to the fuselage, components which are anchored to the fuselage and will thus transmit its loads to the respective fuselage section.

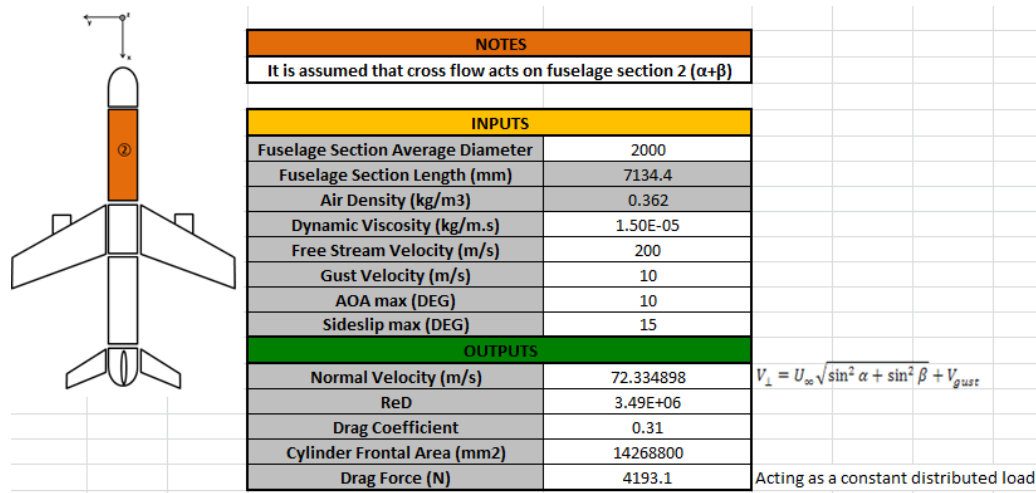


Figure E. 10 - Typical spread sheet for the fuselage aerodynamic analysis.

I. Plots

In a folder called «**Combined Loads**», the user can find the plots of the maximum shear force, bending moment and torsion at each point along the spanwise directions of the wing, vertical tail and horizontal tail and along the length of the fuselage. However, the reader should note that these workbooks compute the maximum and minimum loads for a particular velocity, which means that in order to have the absolute maximum and minimum loads different values for the velocity should be analysed.

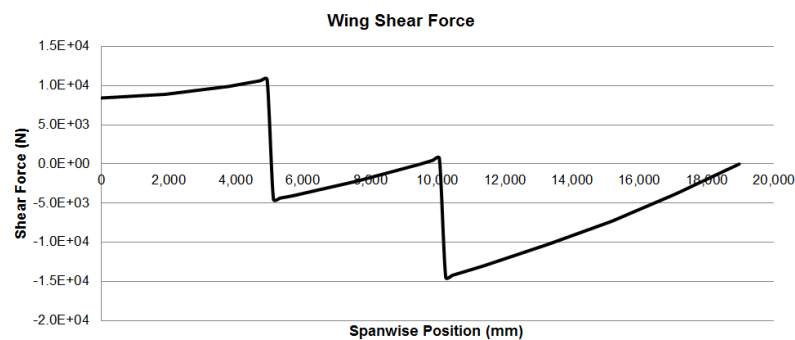


Figure E. 11 – Example of Wing maximum shear force on the horizontal plane

J. Endnote

It is the user responsibility to compute the critical load combinations, which means that one of the tasks is to combine the partial loads of the wing, empennage, landing gears and fuselage in an effective way, so that the actual limit loads are effectively being computed, since the workbooks created do not directly lead to the maximum loads acting at each point.